(2)

AD-A196 456

AFWAL-TR-87-3098
PART I

UNSTEADY LOW-SPEED WINDTUNNEL TEST OF A STRAKED DELTA WING, OSCILLATING IN PITCH

PART I: GENERAL DESCRIPTION AND DISCUSSION OF RESULTS

A. M. Cunningham, Jr.

GENERAL DYNAMICS
FORT WORTH DIVISION
P. O. Box 748
FORT WORTH, TEXAS 76101

R. G. den Boer
C. S. G. Dogger
E. G. M. Geurts
A. J. Persoon
A. P. Retel
R. J. Zwaan

NATIONAL AEROSPACE LABORATORY (NLR)
AMSTERDAM, NETHERLANDS

APRIL 1988

FINAL REPORT FOR PERIOD JUNE 1985-AUGUST 1987

FLIGHT DYNAMICS LABORATORY
AIR FORCE WRIGHT AERONAUTICAL LABORATORIES
AIR FORCE SYSTEMS COMMAND
WRIGHT-PATTERSON AIR FORCE BASE, OHIO 45433-6553

NOTICE

When Government drawings, specifications, or other data are used for any purpose other than in connection with a definitely related Government procurement operation, the United States Government thereby incurs no responsibility nor any obligation whatsoever; and the fact that the government may have formulated, furnished, or in any way supplied the said drawings, specifications, or other data, is not to be regarded by implication or otherwise as in any manner licensing the holder or any other person or corporation, or conveying any rights or permission to manufacture use, or sell any patented invention that may in any way be related thereto.

This report has been reviewed by the Office of Public Affairs (ASD/PA) and is releasable to the National Technical Information Service (NTIS). At NTIS, it will be available to the general public, including foreign nations.

This technical report has been reviewed and is approved for publication.

Don W. Kinsey

DON W. KINSEY
Project Engineer

Bohdan G. Kunciw

BOHDAN G. KUNCIW, MAJ, USAF
Chief, Aerodynamics & Airframe Branch
Aeromechanics Division

FOR THE COMMANDER

Alfred C. Draper

ALFRED C. DRAPER
Acting Chief
Aeromechanics Division

"If your address has changed, if you wish to be removed from our mailing list, or if the addressee is no longer employed by your organization please notify AFWAL/FIMM*, W-PAFB, OH 45433 to help us maintain a current mailing list".*

Copies of this report should not be returned unless return is required by security considerations, contractual obligations, or notice on a specific document.

UNCLASSIFIED
SECURITY CLASSIFICATION OF THIS PAGE

REPORT DOCUMENTATION PAGE

Form Approved
OMB No. 0704-0188

1a. REPORT SECURITY CLASSIFICATION UNCLASSIFIED	1b. RESTRICTIVE MARKINGS None
2a. SECURITY CLASSIFICATION AUTHORITY	3. DISTRIBUTION/AVAILABILITY OF REPORT Approved for public release; distribution is unlimited
2b. DECLASSIFICATION/DOWNGRADING SCHEDULE	
4. PERFORMING ORGANIZATION REPORT NUMBER(S)	5. MONITORING ORGANIZATION REPORT NUMBER(S) AFWAL-TR-87-3098, PART I
6a. NAME OF PERFORMING ORGANIZATION General Dynamics 6b. OFFICE SYMBOL (If applicable)	7a. NAME OF MONITORING ORGANIZATION Air Force Wright Aeronautical Laboratories Flight Dynamics Laboratory/AFWAL/FIMM
6c. ADDRESS (City, State, and ZIP Code) P.O. Box 748 Fort Worth TX 76101	7b. ADDRESS (City, State, and ZIP Code) Wright-Patterson AFB OH 45433-6553
8a. NAME OF FUNDING/SPONSORING ORGANIZATION 8b. OFFICE SYMBOL (If applicable)	9. PROCUREMENT INSTRUMENT IDENTIFICATION NUMBER F33615-85-C-3013
8c. ADDRESS (City, State, and ZIP Code)	10. SOURCE OF FUNDING NUMBERS PROGRAM ELEMENT NO: 62201F PROJECT NO: 2404 TASK NO: 10 WORK UNIT ACCESSION NO.: 94

11. TITLE (Include Security Classification)
UNSTEADY LOW-SPEED WIND TUNNEL TEST OF A STRAKED DELTA WING, OSCILLATING IN PITCH, PART I: GENERAL DESCRIPTION AND DISCUSSION OF RESULTS

12. PERSONAL AUTHOR(S)
Cunningham, A. M., General Dynamics* (See Reverse)

13a. TYPE OF REPORT	13b. TIME COVERED	14. DATE OF REPORT (Year, Month, Day)	15. PAGE COUNT
FINAL	FROM Jun 85 TO Aug 87	1988 April	140

16. SUPPLEMENTARY NOTATION

17. COSATI CODES

FIELD	GROUP	SUB-GROUP
01	01	
20	04	

18. SUBJECT TERMS (Continue on reverse if necessary and identify by block number)
Unsteady Flow, Vortex Flow, Wind Tunnel Test

19. ABSTRACT (Continue on reverse if necessary and identify by block number)

Results of a wind tunnel test of an oscillating straked wing. The report provides unsteady airloads and pressure distributions for a range of incidences (-8 to 50 deg.) and amplitudes (1 to 16 deg.). The wind speed was 80 meters/second, which provided reduced frequencies up to 0.50 based on root chord. The zeroth and first harmonic as well as the continuous time history of the pressure and overall loads were measured. Flow visualization was performed for flow of 30 meters/second using a pulsating laser light sheet.
This part presents the description of this wind tunnel test and preliminary discussions of results obtained from the test. Details are provided on the model, instrumentation and support system as well as test program condition/run number cross-reference tables for use with the data base presented in parts II through VI of this report. Model geometry and force data processing procedures are presented in the appendices. Also presented in the appendices are updated values of force data obtained from the steady tests (See reverse)

20. DISTRIBUTION/AVAILABILITY OF ABSTRACT ☒ UNCLASSIFIED/UNLIMITED ☐ SAME AS RPT. ☐ DTIC USERS	21. ABSTRACT SECURITY CLASSIFICATION UNCLASSIFIED
22a. NAME OF RESPONSIBLE INDIVIDUAL Don W. Kinsey	22b. TELEPHONE (Include Area Code) (513) 255-2481 22c. OFFICE SYMBOL AFWAL/FIMM

DD Form 1473, JUN 86 Previous editions are obsolete. SECURITY CLASSIFICATION OF THIS PAGE
UNCLASSIFIED

12. PERSONAL AUTHOR(S) CONTD

* den Boer, R. G.,	National	Aerospace	Laboratory,	The	Netherlands
Dogger, C. S.,	"	"	"	"	"
Geurts, E.G.M.,	"	"	"	"	"
Persoon, A. J.,	"	"	"	"	"
Retel, A. P.,	"	"	"	"	"
Zwaan, R. J.,	"	"	"	"	"

19. ABSTRACT CONTD

of the model suspended by a wire balance.

FOREWORD

This report summarizes the results of the windtunnel test of an oscillating straked wing conducted under a cooperative program of research between General Dynamics Fort Worth Division, Fort Worth, Texas, and the National Aerospace Laboratory (NLR), The Netherlands. The model and support system was designed and fabricated at NLR under a separate program with General Dynamics and NLR funding. The test preparation, windtunnel test and reporting were performed at NLR under Air Force Contract F33615-85-C-3013, for the Flight Dynamics Laboratory of the Air Force Wright Aeronautical Laboratories, Wright-Patterson Air Force Base, Ohio. The work was administered by Mr. D.W. Kinsey of the Aeromechanics Division (AFWAL/FIM). Additional technical monitoring support was provided by Mr. T. Cord of the Flight Control Division (AFWAL/FIG).

The program manager and principal investigator was Dr. A.M. Cunningham Jr. at General Dynamics and Mr. R.G. den Boer was the principal investigator at NLR. Mr. den Boer was assisted by the following NLR specialists: C.S.G. Dogger, E.G.M. Geurts, A.J. Persoon, A.P. Retèl and R.J. Zwaan.

This report consists of six parts. Part I presents a general description of the model and test program and a discussion of the results. Part II contains the steady pressure distribution plots and the major part of the zeroth and first order harmonic unsteady pressure distribution plots. Part III contains the remainder of the unsteady pressure distribution plots and plots of the steady and the zeroth and first order harmonic unsteady overall loads. Part IV contains time history plots of the unsteady pressures and overall loads. Part V contains power spectral density plots of the overall loads at harmonic oscillation and time history plots of overall loads for (1-cos) model motions. Part VI contains results of the flow visualization program.

ACKNOWLEDGEMENT

The authors wish to express gratitude to Mr. N.G. Verhaagen of the Aerospace Department of the Technical University of Delft for his cooperation in preparatory tests.

The authors make reference to the following persons who contributed substantially to this project: Messrs. T. Horsman, Ph. Kok, E.W.M. Slijkerman. Reference is also made to Mr. H. Kannemans, who was involved in an orientating windtunnel test up to December 1, 1983, when he started working at the Flight Test Instrumentation Department of NLR, and to Mr. J.J. Horsten, who was principal investigator up to September 1, 1985, when he entered the service of Martinair.

CONTENTS

CONTENTS (Cont'd)

(138 pages in total)

LIST OF TABLES

LIST OF ILLUSTRATIONS

LIST OF ILLUSTRATIONS (Cont'd)

LIST OF ILLUSTRATIONS (Cont'd)

LIST OF SYMBOLS

ALPHA, α	wing incidence	(deg)
b	local wing span	(m)
bw	wing span (bw = 0.8000)	(m)
BETA, β	sideslip angle	(deg)
c	local chord	(m)
CD	wing drag force coefficient	
Cl	wing rolling moment coefficient	
(Cl)m	mean wing rolling moment coefficient (Cl)m = l/(Q*S*bw)	
(Cl)i	unsteady wing rolling moment coefficient (Cl)i = l/(Q*S*bw*dα) (Cl)i = Re(Cl) + i Im(Cl)	
CL	wing lift force coefficient	
Cm	wing pitching moment coefficient ref. axis = rotation axis x/cr = 73.27 %	
(Cm)m	mean wing pitching moment coefficient (Cm)m = m/(Q*S*cr) ref. axis x/cr = 73.27 %	
(Cm)i	unsteady wing pitching moment coefficient ref. axis x/cr = 73.27 % (Cm)i = m/(Q*S*cr*dα) (Cm)i = Re(Cm) + i Im(Cm)	
Cn	wing yawing moment coefficient	
(Cn)m	mean wing yawing moment coefficient (Cn)m = n/(Q*S*bw)	
(Cn)i	unsteady wing yawing moment coefficient (Cn)i = n/(Q*S*bw*dα) (Cn)i = Re(Cn) + i Im(Cn)	
CN	wing normal force coefficient	
(CN)m	mean wing normal force coefficient (CN)m = N/(Q*S)	
(CN)i	unsteady wing normal force coefficient (CN)i = N/(Q*S*dα) (CN)i = Re(CN) + i Im(CN)	
Cp	pressure coefficient	
(Cp)m	mean pressure coefficient	
(Cp)i	unsteady pressure coefficient (Cp)i = p_i/(Q*dα) (Cp)i = Re(Cp) + i Im(Cp)	
cr	root chord (cr = 0.7855)	(m)
CT	wing tangential force coefficient	
(CT)m	mean wing tangential force coefficient (CT)m = T/(Q*S)	

LIST OF SYMBOLS (Cont'd)

(CT)i	unsteady wing tangential force coefficient (CT)i = T/(Q*S*dα) (CT)i = Re(CT) + i Im(CT)	
CY	wing side force coefficient	
(CY)m	mean wing side force coefficient (CY)m = Y/(Q*S)	
(CY)i	unsteady wing side force coefficient (CY)i = Y/(Q*S*dα) (CY)i = Re(CY) + i Im(CY)	
(d)i	unsteady displacement of accelerometer relative to the angular displacement of the wing (d)i = Re(d) + i Im(d)	(mm)
D	wing drag force	(N)
DALPHA,dα	harmonic oscillation: amplitude of unsteady wing incidence (1-cos) inputs : magnitude of wing incidence variation	(deg,rad)
f, FREQ	frequency	(Hz)
HARM	harmonic component (HARM = 0: mean) (HARM = 1: first harmonic)	
i	SQRT(-1)	
l	wing rolling moment (figure 1)	(Nm)
L	wing lift force	(N)
m	wing pitching moment (figure 1) ref. axis x/cr = 73.27 %	(Nm)
MACH	freestream Mach number	
n	wing yawing moment (figure 1)	(Nm)
N	wing normal force (figure 1)	(Nm)
NO	number of pressure transducer	
p	pressure at model surface	(Pa)
ps	static pressure	(Pa)
pt	total pressure	(Pa)
PHI, φ	phase angle	(deg)
Q	dynamic pressure	(Pa)
REDFR	reduced frequency, REDFR = pi * f * cr/V	
RUN	run number	
S	wing area (S = 0.2640)	(m**2)
t	time	(s)
T	wing tangential force (figure 1)	(N)
T	stagnation temperature in settling chamber	(deg C)

LIST OF SYMBOLS (Cont'd)

T	harmonic oscillation: period of oscillation	(s)
	(1-cos) input: duration of (1-cos) input	(s)
V	freestream velocity	(ms**-1)
x	chordwise coordinate in wing reference plane apex: x=0 (figures 1, 5)	(m)
x'	coordinate in direction of longitudinal test section axis (see figure 9)	(m)
xref	reference x-value	(m)
y	spanwise coordinate in wing reference plane (see figures 1, 5); y-axis is the rotation axis; x/cr = 73.27 %	(m)
y'	spanwise coordinate (see figure 9)	(m)
yref	reference y-value	(m)
Y	wing side force (see figure 1)	(N)
z	coordinate in plane of symmetry normal to wing reference plane (see figures 1,5)	(m)
z'	coordinate normal to x'-y' plane (see figure 9)	(m)

GREEK

α,ALPHA	wing incidence	(deg)
d_α,DALPHA	harmonic oscillation: amplitude of unsteady wing incidence	(deg,rad)
	(1-cos) input: magnitude of wing incidence variation	
β,BETA	sideslip angle	(deg)
φ, PHI	phase angle	(deg)
τ	pulse width	

SUBSCRIPTS

a	adjusted
g	geometric
m	mean
i	unsteady
ref	reference

1 INTRODUCTION

1.1 Motive

Straked wings are currently becoming common features of advanced fighter aircraft. The strakes are designed to generate vortices from highly swept leading edges which stabilize flow over the wing and provide additional lift up to high angles of attack. In this way the strakes contribute much to high maneuvrability. The vortex lift capability of straked wings has been extensively explored and experimental data concerning aerodynamic loading are available for various planforms and Mach numbers. Advanced calculation methods to predict the vortex flow are maturing.

The knowledge of unsteady loading on straked wings is less developed, both in the cases where the loading is due to wing oscillations - as required for aircraft stability and flutter analysis - and in cases where fluctuations in the flow are induced by vortex burst (or vortex breakdown) as required for stall and buffet predictions. The common practice in flutter analysis, for example, is that flutter clearance calculations for straked wing fighters are still based on attached flow without leading edge vortices. This is necessary because a lack of adequate calculation methods for unsteady vortex flow which must be validated by experiment. The immediate question then arises if such a procedure can guarantee sufficiently conservative predictions, or, if so, is it unreasonably conservative.

This situation has given rise to a cooperative project of General Dynamics (GD) and the National Aerospace Laboratory (NLR), with funding provided by the Air Force Wright Aeronautical Laboratories (AFWAL), concerning a windtunnel experiment with an oscillating straked wing. This experiment will extend the knowledge of unsteady vortex flow, and provide a data base for the validation of computer codes for unsteady airloads.

1.2 Some physical aspects

A brief description of some physical aspects of the unsteady vortex flow is given here. First the main characteristics of the steady flow are considered. In figure 2 a straked wing at incidence is shown. Vortices are shed from the leading edges of the strake and the wing. The sharp strake leading edges generate vortex sheets even at low incidence which roll up spirally into the strake vortices and flow downstream over the wing. The vortices induce strong lateral velocities at the strake upper

surface, giving rise to suction peaks at the position of the vortex cores (see upper left inset). When the lateral velocities are large enough, secondary flow separations occur, leading to secondary vortices spiralling opposite to the primary vortices.

At moderate incidences vortex sheets start to develop from the wing leading edges, starting at the kinks. As a result, the spanwise pressure distribution now shows two pressure peaks (see upper right inset).

At higher incidences vortex burst or vortex breakdown occurs initially for the wing vortices followed later by the strake vortices. An important consequence of vortex burst is that the corresponding suction peaks become weaker and that the vortices lose their ability to produce additional lift. A normal behaviour of vortex burst is that it will move upstream when the incidence increases. At still higher incidences large-scale boundary layer or stall separation occurs, starting often at the trailing edge.

The explanation of the above vortex flow becomes increasingly complicated in case of interactions of strake and wing vortices, their influence on vortex burst and flow separation and, at high enough speeds their interaction with shock waves. The analysis of these phenomena is still the subject of many investigations (e.g. Ref. 1).

When the straked delta wing is oscillating, the strength and the position of the wing and strake vortices will oscillate. As the vortices are being fed through the vortex sheets emanating from the leading edges, it is to be expected that the oscillations of vortex strength and position will lag the wing oscillation. Phenomena like vortex burst and stall separation have shown hysteresis effects in steady measurements so that it might be conjectured that in the unsteady case these effects will cause an additional lagging.

1.3 Objectives

With the description of the problem area in section 1.1 and the various physical aspects in section 1.2 as background the objectives of the windtunnel experiment were formulated as follows:

- to obtain a physical insight of the vortex flow
- to set up a data base of unsteady aerodynamic data for computer code validation; and
- to study the dynamic aspects of vortex bursts, up to high angles of attack at which vortex breakdown occurs close to the strake leading edge.

In order to achieve these objectives, some basic decisions were made:

a. The experiment was restricted to low speeds to keep the already complicated flow from being further complicated by compressibility effects. Continued experiments in future may hopefully cover the transonic speed range.

b. Preference was given to a balance to measure the overall aerodynamic loads. Because of the large pressure gradients it was expected that no practical grid of pressure pickups installed in the windtunnel model would be dense enough to provide accurate aerodynamic loads through integration. Measurements of pressure distributions would only be applied in a few strategically chosen sections.

c. The aerodynamic load and pressure measurements would be supplemented with information about the flow above the model upper side. Flow visualization was used to study the position of the vortices and vortex cores, development of vortex burst, etc. Application of a laser light screen technique in a previous windtunnel test had already proven to be feasible (see Ref. 2) to study the position of the vortex cores in steady flow (see Fig. 3). Also the means to apply a chopped laser light screen were investigated for unsteady flow.

2 TEST SETUP

2.1 Windtunnel

The tests were conducted in the low speed windtunnel LST 3x2.25 m^2 of NLR in the Noordoostpolder (North-East Polder) of The Netherlands. The tunnel is a closed-type windtunnel and has interchangeable test sections with a total length of 8.75 m. The test sections are provided with turntables in the floor and ceiling. The tunnel has a maximum attainable windspeed of about 85 m/s.

2.2 Model and model support

An overall view of the test setup is shown in figure 4. The geometry of the model is indicated in figure 5. It is a straked delta wing, with a span of 800 mm, a root chord of 785.5 mm and tip chords of 120 mm. As the model was not intended to represent a real aircraft, the parts which might complicate the aerodynamics, like fuselage and empennage, were left

out. The outboard wing has an NACA 64A005 airfoil and a leading edge sweep of 40 deg. The strake has a sharp leading edge with a sweep of 76 deg. The spanwise cross-section of the strake has a diamond shape with a half top angle of 11.4 deg (see figure 5). At the centre, the diamond shape is rounded with a radius which varies linearly from 0 mm at the apex x=0 mm, to a radius of 80 mm at x=333.7 mm and back to a radius of 0 mm at x=437.0 mm. At the kink in the leading edge, where the strake joins the wing, the thickness distribution is smoothed.

The middle of the main wing was thickened to accommodate the balance. The sides of this thicker region were rounded with a radius of 80 mm and the top is a flat surface, parallel to the model reference plane (see Fig.5). A more detailed description of the model geometry is presented in appendix A.

The model was designed (see Ref. 3) and fabricated at NLR. It was made of a magnesium alloy to reduce inertia loads. The overall mass of the model, including its instrumentation, but without the balance was 5.9 kg. The instrumentation is described in section 2.3. For the visualization tests a smoke tube was attached to the lower side of the model, with its opening very close to the apex (see Fig. 6b-c). The optimal position of the smoke tube was determined in a separate test (see Ref. 4), although during the final test the tube could be shifted in x- and z-directions and its incidence could be changed.

The support mechanism (see Figs. 4,6a), also designed and built at NLR, was mounted on the turntable in the floor of the test section to allow model sideslip. By a system of struts the model was supported in such a way that it could perform a pitching motion about an axis at 73.3 % root chord. The support elements were aerodynamically shaped and two of them were used as conductors for the instrumentation wiring.

2.3 Model instrumentation

The instrumentation of the model consisted of:

- 1 six-component balance,
- 1 displacement transducer,
- 1 temperature transducer,
- 9 accelerometers,
- 42 miniature pressure transducers.

The location of the instrumentation in the model is indicated in table 1 and figure 5.

For measuring the forces and moments an existing six-component balance (NLR 635) was used. With this balance forces and moments can be measured up to: 450 N in tangential force, 1200 N in side force, 3000 N in normal force, 90 Nm in roll, 110 Nm in pitch and 70 Nm in yaw.

With a Sangamo AFG 5.0 S linear variable differential transducer (LVDT) mounted between the model and support, the oscillation amplitude and the mean steady wing incidence were measured. This provided the correct geometric incidence which included the deformation of the balance.

The vibration modes were measured with five Endevco 2220 C accelerometers of the piezo-electric type (range: up to 10E4 m/s^2) and with four Kulite GY-155 accelerometers of the piezo-resistive type (range: up to 500 m/s^2).

Three types of pressure transducers were used:

- 10 Endevco 8507-5
- 12 Kulite CQL-080-5D
- 20 Kulite XCS-093-5D

These transducers were mounted in such a way that they were electrically isolated, free of local model deformation and not influenced by the model accelerations. They were divided over four strategically chosen sections:

- a spanwise section on the strake to obtain data in the conical flow region for the verification of conical flow phenomena (10 pressure transducers at $x/cr = 0.4042$),
- a spanwise section just behind the kink to show the development of the leading edge wing vortex starting from the kink (18 pressure transducers at $x/cr = 0.6588$),
- a spanwise section at the rear part of the main wing for measurement of buffet phenomena (8 pressure transducers at $x/cr = 0.9682$),
- a chordwise section at the main wing panel to show the development of vortex burst as a function of incidence (8 pressure transducers at $2y/b = 0.4000$).

The sensitivity of the pressure transducers shows a small variation with temperature. By measuring the temperature of the model with a Unicurve thermistor, UUT 45J1, the correct sensitivity of the pressure transducers could be applied.

2.4 Model excitation

Excitation was provided by an electro-hydraulic shaker system, designed by Keelavite Hydraulics Ltd. It consists of a hydraulic power supply, a combined linear actuator and servovalve and a feedback control unit (see Ref. 5). The hydraulic actuator could deliver a maximum static force of 13000 N and a dynamic force of 8000 N at a total piston stroke of 35 mm at low frequencies to 16 mm at 16 Hz.

The hydraulic actuator was suspended in a box which was bolted rigidly to the turntable. The piston was connected to a crank which converted the linear motion into a rotational motion. By the driving rod this motion was transmitted to the yoke, which supported one side of the balance. On the other side of the balance the model was clamped. During most of the runs the model was forced into a sinusoidal motion. In a limited number of runs, a (1-cos) motion was used.

2.5 Equipment for measurement of overall loads and pressures

The windtunnel tests were performed using a computer controlled multi-channel transfer function analyzer, called PHAROS (Processor for Harmonic Analysis of the Response of Oscillating Surfaces). A description of this system is given in reference 6. The system is capable of analyzing the incoming data from 48 channels simultaneously. By means of a switch panel this process was conducted twice at each test point so that 96 different signals could be recorded.

In figure 7 a block-diagram of the test setup is shown, including the PHAROS system. The two-phase oscillator of PHAROS controlled the hydraulic actuator, which provided the model excitation. The response signals of the instrumentation were acquired by PHAROS for analysis. The electrical signals were fed through conditioners into transfer function analyzers to obtain the mean component and the real and imaginary parts of the harmonic components. These data were then stored on a disc of the computer and a quick-look analysis was made. The analysis of each test run was performed in about 3 minutes, including plots and tables of all measured quantities (see also section 4.1). Thus, immediate access to detailed preliminary pressure and force data was possible during the test.

2.6 Equipment for flow visualization

In figure 8 a schematic overview is given of the visualization test setup. On the left-hand side a top view is shown of the windtunnel test section with the windtunnel model and the flow visualization equipment beside it. The smoke tube underneath the strake injected smoke into the flow in upstream direction near the stagnation point. In this way the smoke, mixed with air, was sucked into the vortices over the model. By means of a 5 Watt argon ion laser and a cylindrical lens, a light screen was formed which was perpendicular to the model reference plane when the model was placed at its mean incidence. The flow patterns were made visible by the light scattered by the smoke particles in the light sheet which is shown in the figure at the right.

In order to record the flow characteristics at fixed phase angles with respect to the model motion, a chopped laser light screen was used. By means of an acousto-optic modulator the laser light screen was made intermittant. The modulator was controlled by a special device developed at NLR, which generated electronic pulses in phase with the same digital oscillator signal that controlled the model motion. The pulse signal was then converted into an amplitude-modulated high frequency signal by a driver which excited the acousto-optic modulator. When no modulation was applied, the laser beam was interrupted by a mirror and reflected to a black absorber. In case of 100% modulation tne modulator deflected the laser beam about 6 mRad. After that the beam passed the interrupt mirror and was led into the optical parts, including a cylindrical lens, to produce the light screen.

The optical elements could be rotated about the optical axis to place the light screen perpendicular to the wing, when the model was at mean incidence. At a distance of 2.50 m downstream of the rotation axis of the model an Olympus OM4 (35mm SLR) photocamera was installed with its optical axis in the symmetry plane at the same level as the rotation axis of the model. Photographs were taken by remote control with a 250 filmback and a 100 mm lens. The photographs were taken to determine the vortex core position at different phase angles of the model motion.

To enable the study of phenomena like vortex burst, also video recordings were made with a Charged Coupled Device (CCD) camera, positioned beside the tunnel wall.

3 PREPARATORY TESTS

The model was supported by a structure consisting of several struts (see Fig. 4). To estimate the interference with the flow, steady measurements were performed in a separate preparatory test with the model suspended by wires to an overhead balance system (see Ref. 7). Support interference corrections were derived, which were applied later in postprocessing the results of the main test. In the results of this preparatory test as presented in reference 7, the pitching moment is affected by the drag of the wires, which yield an additional pitching moment. Only the force in the wire attached to the front of the model is used to derive the correct pitching moment as presented in appendix C.

In a separate test (Ref. 8), the vibration modes of the model (on the balance) and the support system were measured. All resonance frequencies were far beyond the highest excitation frequency in the test program (see table 2). Therefore, the influence of elastic deformations of model and support mechanism was negligible.

Another preparatory test was carried out to determine the optimal position of the smoke tube with respect to the model. Use was made of an oscillating dummy model with an adjustable smoke tube. A steady laser light screen was applied. The test was performed in a small windtunnel at the Delft University of Technology, Department of Aerospace Engineering. In this test the optimal conditions for the smoke generation were also investigated (see Ref. 4). The same dummy model was used in a later windtunnel test in which the equipment and procedures for the unsteady flow visualization were tested.

4 PROCEDURES

4.1 Measurement of overall loads and pressure distributions

4.1.1 Transfer functions

The main objective of these measurements was to determine the transfer functions between the mechanical motion of the model as input and the pressures and overall loads as output. By using the PHAROS system (see section 2.5), the zeroth and first harmonics of the measured signals were obtained and stored on the discs of the PHAROS computer. Next, the data

of the balance were corrected for inertial and gravitational loads, according to the method of appendix B. All quantities were normalized with the response of the displacement transducer for the model motion. Then a quick-look printout of all measured quantities was produced on-line in tables and plots. The complete procedure of data acquisition and presentation required about 3 minutes for each test run.

After the windtunnel test the final data reduction of these harmonic data was made on the HP21/MXE computer of the PHAROS system. The aerodynamic quantities obtained after each test run were:

- one chordwise and three spanwise distributions of the mean steady pressure coefficients (Cp)m
- one chordwise and three spanwise distributions of the unsteady pressure coefficients Re(Cp) and Im(Cp), normalized with the angular displacement of the wing derived from the output of the LVDT
- zeroth and first harmonics of force and moment coefficients, measured with the NLR 635 balance, again normalized as mentioned above
- amplitudes and displacements, derived from accelerometer signals normalized as mentioned above.

4.1.2 Time recordings

Time recordings of pressures and overall loads were also made to enable the study of:

- higher harmonics in case of strong nonlinearities
- power spectra in case of vortex burst and strong flow separation effects
- cross-correlation functions in space and time when following the development of vortex burst and boundary layer separation.

In the processing of the recordings of the overall loads to time history plots of overall aerodynamic coefficients, the procedure indicated in appendix B is used.

4.2 Incidence, blockage and dynamic pressure distribution

4.2.1 Incidence

In this windtunnel test, a very large range of incidences and amplitudes was covered. Although the output of the LVDT was proportional with its elongation, the elongation itself varied nonlinearly with the inci-

dence. During the experiment this nonlinear relationship was not yet determined and a preliminary relationship between output of the LVDT and incidence and amplitude was used. For that reason these preliminary adjusted values (αa and $d\alpha a$ are presented in the tables which give an overview of the test program (tables 4 to 12). However, in the postprocessing the nonlinearity was taken into account and the correct geometric incidence (αg) and amplitude ($d\alpha$) were obtained. These values (measured by the LVDT) were not influenced by the deformation of the balance. Next, additional corrections to αg were applied to enable comparison to free-flight conditions, as the incidence was affected by the presence of the support system and the windtunnel walls. First a zero-lift correction was applied to correct for the influence of the support system. This correction (-0.05 deg) is the difference in incidence at zero lift, between the steady tests in wires (see Ref. 7) and the steady tests on the strut support. In both tests the wing model was equipped with wire suspension blocks. Secondly an upwash correction according the method of references 9 and 10 was applied to take into account the influence of the tunnel walls.

4.2.2 Blockage

Due to the presence of the model in the test section, the effective dynamic pressure is increased by so-called "blockage" effects. The solid blockage can be neglected, due to the small volume of the model. The wake blockage is primarily caused by the flow separation (bluff body drag) and can be estimated from the lift vs. drag curve according to the method of references 9, 10 and 11.

During the windtunnel test the lift vs. drag curve, determined previously for the model suspended by wires (see Ref. 7), was used to adjust the tunnel speed in such a way that the dynamic pressure, corrected for blockage effects, was almost independent of the incidence. In the postprocessing, correction for the blockage effect is done on basis of the lift vs. drag curve as measured during the steady part of the test with the model on the struts.

4.2.3 Dynamic pressure distribution

In order to get some information of the dynamic pressure distribution around the model in relation to the dynamic pressure, measured by the tunnel reference system, some dynamic pressures were measured for zero-lift conditions. The pressures were measured in a plane normal to the longitudinal test section axis (y'-z' plane) at the position of the pitching axis of the model. The pressures measured by the tunnel reference system were corrected to values in the empty test section. The dynamic pressures measured by the pitot static tube, divided by the dynamic pressure in the empty test section (Qref) are given in table 3 and figure 9. These data were intended for possible future investigations, but were not used in this report.

4.3 Flow visualization

In figure 10 the principle of the chopped laser light screen technique is shown. The upper part of the figure shows the time history of the model motion and the lower part shows the time history of the light pulses which generate the laser light screen. The phase difference between model motion and light pulses could be varied over the entire period of 360 deg. The pulse duration could be varied between 1 and 8 deg.

For recording vortex position data, the Olympus OM 4 still photo camera was used (see figure 8) with Kodak Tri-X as film, upgraded to 1600 ASA.

As the light screen was present only during a fraction of the cycle (2.2 % maximum), several pulses were needed for one exposure. Consequently the quality of the photographs was strongly influenced by the model motion during the light pulses (depending on pitch rate and pulse width), and the time-averaging effect, i.e. the number of pulses needed for one exposure. This was not a serious drawback. In a preparatory test (see section 3), the photographs taken were very suitable for the purpose of determining vortex core positions at different phase angles of the model motion.

For qualitative dynamic information the CCD video camera was used. Although this camera has a smaller resolution than the photocamera, a complete picture could be generated from each light pulse, due to the high sensitivity.

5 TEST PROGRAM

5.1 Overall loads and pressure measurements

5.1.1 Steady tests

The steady tests, performed at zero sideslip and at a velocity of 80 m/s, covered an angle of attack range of -8 to 50 deg. To enable comparison with the steady test of the model suspended by wires (see Ref. 7), steady tests were performed with the model supported by the struts, both with and without wire suspension blocks mounted in the wings. The effect of the wire suspension blocks had to be examined to determine their effect on the zero lift correction (see section 4.2.1).

A survey of the steady test program, including the run numbers, is shown in table 4.

5.1.2 Unsteady tests

The unsteady tests covered a wide range of incidences (-8 to 50 deg), frequencies (1 to 16 Hz) and amplitudes (1 to 16 deg). Most of the pressure and load measurements were performed at 80 m/s windspeed, zero sideslip and at harmonic oscillation, with reduced frequencies based on the root semi-chord up to 0.5. A survey of this part of the unsteady testprogram, including the runnumbers, is shown in table 5.

The influence of the windspeed was studied by repeating a number of runs at 30 m/s (same windspeed as in the visualization runs) and 55 m/s (see tables 6 and 7). The frequencies were adjusted at the same time to correspond with the reduced frequencies as applied in the 80 m/s runs. At 80 m/s also runs with sideslip were performed (see tables 8 and 9).

In all runs with harmonic oscillation, the zeroth and first harmonic components of the pressures and overall loads were measured, and time recordings were made. A survey of the runnumbers for which time histories of the pressure distributions are presented is given in table 10. Table 11 presents a survey of the runnumbers for which time history plots of the overall loads at harmonic oscillation are presented. In this table the components of the balance and the corresponding power spectral density plots with their plotnumbers are indicated. In total, about 1000 runs with harmonic oscillation were performed.

In the results of the steady measurements (see figure 11) some characteristic incidence ranges can be distinguished:

up to 9 deg: attached ("linear") flow
9 to 19 deg: fully developed vortex flow
19 to 36 deg: vortex burst extending from trailing edge
beyond 36 deg: vortex burst penetrating the strake, almost fully stalled flow.

Special emphasis was placed on incidences which marked transition of the flow characteristics, or were typical for the flow characteristics in some incidence range. These actual incidences were 9, 19, 22, 36 and 42 deg, which correspond to the adjusted incidences referred to in the tables (αa = 8, 18, 22, 38, 46 deg). At these incidences a dense grid of amplitude and frequency values was measured.

5.2 Load measurements at (1-cos) inputs

This part of the test program consisted only of unsteady runs in which a (1-cos) signal was used as input, to simulate maneuvers. Time history recordings were made of the response signals of the six components of the balance, using the model motion signal as a reference.

The adjusted incidence (αa) at the start of the input is varied from 8 to 46 deg. The duration of the (1-cos) inputs is varied from 0.083 to 0.500 s, the magnitude of the wing incidence variation was 8, 16, 24 and 32 deg. A survey of the test program, including the runnumbers, is presented in table 12. At the same test conditions, also the first half (increasing incidence) and second half (decreasing incidence) were performed separately, with some time in between to allow the flow to stabilize.

5.3 Flow visualization experiments

The intention of the flow visualization program was to obtain information about the flow over the upper side of the model. This was done at the five characteristic incidences, mentioned in section 5.1.2, both by photographs and video recordings as described in sections 2.6 and 4.3 at a low windspeed (30 m/s) to obtain good smoke visualization. A survey of the test conditions is given in table 13 a through c.

During the visualization tests the phase angle of the pulsation with respect to the model motion was varied over a complete cycle in steps of

45 deg. At three chord positions, corresponding with the location of the pressure transducers, at five incidences, amplitudes and reduced frequencies corresponding with the 80 m/s runs, the smoke patterns in the light screen were registered on photofilm to determine the positions of the vortex cores, as well as on video, to obtain qualitative data of the dynamic flow phenomenae. Over 1200 cases were completed.

6 PRESENTATION OF RESULTS

The presentation of the test results is given in six parts of the report. The present part, part I, contains some examples of the test data and surveys of all testruns. Some general figures, derived from the test are also given.

Parts II and III present the plots of the zeroth and first order harmonic components of the pressure distributions for the runs as presented in the tables 4 through 9 in this part. In part III the zeroth and first order harmonic components of the overall loads, plotted vs. incidence, amplitude and frequency are also presented. The printed values have also been included on microfiche. All harmonic data are available on magnetic computer tape in order to enable easy data handling. The corresponding formats are given in table 14. Table 15 gives an example of a print of a steady test run and table 16 of an unsteady test run as presented on microfiche. The test conditions have been listed on the right-hand side in the upper table. The steady and unsteady pressures of the four sections are given as pressure coefficients together with their sectional coordinates. The overall forces and moments, obtained from the balance are presented as steady and unsteady aerodynamic coefficients. The sign definitions of the body-fixed coordinate system are given in figure 1. The corresponding pressure plots are shown in figures 12 and 13. The displacements derived from the accelerometers are presented both relative to LVDT 2 and in absolute form. LVDT 2 is the transducer in the model, whereas LVDT 1 is the transducer in the hydraulic actuator. When the pressure transducers or the accelerometers did not operate properly the values were not presented. In the next chapter more attention will be given to these harmonic data.

Part IV presents the plots of the time recordings of pressures and overall loads for the runs with harmonic excitation. A survey of the run-

numbers for which these pressure plots are presented in part IV is given in table 10 of this part and an example of such a time recording for the four sections and the eight phase angles is presented in figure 14. Table 11 presents a survey of the runnumbers for which the time histories of the overall loads are plotted; an example of the overall loads vs. incidence, derived from the time recordings of the balance signals is given in figure 15.

Part V presents a selection of the power spectral density plots of the overall loads at harmonic excitation, corresponding with the time history plots of the overall loads as presented in part IV (runnumbers, component and plotnumbers are presented in table 11 of this part). The responses of the overall loads to (1-cos) input signals (runnumbers presented in table 12) are also presented. An example of such a time history is given in figure 16.

Part VI presents the results of the flow visualization by prints as well as plots of the variation of the vortex core positions during a cycle of the model motion at various incidences, amplitudes and frequencies. This part presents some selected cases in tables 17 through 22, which will be discussed further in section 7.3. The corresponding photographs and plots of the measured positions of the vortex cores for the 8 phase angles are presented in figures 31 to 43. When measurement of the vortex core positions was impossible no values were presented in prints and plots. The photographs for the eight phase angles at the aft light-sheet position, x/c = 96.82 %, are also included. Although it was impossible to measure the core positions in many of these photos, they still provide substantial qualitative information about the flow phenomena under these conditions. Some plots (figures 44, 45) are also enclosed in this part to demonstrate the influence of amplitude and frequency on the time history of the vortex core position.

7 BRIEF DISCUSSION OF SOME RESULTS

In this chapter a selection of windtunnel test data is discussed. A summary description was also given in reference 12 and a preliminary analysis of harmonic data is presented in reference 13.

7.1 Overall loads

The variation of the steady normal force coefficient and the moment coefficient with incidence is shown in figure 11. The different types of flow are also indicated. Up to about 9 deg, a linear variation of CN and Cm with incidence is observed. Beyond 9 deg the slopes increase due to the development of vortex flows over both the strake and wing. At about 19 deg incidence, vortex burst starts at the wing trailing edge. Suction at the aft part of the wing is diminished, while suction on the front part still increases due to the increase of the strength of the strake vortex. Beyond 19 deg incidence, the vortex burst moves upstream, however, both CN and Cm still increase, though, at a smaller rate than before. At about 36 deg the increase of suction at the upstream part of the wing due to increasing incidence and the drop of suction at the downstream part of the wing due to the growth of the vortex burst region, counterbalance eachother which leads to maximum values of CN and Cm. Beyond 36 deg the flow over the entire wing and strake collapses rapidly into an almost completely separated flow.

The effects observed in the steady plots are also reflected in the unsteady plots. This is demonstrated in the figures 17 and 18. A very distinct change in the unsteady pitching moment coefficient is observed at about 19 deg (onset of vortex burst) and at 36 deg where the phase angle of the unsteady pitching moment changes about 180 deg. The effect of frequency on the first harmonic components of the pitching moment coefficient is shown in figure 19.

Figure 20 shows the real part of the first harmonic of the pitching moment coefficient vs. frequency for several amplitudes. At the selected incidence of $\alpha = 18.9$ deg Re(Cm) is independent of the frequency (this corresponds with the upper part of figure 19) but does depend on the amplitude. This amplitude dependence is very well organized at this incidence. Both frequency dependence and amplitude dependence show up in the imaginary part of the first harmonic of the pitching moment coefficient (see figure 21).

The results of the three force coefficients vs. amplitude are shown in the figures 22 through 24.

In figure 22 the zeroth harmonic and the real part of the first order harmonic component of the normal force coefficient is presented versus amplitude at $\alpha = 18.9$ deg and $f = 3$ Hz. At this low frequency Re(CN) decreases with amplitude at the higher amplitudes, as can be expected from the steady CN versus α curve, presented in figure 11.

Figure 23 shows the zeroth harmonic of the side force coefficient vs. amplitude for 3 frequencies at $\alpha = 35.9$ deg and $\beta = 5.0$ deg. The range used as vertical axis of the graph is less than 1 % of the total range of the balance (also see section 8.1), however, a good distinction can be made between curves for various frequencies. Figure 24 shows the zeroth harmonic of the tangential force coefficient vs. amplitude for 2 frequencies at 18.9 deg incidence. The effect of the frequency results in a shift of $(C_T)_m$ while the shape remains the same.

Figure 25 shows the effect of sideslip on the unsteady yawing moment coefficient. In the plot all measured amplitude frequency combinations for one particular incidence are shown. The trends for only one amplitude frequency combination are indicated in the figure. A similar treatment is shown in figure 26 for the effect of sideslip on the first harmonic of the rolling moment coefficient. In the left part of the figure the frequency is kept constant and the amplitude is varied, while in the right part the amplitude is constant and the frequency is varied.

7.2 Pressure distribution

Positioning of the transducers was very appropriate for understanding the complex flow phenomena that were encountered in this investigation. Thus, based on consideration of the steady and unsteady pressure distribution, it was possible to make the flow field observations that were described in section 7.1.

During the experiment, the zeroth and first harmonic components of the pressure distribution were presented. After postprocessing, which included correction for blockage effects and determination of the correct incidence, the same presentation was used again. Figure 12 shows an example of the pressure coefficients of a steady test run and figure 13 shows the same for an unsteady test run. In figure 27 an overview is given of the development of the steady pressure distribution with incidence. The chosen incidences are the ones which are selected for the flow visualization program. In section 1 the presence of the strake vortex is indicated by position of the strake vortex at about 45 % and the wing vortex at about 80 % of the local semi-span. Up to about 19 deg the pressures grow with incidence. At incidences greater than about 19 degrees the effect of the wing vortex on the pressure distribution decreases. Beyond an incidence of 36 deg the wing vortices have disappeared due to flow separation, while beyond 42 deg the strake vortices have also disappeared.

At the trailing edge section 3 shows the effect of vortex burst. Section 4 shows the pressure distribution of the chordwise section with its characteristic suction peak on the nose. At incidences greater than about 36 deg trailing edge separation occurs, while at incidences greater than about 42 deg flow separation on the nose occurs.

By combining plots of unsteady runs, one can easily get good insight into the influence of the different parameters: figure 28 shows the influence of incidence and figure 29 shows the influence of amplitude on the pressure distribution at section 2.

An impression of the contribution of the higher harmonics can be obtained from the tape recordings by time history plots (see figure 14) or spectra. As another example, figure 30 shows the time history of the pressure distribution at section 2 for the flow condition as presented at 6.98 deg amplitude in figure 29. The pressure signal at the suction peak, which can be associated with the wing vortex (80 % local semi-span), shows a nonlinear behaviour, which is expressed in a significant second harmonic component in the spectra.

7.3 Vortex core positions

In this section examples of the time history of the unsteady flow are presented in figures 31 through 43. Flow patterns have been photographed for eight phase angles at three spanwise sections and in these photographs the positions of the vortex cores have been determined as shown in the figures.

At the strake section (x/cr = 40.42 %) one test condition was chosen: α = 18.94 deg, $d\alpha$ = 3.58 deg, f = 1.88 Hz. The photographs of this case are shown in figure 31 and the measured positions of the cores are presented in table 17 and figure 32. The spanwise position of the vortex core, depending on the phase angle, is situated at about 70%, which corresponds to the steady pressure distribution at section 1 in figure 27(3). At these test conditions a stable vortex flow exists at this section.

At the section just behind the kink (x/cr = 65.88 %) five test conditions were chosen. Not only the strake vortex, but also the wing vortex is present in this section. The situation in figures 33 and 34 is rather straight forward. At an incidence α = 18.93 deg and an amplitude of $d\alpha$ = 6.93 deg we still have stable vortex flow during the cycle. Because it was attempted to optimize the smoke conditions for the wing vortex, the core positions of the strake vortices were overexposed and could not

always be measured (see table 18). The spanwise coordinate of the wing vortex cores (~ 80 %) corresponds with the position of the pressure peak in section 2 in the figures 27 and 28. In the figures 35, 36 and 37, 38 the incidence and frequency are the same, but a different amplitude is used. Plotting the nondimensionalized z-position of the vortex cores versus phase angle (see figure 44) shows that the distance of the vortex cores from the model increases with the amplitude. The vortex flow at the left side breaks up at the higher amplitude at a phase angle of $\varphi = 90$ deg (see figure 37). In these situations such smoke conditions were created that the vortex core positions could be determined for both the strake vortex and the wing vortex (see tables 19 and 20). In the test conditions corresponding to the figures 37 through 42 the same incidence and about the same amplitude were maintained, but 3 different frequencies were used. In figure 45 the nondimensionalized z-position is plotted versus phase angle. There seems to be a phase shift between the measurements at 1.13 Hz and 6 Hz, but the measurements at 3 Hz mystify the picture. Also an increasing frequency seems to postpone the vortex burst (see the photographs at the phase angles $\varphi = 90$ and $\varphi = 135$ degrees). The determined positions are presented in the tables 20 to 22.

At the trailing edge section (x/cr = 96.82 %) as shown in figure 43 the flow changes from burst vortices at $\varphi = 0$ degrees to fully separated flow at a phase angle of 90 degrees, and to stable vortex flow at 270 degrees phase angle.

8 FINAL COMMENTS

8.1 Deformation and accuracy of the balance

For computer code evaluation, accurate overall loads are indispensable. A balance is used for this purpose, although it will be a weak element in the support of the model. The balance signals will also be affected by inertia loads. In this test the resonance frequencies of the support system (including the balance) were far beyond the highest excitation frequency. Subsequently, the influence of these vibration modes on the model motion were negligible. Due to the small inertia properties of the model and the low test frequencies, inertia loads were small, hence by measuring the model motion, corrections for inertia loads were made by using wing model mass properties. In this way, overall loads will be

obtained which are expected to be more accurate than airloads obtained by integration of a large number of pressures, measured at the model surface, especially when large pressure gradients occur.

The maximum forces and moments which can be measured with the NLR 635 balance are mentioned in section 2.3. Assuming that the balance can measure accurately at less than 1% of its total range, the nondimensionalized force and moment coefficients can be calculated corresponding to a 1% load. Comparing these values to the measured values, it can be concluded that the ranges of all symmetrical components conform to the acting loads upon the balance. However the loads of the asymmetrical components are acting in the lower 10% of the total range. Nevertheless it can be said that the accuracy of the measurements will be better than 1% of their total range.

8.2 Instrumentation

Just before the test period, transducer 3 of the 42 pressure transducers was found unusable in both steady and unsteady measurements. The transducers 6, 27 and 42 were unusable in the steady measurements and the transducers 29 and 37 in the unsteady measurements. The measured values of these transducers were not presented in the print out and plots. This presentation was also used with the transducers which were unreliable or failed during the tests. The transducers in pressure section 1 on the strake were highly susceptible to failure as a consequence of the high acceleration levels encountered in this section.

Accelerometers 5 and 6 gave very poor signals before the test period and were not presented in any run. Furthermore only the results with accelerometers 1, 7 and 8 seemed reliable. The other accelerometers were not reliable in all cases, which can be seen in the last column of the LVDT/-Accelerometer table in the print out, in which the calculated amplitude divided by the measured amplitude is presented.

Two of the supporting struts were used as conduits for the instrumentation wiring. To minimize loads on the balance due to the instrumentation wiring sufficient slack was provided between the supporting struts and model.

8.3 Backlash in wing support bearings

During the windtunnel test all signals could be monitored on an oscilloscope. By monitoring the LVDT signal, an increase in backlash in the bearings of the wing support could be detected, in which case the bearings could be adjusted and the backlash removed.

8.4 Visualization

During the visualization at the three spanwise sections a large number of photographs was taken with the aim to measure the positions of the vortex cores. This was not possible in all cases; especially for section 2 (just behind the kink) it was not always possible to inject the right amount of smoke in both vortex systems. When more smoke was injected, the wing vortices could be photographed correctly, but the strake vortices were overexposed; when less smoke was injected the wing vortices could not be detected on the photographs. At the third section, the vortices were burst in many of the tests and only qualitative information could be obtained from the photographs.

The video recordings also provided much qualitative information of the flow, especially at vortex burst, because no time averaging over several light pulses was needed for proper exposure.

8.5 The effect of the wire suspension blocks

In one of the preparatory tests as discussed in chapter 3, measurements were carried out on the model suspended by wires (see Ref. 7). This was done in order to make an estimate of the interference of the model support system used in the test described in this report. To be able to attach the wires in the preparatory test, special wire suspension blocks had to be installed in the model. In figure 46 the effect of the wire suspension blocks on the lift and drag curves for the model on the strut support is presented. The graphs with and without wire suspension blocks are presented next to each other because placing the two curves in one figure shows no difference. Therefore the effect of the wire suspension blocks can be neglected in the zero lift correction as described in section 4.2.1.

9 CONCLUDING REMARKS

The aims, mentioned in section 1 have been achieved.

- A large data base of both overall forces and moments as well as pressure distributions has been created. It is expected that this data base will be useful for the evaluation of advanced computer codes for the determination of unsteady aerodynamic quantities for conditions at high angles of attack.
- From photographs quantitative information about the vortex core positions is made available to better understand the unsteady vortex flow.
- Video and photograph registrations made during this experiment will contribute significantly to enlarge the physical insight into both steady and unsteady vortex flow phenomena.

10 REFERENCES

1	Boersen, S.J. Elsenaar, A.	The international vortex flow experiment, a test case for compressible Euler code evaluation. NLR MP 86076 U (1986)
2	Kannemans, H.	Laser-light sheet visualization and in field total pressure measurements in steady vortex flow over delta and double delta wings. NLR TR 83057 L (1983)
3	Horsten, J.J.	Design of the GD/NLR straked wing model and support system. Memorandum AE-85-005 U (1985)
4	Persoon, A.J. Retel, A.P.	Some experiments with flow visualization of vortices over a vibrating straked wing. Memorandum AE-86-001 L (1986)
5	Poestkoke, R.	Hydraulic test rig for oscillating wind tunnel models. NLR MP 76020 U (1976)

6	Fuykschot, P.H.	PHAROS, Processor for Harmonic Analysis of the Response of Oscillating Surfaces". NLR MP 77012 U (1977)
7	de Vries, O.	Force measurements in a low speed windtunnel on a model of a straked wing, suspended in wires. NLR TR 86047 C (1986)
8	den Boer, R.G. Persoon, A.J.	Vibration test of the GD/NLR straked wing model and support mechanism. Memorandum AE-85-014 U (1985)
9	Maskell, E.C.	A theory of blockage effects on bluff bodies and stalled wings in a closed windtunnel. RAE Report No.Aero 2685 (Nov.1963)
10	Garner, H.C. Rogers, E.W.E. Acum, W.E.A. Maskell, E.C.	Subsonic wind tunnel wall correction. AGARDograph 109 (1966)
11	Vayssaire, J.C.	Correction de blockage dans les essais en soufflerie effects des decollements. AGARD-CP-102
12	den Boer, R.G. Cunningham, A.M.	A windtunnel investigation of low speed of the flow about a straked delta wing, oscillating in pitch. AIAA paper 87-2493. Atmospheric Flight Mechanics Conference, Monterrey, August 17-19, 1987
13	Cunningham, A.M. den Boer, R.G.	Harmonic analysis of force and pressure data results for an oscillating straked wing at high angles. AIAA paper 87-2494. Atmospheric Flight Mechanics Conference, Monterrey, August 17-19, 1987

TABLE 1

Positions of pressure transducers and accelerometers (x 100 %), see figure 5

PRESSURE TRANSDUCERS

sec	no	x/c	2y/b
I	1	40.42	6.81
	2	40.42	20.43
	3	40.42	34.06
	4	40.42	47.68
	5	40.42	54.48
	6	40.42	61.29
	7	40.42	68.10
	8	40.42	74.92
	9	40.42	81.73
	10	40.42	88.54
II	11	65.88	13.11
	12	65.88	26.00
	13	65.88	32.44
	14	65.88	38.89
	15	65.88	42.93
	16	65.88	46.93
	17	65.88	50.98
	18	65.88	55.02
	19	65.88	59.02
	20	65.88	63.07
	21	65.88	67.07
	22	65.88	71.11
	23	65.88	75.56
	24	65.88	80.00
	25	65.88	84.44
	26	65.88	88.89
	27	65.88	93.33
	28	65.88	97.78

sec	no	x/c	2y/b
III	29	96.82	20.00
	30	96.82	30.00
	31	96.82	40.00
	32	96.82	50.00
	33	96.82	60.00
	34	96.82	70.00
	35	96.82	80.00
	36	96.82	90.00
IV	37	5.72	40.00
	22	16.61	40.00
	38	29.21	40.00
	39	41.82	40.00
	40	54.42	40.00
	41	67.02	40.00
	42	79.62	40.00
	31	92.22	40.00

SECTION	c	b/2
I	785.5	79.16
II	785.5	225.0
III	785.5	400.0
IV	321.38	400.0

ACCELEROMETERS b/2 = 400.0 mm

no	x/cr	2y/b
1	82.75	86.25
2	92.94	86.25
3	82.75	-86.25
4	92.94	-86.25
5	92.94	-37.50
6	93.70	0.00
7	46.72	0.00
8	21.26	0.00
9	62.38	-37.50

TABLE 2

Vibration modes with corresponding frequencies of the installed model

mode number	freq.	type
1	38.66	roll
2	45.36	roll + pitch
3	53.03	pitch
4	111.87	model bending
5	31.97	yaw
6	80.03	Y-displacement on support

TABLE 3

Dynamic pressure distribution (model at zero lift)

y' (mm)	z' (mm)	Qpitot/Qref
200.0	50.0	1.0627
100.2	50.0	1.0830
0.1	50.0	1.1006
-99.9	50.0	1.0796
-199.5	50.0	1.0572
-300.0	50.0	1.0344
-400.0	50.0	1.0155
-500.0	50.0	1.0102
199.7	150.6	1.0281
99.9	150.6	1.0354
0.0	150.6	1.0384
-100.1	150.6	1.0338
-200.2	150.6	1.0265
-300.0	150.6	1.0175
-400.6	150.6	1.0117
-500.6	150.6	1.0080
199.9	249.2	1.0158
100.1	249.2	1.0187
0.1	249.2	1.0193
-100.0	249.2	1.0176
-200.0	249.2	1.0153
-300.0	249.2	1.0116
-400.2	249.2	1.0090
-500.4	249.2	1.0068
0.0	450.0	1.0078
0.0	450.0	1.0077
-149.6	-50.0	1.2146
-200.0	-50.0	1.1416
-300.0	-50.0	1.0736
-400.0	-50.0	1.0290
-499.7	-50.0	1.0168
-600.1	-50.0	1.0115

TABLE 4

Steady test program (β = 0 deg, V ~ 80 m/s)

V = 80 m/s
β = 0 deg

α_a	RUN NR.
-10	3
-8	4
-6	5
-4	6-23
-2	7
0	8-9
2	10
4	11-62
6	12
8	13-63
10	14-24
12	15-64
14	16
16	17-65
18	18
20	19-25-27-34
20	55-66-72-73
22	20-28-35
24	21-29-36-67
26	22-30-37
28	38-68
30	39
32	40-69-74
34	41
36	42-70
38	43-54-56
40	44-53-57-71
42	45-58
44	46
46	47
48	48
50	49
52	50
54	51
55	52-59

without wire suspension blocks

α_a	RUN NR.
4	1060
8	1061
12	1063
14	1064
16	1065
18	1066
20	1067
22	1068
26	1069
30	1070
34	1071
36	1072
38	1073
40	1074

with wire suspension blocks

TABLE 5
Unsteady test program (β = 0 deg, V ~ 80 m/s)

V = 80 m/s
β = 0 deg

α_a	f	$d\alpha_a$								
		2	4	6	8	10	12	14	16	18
-4	3	430	431							
	5	432	433							
	8	434	435							
	12	436								
-4	16	437								
0	3	438	439		440					
	5	441	442		443					
	8	444	445		446					
	12	447								
0	16	448								
4	3	449	450		451		452			
	5	453	454		455		456			
	8	457	458		459					
	12	460								
4	16	461								
8	3	462	463 1033		464 1034		465		466 1035	
	5	467	468 1036		469 1037		470		471 1040	
	8	472	473 1041		474 1042					
	12	475								
8	16	476 1043								

TABLE 5 (cont'd)

V = 80 m/s
β = 0 deg

α_a	f	$d\alpha_a$ 2	4	6	8	10	12	14	16	18
12	2		76		77					
	3	477	478 479		479 498		480			
	5	481	482 499		483 500		484			
	8	485	486 501		487 502					
	12	488 503								
12	16	489 504								
16	2	78	79	80	81	82	83			
	3	84 490	85 491	86	87 492	88	89			
	4	90	91	92	93	94	95			
	5	97 493	98 494	99	100 495	101	102			
	8	496 505	506	507	508					
	12	509								
16	16	510								
18	2	103	104 951	105	106 952	107	108	109 953		
	3	110	111 984	112	113 985	114	115	116 986		
	4	117	118 954	119	120 955	121	122	123 956		
	5	124	125 987	126	127 988	128	129	130 989		

TABLE 5 (cont'd)

V = 80 m/s
β = 0 deg

α_a	f	$d\alpha_a$ 2	4	6	8	10	12	14	16	18
	8	511	512 957	513	514 958					
	12	515								
18	16	516 959								
20	2	131	132 960	133	134 961	135	136	137	138 962	
	3	139	140	141	142	143	144	145	146	
	4	147	148 963	149	150 964	151	152	153	154 965	
	5	155	156	157	158	159	160	161	162	
	8	517	518 966	519	520 967					
	12	521								
20	16	522 968								
22	2	173	172 969	174	175 970	176	177	178	179 971	180
	3	181	182 978	183	184 979	185	186	187	188 980	189
	4	190	191 972	192	193 973	194	195	196	197 974	198
	5	199	200 981	201	202 982	203	204	205	206 983	207
	6	523	524	525	526	527	528			
	8	529	530 975	531	532 976					
	10	533	534							
	12	535								
22	16	536 977								

TABLE 5 (cont'd)

V = 80 m/s
β = 0 deg

α_a	f	$d\alpha_a$								
		2	4	6	8	10	12	14	16	18
24	2	208	209	210	211	212	213	214	215	
	5	216	217	218	219	220	221	222	223	
	8	537	538	539	540					
	12	541								
24	16	542								
26	3	224	225 425	226	227	228	229	230		
	5	231	233	234	235	236	237	238		
	8	543	544	545	546					
	12	547								
26	16	548								
28	3	239	240 426	241	242	243	244			
	5	245	246	247	248	249	250			
	8	549	550	551	552					
	12	553								
28	16	554								
30	3	251	252 265 427	253	254 266	255				
	5	256	257 267	258	259 268	260				
	8	555 567	556	557 569	558					
	12	559 570								
30	16	560 571								

TABLE 5 (cont'd)

V = 80 m/s
β = 0 deg

α_a	f	$d\alpha_a$								
		2	4	6	8	10	12	14	16	18
32	3	269	261 270 428	271	262 272	273	274			
	5	275	263 276	277	264 278	279	280			
	8	561 572	562 573	563	564 574					
	12	565 575 576								
32	16	566								
34	3	281	282	283	284	285	286	287		
	5	288	289	290	291	292	294	295		
	8	577	578	579	580					
	12	581								
34	16	582								
36	3	296	297	298	299	300	301	302	303	
	5	304	305	306	307	308	309	310	311	
	8	583	584	585	586					
	12	587								
36	16	588								
38	2	314	315	316	317	318	319	320	321	
	3	322	323 1044	324	325 1045	326	327	328	329 1046	
	4	330	331	332	333	334	335	336	337	
	5	338 719	339 720 1047	340 721 1048	341 722	342 723	343 724	344 725	346 726 1049	

TABLE 5 (cont'd)

V = 80 m/s
β = 0 deg

α_a	f	$d\alpha_a$ 2	4	6	8	10	12	14	16	18
	6	590 656	591 657	592 658	593 659	594 660				
	8	589 661	595 662 1050	596 663	597 664 1051					
	10	665	599 666							
	12	598 600 677								
38	16	601 668 1052								
40	3	367	368	369	370	371	372	373		
	5	374	375	376	377	378	379	380		
	8	602	603	604	605					
	12	606								
40	16	608								
42	3	381	382	383	384	385	386			
	5	387	388	389	390	391	392			
	8	609	610	611	612					
	12	613								
42	16	615								
44	3	393	394	395	396	397				
	5	398	399	400	401	402				
	8	616	617	618	619					
	12	620								
44	16	621								

TABLE 5 (cont'd)

$\bar{V}$ = 80 m/s
β = 0 deg

α_a	f	$d\alpha_a$								
		2	4	6	8	10	12	14	16	18
46*	3	403 653	404 655 1053	405	406 1054					
	5	407	408 1055	409	410 1056					
	8	623 669	624 670 1057	625 671	626 672 1058					
	12	627 673								
46	16	628 674 1059								
48	3	411	412	413						
	5	414	415	416						
	8	629	630	631						
	12	632								
48	16	633								
50	3	417	418							
	5	419	420							
	8	634	635							
	12	636								
50	16	637								
52	3	422								
	5	421								
	8	638								
	12	639								
52	16	640								

*	α_a	f	$d\alpha_a$
RUN 651:	46	3	0.1
RUN 652:	46	3	1
RUN 654:	46	3	3

TABLE 5 (concluded)

V = 80 m/s
β = 0 deg

α_a	f	$d\alpha_a$								
		2	4	6	8	10	12	14	16	18
54	3	423 (1°)								
	5	424 (1°)								
	8	641 (1°)								
	12	642 (1°)								
54	16	643 (1°)								

TABLE 6
Unsteady test program (β = 0 deg, V ~ 55 m/s)

V = 55 m/s
β = 0 deg

α_a	f	$d\alpha_a$								
		2	4	6	8	10	12	14	16	18
8	2.06		790		791				792	
	3.44		793		794				795	
	5.50		796		797					
8	11.0		798							
16	2.06		832		833		834			
	3.44		835		836		837			
	5.50		838		839					
16	11.0	840								
18	2.06		841		842			843		
	3.44		844		845			846		
	5.50		847		848					
18	11.0	849 859								
20	2.06		850		851				852	
	3.44		853		854				855	
	5.50	858	856		857					
20	11.0	860								
22	2.06		861		862				863	
	3.44		864		865				866	
	5.50		867		868					
22	11.0	883								

TABLE 6 (cont'd)

$V = 55$ m/s
$\beta = 0$ deg

α_a	f	$d\alpha_a$ 2	4	6	8	10	12	14	16	18
24	2.06		874		875				876	
	3.44		877		878				879	
	5.50		880		881					
24	11.0	882								
36	2.06		675		676				677	
	3.44		678		679				680	
	5.50		681		682					
36	11.0	683								
38	2.06		684		685				686	
	3.44		687		688				689	
	5.0	718								
	5.50		690		691					
38	11.0	692								
42	2.06		693		694				695	
	3.44		696		697		698			
	5.50		699		700					
42	11.0	701								
44	2.06		702		703	704				
	3.44		705		706	707				
	5.50		708		709					
44	11.0	710								

TABLE 6 (concluded)

$V = 55$ m/s
$\beta = 0$ deg

α_a	f	$d\alpha_a$								
		2	4	6	8	10	12	14	16	18
46	2.06		711		712					
	3.44		713		714					
	5.50		715		716					
46	11.0		717							

TABLE 7
Unsteady test program (β = 0 deg, V ~ 30 m/s)

V = 30 m/s
β = 0 deg

α_a	f	$d\alpha_a$ 2	4	6	8	10	12	14	16	18
8	1.13		819		820				821	
	1.88		822		823				824	
	3.0		825		826				827	
	6.0	828	829		830					
8	12.0	831								
18	1.13		897		898			899		
	1.88		900		901			902		
	3.0		903		904			905		
	6.0	906	907		908					
18	12.0	909								
22	1.13		884		885				886	
	1.88		887		888				889	
	3.0		890		891				892	
	6.0	893	894		895					
22	12.0	896								
38	1.13		727		728				729	
	1.88		730		731				732	
	3.0		733		734				735	
	6.0	736	737		738					
38	12.0	739								

TABLE 7 (concluded)

$V = 30$ m/s $\beta = 0$ deg

α_a	f	$d\alpha_a$								
		2	4	6	8	10	12	14	16	18
46	1.13		741		742					
	1.88		743		744					
	3.0		745		746					
	6.0	747	748		749					
46	12.0	750								

TABLE 8
Unsteady test program (β = +5 deg, V ~ 80 m/s)

V = 80 m/s
β = 5 deg

α_a	f	$d\alpha_a$								
		2	4	6	8	10	12	14	16	18
8	3		799		800				801	
	5		802		803				804	
	8	806	805		807					
8	16	808								
18	3		941		942			943		
	5		944		945			946		
	8	947	948		949					
18	16	950								
22	3		911		912				913	
	5		914		915				916	
	8	917	918		919					
22	16	920								
38	2		751		752				753	
	3		754		755				756	
	5		757		758				759	
	8	760	761		762					
38	16	763								
46	3		782		783					
	5		784		785					
	8	786	787		788					
46	16	789								

TABLE 9
Unsteady test program (β = -5 deg, V ~ 80 m/s)

V = 80 m/s
β = -5 deg

α_a	f	$d\alpha_a$ 2	4	6	8	10	12	14	16	18
8	3		809		810				811	
	5		812		813				814	
	8	815	816		817					
8	16	818								
18	3		931		932			933		
	5		934		935			936		
	8	937	938		939					
18	16	940								
22	3		921		922				923	
	5		924		925				926	
	8	927	928		929					
22	16	930								
38	3		764		765				766	
	5		767		768				769	
	8	770	771		772					
38	16	773								
46	3		774		775					
	5		776		777					
	8	778	779		780					
46	16	781								

TABLE 10
Runnumbers for which plots are presented of time histories of the pressure distributions

V = 80 m/s
β = 0 deg

α_a	f	$d\alpha_a$ = 2	4	6	8	10	12	14	16	18
8	3		1033		1034				1035	
	5		1036		1037				1040	
	8		1041		1042					
8	16	1043								
18	2				952			953		
	3				985			986		
	4		954		955					
	5		987		988			989		
	8		957		958					
18	16	959								
20	2		960		961			962		
	4		963		964			965		
	8		966		967					
20	16	968								
22	2		969		970			971		
	3		978		979			980		
	4		972		973			974		
	5		981		982			983		
	8		975		976					
22	16	977								

TABLE 10 (concluded)

V = 80 m/s
β = 0 deg

α_a	f	$d\alpha_a$								
		2	4	6	8	10	12	14	16	18
38	3		1044		1045			1046		
	5		1047		1048			1049		
	8		1050		1051					
38	16	1052								
46	3		1053		1054					
	5		1055		1056					
	8		1057		1058					
46	16	1059								

TABLE 11a
Runnumbers and corresponding plotnumbers of time histories and power spectral densities of overall loads at harmonic oscillation ($V \approx 80$ m/s, $\beta = 0$ deg)

$V = 80$ m/s
$\beta = 0$ deg

α_a	f	$d\alpha_a$ = 8	12	16	18
0	3	440 -			
	5	443 -			
	8	446 -			
4	3	451 -	452 -		
	5	455 -	456 -		
	8	459 -			
8	3	464 -	465 -	466 -	
	5	469 -	470 -	471 -	
	8	474 -			
12	3	479 m 3202	480 N 3204 m 3203		
	5	483 m 3207	484 m 3208		
	8	487 m 3211			
16	3	87 -	89 -		
	5	100 -	102 -		
18	3	113 N 1108	115 m 1109		
	5	127 -	129 -		
	8	514 N 3244 m 3243			
20	3	142 -	144 -	146 -	
	5	158 -	160 -	162 m 1112	
	8	520 N 3256 m 3255			

TABLE 11a (cont'd)

V = 80 m/s
β = 0 deg

α_a	f	$d\alpha_a$ 8	12	16	18
22	3	184 m 1125	186 m 1127	188 m 1129	189 m 1130
	5	202 m 1143	204 m 1145	206 m 1147	207 m 1148
	8	532 m 3270			
24	3	211 m 1152	213 m 1154	215 m 1156	
	5	219 m 1160	221 m 1162	223 m 1164	
	8	540 m 4104			
26	3	227 m 1168	229 m 1170		
	5	235 -	237 m 1202		
	8	546 N 4111 m 4110			
28	3	242 m 1207	244 m 1209		
	5	248 m 1213	250 m 1215		
	8	552 m 4117			
30	3	254 m 1218			
	5	259 m 1223			
	8	558 m 4123			
32	3	262 m 1226	274 N 1243 m 1242		
	5	264 m 1228	280 N 1255 m 1254		
	8	564 m 4129			

TABLE 11a (concluded)

V = 80 m/s
β = 0 deg

α_a	f	$d\alpha_a$ 8	12	16	18
34	3		286 N 1267 m 1266		
	5	291 N 2103 m 2102	294 -		
	8	580 N 4150 m 4149			
36	3	299 N 2117 m 2116	301 N 2121 m 2120		
	5	307 N 2133 m 2132	309 N 2137 m 2136		
	8	586 N 4162 m 4161			
38	3	325 N 2165 m 2164	327 N 2169 m 2168	329 N 2173 m 2172	
	5	341 N 2222 m 2221	343 N 2226 m 2225	346 N 2232 m 2231	
	8	597 N 5116 m 5115			
40	3	370 -	372 -		
	5	377 -	379 -		
	8	605 N 5132			
42	3	384 N 2268 m 2267	386 N 2272 m 2271		
	5	390 N 3106 m 3105	392 N 3110 m 3109		
	8	612 -			
44	3	396 N 3118 m 3117			
	5	401 N 3128 m 3127			
	8	619 N 5156 1 5157 m 5155			
46	3	406 N 3138 m 3137			
	5	410 N 3146 m 3145			
	8	626 N 5169 m 5168			

TABLE 11b
Runnumbers and corresponding plotnumbers of time histories and power spectral densities of overall loads at harmonic oscillation (V ~ 80 m/s, β = 5 deg)

V = 80 m/s β = 5 deg

α_a	f	$d\alpha_a$ 8	12	16	18
8	3	800 N 7105 1 7106 m 7104		801 N 7108 1 7109 m 7107	
	5	803 N 7114 1 7115 m 7113		804 N 7116 1 7117	
	8	807 N 7125 1 7126 m 7124			
18	3	942 N 8103 1 8104 m 8102			
	5	945 N 8112 1 8113 m 8111			
	8	949 N 8124 1 8125 m 8123			
22	3	912 N 7163 1 7164 m 7162		913 N 7166 1 7167 m 7165	
	5	915 N 7172 1 7173 m 7171		916 1 7201 m 7174	
	8	919 N 7209 1 7210 m 7208			
38	3	755 N 5241 1 5242 m 5240		756 N 5244 1 5245 m 5243	
	5	758 N 5250 1 5251 m 5249		759 N 5253 1 5254 m 5252	
	8	762 N 5262 1 5263 m 5261			
46	3	783 N 6252 1 6253 m 6251			
	5	785 N 6258 1 6259 m 6257			
	8	788 N 6267 1 6268 m 6266			

TABLE 11c

Runnumbers and corresponding plotnumbers of time histories and power spectral densities of overall loads at harmonic oscillation (V ~ 80 m/s, β = -5 deg)

V = 80 m/s
β = -5 deg

α_a	f	$d\alpha_a$ 8	12	16	18
8	3	810 N 7134 l 7135 m 7133		811 N 7137 l 7138 m 7136	
	5	813 N 7143 l 7144 m 7142		814 N 7146 l 7147 m 7145	
	8	817 N 7154 l 7155 m 7153			
18	3	932 N 7248 l 7249 m 7247			
	5	935 N 7257 l 7258 m 7256			
	8	939 N 7269 l 7270 m 7268			
22	3	922 N 7218 l 7219 m 7217		923 N 7221 l 7222 m 7220	
	5	925 N 7227 l 7228 m 7226		926 N 7230 l 7231 m 7229	
	8	929 N 7239 l 7240 m 7238			
38	3	765 N 5271 l 5272 m 5270		766 N 5274 l 6201 m 5273	
	5	768 N 6206 l 6207 m 6205		769 N 6209 l 6210 m 6208	
	8	772 N 6218 m 6217			
46	3	775 N 6226 l 6227 m 6225			
	5	777 N 6234 l 6235 m 6233			
	8	780 N 6243 l 6244 m 6242			

TABLE 12

Unsteady test program ((1-cos) inputs)

(β = 0 deg, V ~ 80 m/s)

V = 80 m/s
β = 0 deg

α_a	T	$d\alpha_a$								
		4	8	12	16	20	24	28	32	36
8	0.500		3047		3053		3058		3062	
	0.330		3048		3054		3059		3063	
	0.250		3049		3055		3060		3064	
	0.200		3050		3056		3061		3065	
	0.125		3051		3057					
8	0.083		3052							
16	0.500						3066			
	0.333						3067			
	0.250						3068			
16	0.200						3069			
22	0.500		3013		3019		3024		3028	
	0.330		3014		3020		3025		3029	
	0.250		3015		3021		3026		3030	
	0.200		3016		3022		3027		3031	
	0.125		3017		3023					
22	0.083		3018							
24	0.500				3070					
	0.330				3071					
	0.250				3072					
	0.200				3073					
24	0.125				3074					

TABLE 12 (concluded)

$V = 80$ m/s
$\beta = 0$ deg

α_a	T	$d\alpha_a$								
		4	8	12	16	20	24	28	32	36
30	0.500						3032			
	0.333						3033			
	0.250						3034			
30	0.200						3035			
32	0.500		3075							
	0.333		3076							
	0.250		3077							
	0.200		3078							
	0.125		3079							
32	0.083		3080							
38	0.500				3036					
	0.333				3037					
	0.250				3038					
	0.200				3039					
38	0.125				3040					
46	0.500		3041							
	0.333		3042							
	0.250		3043							
	0.200		3044							
	0.125		3045							
46	0.083		3046							

TABLE 13a

Visualization test program (photographs) at x/cr = 40.42

x/c = 40.42 %
V = 30 m/s
β = 0 deg

α	dα	f	table part VI
9.98	4.04	1.13	1
9.87	8.11	1.13	2
9.28	16.59	1.13	3
10.01	3.78	1.88	4
9.91	7.60	1.88	-
9.38	15.51	1.88	5
10.00	3.74	3.0	6
9.88	7.47	3.0	7
9.42	15.23	3.0	8
10.00	3.68	6.0	9
9.88	7.36	6.0	-
18.96	3.82	1.13	-
18.92	7.65	1.13	10
18.78	13.50	1.13	11
18.94	3.58	1.88	12
18.93	7.15	1.88	13
18.79	12.63	1.88	14
18.97	3.54	3.0	-
18.92	7.07	3.0	-
18.83	12.42	3.0	-
18.98	3.46	6.0	-
18.93	6.93	6.0	-
22.45	3.79	1.13	-
22.41	7.57	1.13	-
22.29	15.19	1.13	-
22.46	3.54	1.88	-
22.42	7.09	1.88	-
22.29	14.24	1.88	-
22.44	3.51	3.0	15
22.42	6.98	3.0	16
22.28	14.00	3.0	17
22.50	3.44	6.0	18
22.42	6.88	6.0	19

α	dα	f	table part VI
35.84	3.73	1.13	20
35.89	7.48	1.13	21
36.03	15.23	1.13	22
35.84	3.51	1.88	-
35.87	7.02	1.88	23
36.01	14.26	1.88	24
35.86	3.44	3.0	25
35.87	6.93	3.0	26
36.02	14.03	3.0	-
35.86	3.37	6.0	27
35.85	6.79	6.0	-
42.32	3.90	1.13	-
42.39	7.80	1.13	-
42.29	3.66	1.88	-
42.39	7.33	1.88	-
42.30	3.61	3.0	-
42.38	7.42	3.0	-
42.31	3.51	6.0	-
42.40	7.09	6.0	-

TABLE 13b
Visualization test program (photographs) at x/cr = 65.88

x/c = 65.88 %
V = 30 m/s
β = 0 deg

α	dα	f	table part VI
9.98	4.04	1.13	28
9.87	8.11	1.13	29
9.28	16.59	1.13	30
10.01	3.78	1.88	31
9.91	7.60	1.88	32
9.38	15.51	1.88	33
10.00	3.74	3.0	34
9.88	7.47	3.0	35
9.42	15.23	3.0	36
10.00	3.68	6.0	37
9.88	7.36	6.0	38
18.96	3.82	1.13	39
18.92	7.65	1.13	40
18.78	13.50	1.13	41
18.94	3.58	1.88	42
18.93	7.15	1.88	43
18.79	12.63	1.88	44
18.97	3.54	3.0	45
18.92	7.07	3.0	46
18.83	12.42	3.0	47
18.98	3.46	6.0	48
18.93	6.93	6.0	49
22.45	3.79	1.13	50
22.41	7.57	1.13	51
22.29	15.19	1.13	52
22.46	3.54	1.88	53
22.42	7.09	1.88	54
22.29	14.24	1.88	55
22.44	3.51	3.0	56
22.42	6.98	3.0	57
22.28	14.00	3.0	58
22.50	3.44	6.0	59
22.42	6.88	6.0	60

α	dα	f	table part VI
35.84	3.73	1.13	-
35.89	7.48	1.13	-
36.03	15.23	1.13	61
35.84	3.51	1.88	-
35.87	7.02	1.88	-
36.01	14.26	1.88	-
35.86	3.44	3.0	-
35.87	6.93	3.0	-
36.02	14.03	3.0	62
35.86	3.37	6.0	-
35.85	6.79	6.0	-
42.32	3.90	1.13	-
42.39	7.80	1.13	-
42.29	3.66	1.88	-
42.39	7.33	1.88	-
42.30	3.61	3.0	-
42.38	7.42	3.0	-
42.31	3.51	6.0	-
42.40	7.09	6.0	-

TABLE 13c
Visualization test program (photographs) at x/cr = 96.82

x/c = 96.82 %
V = 30 m/s
β = 0 deg

α	dα	f	table part VI
9.98	4.04	1.13	-
9.87	8.11	1.13	-
9.28	16.59	1.13	-
10.01	3.78	1.88	63
9.91	7.60	1.88	64
9.38	15.51	1.88	-
10.00	3.74	3.0	-
9.88	7.47	3.0	-
9.42	15.23	3.0	-
10.00	3.68	6.0	-
9.88	7.36	6.0	65
18.96	3.82	1.13	-
18.92	7.65	1.13	-
18.78	13.50	1.13	-
18.94	3.58	1.88	-
18.93	7.15	1.88	-
18.79	12.63	1.88	-
18.97	3.54	3.0	-
18.92	7.07	3.0	-
18.83	12.42	3.0	-
18.98	3.46	6.0	-
18.93	6.93	6.0	-
22.45	3.79	1.13	-
22.41	7.57	1.13	-
22.29	15.19	1.13	-
22.46	3.54	1.88	-
22.42	7.09	1.88	-
22.29	14.24	1.88	-
22.44	3.51	3.0	-
22.42	6.98	3.0	-
22.28	14.00	3.0	-
22.50	3.44	6.0	-
22.42	6.88	6.0	-

α	dα	f	table part VI
35.84	3.73	1.13	-
35.89	7.48	1.13	-
36.03	15.23	1.13	-
35.84	3.51	1.88	-
35.87	7.02	1.88	-
36.01	14.26	1.88	-
35.86	3.44	3.0	-
35.87	6.93	3.0	-
36.02	14.03	3.0	-
35.86	3.37	6.0	-
35.85	6.79	6.0	-

TABLE 14

File organization on DELTA model tape

DESCRIPTION	FORMAT
RUN,HARM, ALPHA, Re(DALPHA), IM(DALPHA), FREQ, MACH	2I5,5F10.5
VELOCITY,REDFR,Q,ps,T,BETA,S	2F10.5,F10.2,4F10.5
NO,xref,x/xref,yref,y/yref,(Cp)m, Re(Cp), Im(Cp)	44*(I2,7F10.5,/)
(CN)m,Re(CN),Im(CN),(Cn)m,Re(Cn),Im(Cn)	6F(10.5)
(CY)m,Re(CY),Im(CY),(Cm)m,Re(Cm),Im(Cm)	6F(10.5)
(CT)m,Re(CT),Im(CT),(Cl)m,Re(Cl),Im(Cl)	6F(10.5)
NO,xref,x/xref,yref,y/yref,Re(d),Im(d)	9*(I2,6F10.5,/)

N.B. Improper values represented as: 9999.99

TABLE 15
Example of a print of a steady testrun

STRAKED DELTA

RUN : 18

ALPHA = 19.02 deg		Q = 3874.58 Pa	
MACH = .23		pt = 101625. Pa	
VELOCITY = 81.14 m/s		T = 34.95 deg C	
BETA = 0.00 deg			
FREQ = 0.00 Hz		DALPHA= 0.00 deg	
REDFR = 0.00		HARM = 0	

FORCE COEFFICIENTS	(..)m	Re(..)	Im(..)	MOMENT COEFFICIENTS	(..)m	Re(..)	Im(..)
CN	1.100			Cn	.000		
CY	.005			Cm	.068		
CT	-.013			Cl	-.001		

DISPL.	STAT. mm	AMPL. mm	PHASE RELATIVE TO LVDT2 deg	AMPL. RELATIVE TO LVDT2	CALC. AMPL. mm	CALC./MEAS. AMPL.
LVDT1	.366	0.000	0.0	0.00	0.00	0.000
LVDT2	2.647	0.000	0.0	1.00	0.00	0.000
ACC.1						
ACC.2						
ACC.3						
ACC.4						
ACC.5						
ACC.6						
ACC.7						
ACC.8						
ACC.9						

PRESSURE TRANSDUCERS

SECTION 1 x/cr = 0.4042 b/2 = 79.16 mm

NO	LOCAL SPAN perc.	(Cp)m	Re(Cp)	Im(Cp)
1	6.81	-.439		
2	20.43	-.401		
3	34.06			
4	47.68	-1.244		
5	54.40	-1.588		
6	61.29			
7	68.10	1.782		
8	74.92	-1.393		
9	81.73	-1.229		
10	88.54	-1.195		

SECTION 2 x/cr = 0.6583 b/2 = 225.00 mm

NO	LOCAL SPAN perc.	(Cp)m	Re(Cp)	Im(Cp)
11	13.11	-.304		
12	26.00	-.665		
13	32.44	-.873		
14	38.89	-1.321		
15	42.93	-1.763		
16	46.93	-1.868		
17	50.98	1.601		
[illegible]	55.02	1.453		
19	59.02	1.212		
[illegible]	63.07	1.130		
21	67.07	-1.123		
[illegible]	71.11	1.496		
[illegible]	75.56	2.434		
[illegible]	80.00	3.723		
[illegible]	84.44	-2.586		
[illegible]	88.89	2.076		
[illegible]	93.33			
[illegible]	97.78	1.670		

SECTION 3 x/cr = 0.9682 b/2 = 400.00 mm

NO	LOCAL SPAN perc.	(Cp)m	Re(Cp)	Im(Cp)
[illegible]	29.00	.878		
30	30.00	.186		
[illegible]	40.00	.131		
[illegible]	50.85	.956		
33	60.00	-1.500		
34	70.00	-1.011		
35	80.00	-.531		
[illegible]	[illegible]	.360		

PRESSURE TRANSDUCERS

SECTION 4 2y/b = 0.4000 c = 321.38 mm

NO	LOCAL CHORD perc.	(Cp)m	Re Cp	Im Cp
37	5.72	-4.278		
22	16.61	-1.446		
38	29.21	-1.004		
39	41.82	-1.109		
40	54.42	-1.376		
41	67.02	-1.591		
42	79.62			
31	92.22	.181		

TABLE 16
Example of a print of unsteady testruns

STRAKED DELTA

RUN : 929

ALPHA	= 22.42 deg	Q	= 5611.67 Pa
MACH	= .22	pt	= 101900. Pa
VELOCITY	= 77.15 m/s	T	= 41.95 deg C
BETA	= -5.01 deg		
FREQ	= 8.60 Hz	DALPHA=	6.85 deg
REDFR	= .25	HARM	= 1

PRESSURE TRANSDUCERS

NO	LOCAL CHORD perc.	(Cp)m	Re(Cp)	Im(Cp)

SECTION 1 x/cr = 0.4042 b/2 = 77.16 mm

1	6.31			
2	[illegible]			
3	34.86			
4	47.60			
5	54.46	-1.219	-3.525	-.492
6	61.29		3.296	-.600
7	61.10	-1.415	2.994	-.824
8	74.72			
9	81.73	-1.161	-.354	-.853
10	88.54	-1.109	-2.164	-.871

SECTION 2 x/cr = 0.6583 b/2 = 225.00 mm

11	13.11	-.312	-1.036	-.290
12	26.00	-.709	-2.204	-.296
13	32.44	-.594	2.670	.422
14	[illegible]	-.988	2.645	.715
15	42.93	-1.316	3.219	-.955
16	[illegible]	-1.476	-3.628	-1.091
17	[illegible]	-1.538	4.296	-1.022
18	[illegible]	-1.580	5.075	.629
19	59.02	1.546	-5.906	.513
20	[illegible]	1.510	6.532	-.409
21	67.07	-1.484	7.064	-.443
22	71.11	[illegible]	-7.067	-.694
23	75.56	[illegible]	7.336	1.374
24	80.00	-3.095	.959	[illegible]
25	84.44	3.013	2.413	.237
26	88.37	2.031	.565	.150
27	93.35		.182	.244
28	[illegible]	1.713	.021	-.093

SECTION 3 x/cr = 0.9082 b/2 = 400.00 mm

[illegible]	20.00	.021		
[illegible]	30.00	.062	.056	-.209
[illegible]	40.00	.052	1.051	.142
[illegible]	51.00	[illegible]	[illegible]	.987
[illegible]	60.00	[illegible]	[illegible]	.405
[illegible]	70.00	[illegible]	[illegible]	.193
[illegible]	80.00	[illegible]	[illegible]	[illegible]
[illegible]	91.80	[illegible]	[illegible]	.311

FORCE COEFFICIENTS	(..)m	Re(..)	Im(..)	MOMENT COEFFICIENTS	(..)m	Re(..)	Im(..)
CN	1.063	2.430	1.153	Cn	-.003	-.010	.001
CY	.002	-.002	-.015	Cm	.080	.192	-.025
CT	-.008	.079	.085	Cl	.015	-.104	.140

DISPL.	STAT. mm	AMPL. mm	PHASE RELATIVE TO deg	AMPL. LVDT2	CALC. AMPL. mm	CALC./MEAS. AMPL.
LVDT1	.000	1.211	-179.8	1.19	5.97	4.931
LVDT2	3.177	1.018	0.0	1.00	1.02	1.000
ACC.1		7.918	353.0	7.78	8.92	1.127
ACC.2		16.31	359.4	16.03	18.50	1.134
ACC.3		9.309	339.9	9.15	8.92	.958
ACC.4		17.20	29.4	16.90	18.50	1.075
ACC.5						
ACC.6						
ACC.7		27.21	169.2	26.74	24.96	.917
ACC.8		56.56	187.9	55.57	48.91	.865
ACC.9		16.63	189.8	16.34	10.24	.616

PRESSURE TRANSDUCERS

NO	LOCAL CHORD perc.	(Cp)m	Re Cp	Im Cp

SECTION 4 2y/b = 0.4000 c = 321.38 mm

37	5.72	-3.807		
22	16.61	-1.715	-7.869	-.694
38	29.21	-1.275	-6.995	.114
39	41.82	1.382	6.724	.068
40	54.42	1.292	-5.569	-.169
41	67.03	-1.138	2.740	.090
42	79.63		.420	.445
31	92.22	.032	1.051	.142

TABLE 17
Vortex core positions at section 1,
α = 18.94 deg, dα = 3.58 deg, f = 1.88 Hz

TABLE 12	x/c = 40.42 % b/2 = 79.16 mm	ALPHA = 18.94 deg DALPHA = 3.58 deg			FREQ = 1.88 Hz			
	STRAKE VORTEX				WING VORTEX			
	LEFT		RIGHT		LEFT		RIGHT	
PHI	2y/b	2z/b	2y/b	2z/b	2y/b	2z/b	2y/b	2z/b
0	-0.711	0.411	0.721	0.416				
45	-0.710	0.450	0.711	0.452				
90	-0.719	0.454	0.691	0.454				
135	-0.707	0.443	0.705	0.446				
180	-0.709	0.428	0.721	0.437				
225	-0.716	0.402	0.723	0.404				
270	-0.738	0.381	0.721	0.386				
315	-0.710	0.405	0.719	0.405				

TABLE 18
Vortex core positions at section 2,
α = 18.93 deg, dα = 6.93 deg, f = 6 Hz

TABLE 49	x/c = 65.88 % b/2 = 225.00 mm	ALPHA = 18.93 deg DALPHA = 6.93 deg			FREQ = 6.00 Hz			
	STRAKE VORTEX				WING VORTEX			
	LEFT		RIGHT		LEFT		RIGHT	
PHI	2y/b	2z/b	2y/b	2z/b	2y/b	2z/b	2y/b	2z/b
0					-0.782	0.082	0.794	0.092
45					-0.782	0.115	0.793	0.127
90	-0.438	0.250	0.437	0.259	-0.775	0.153	0.805	0.154
135	-0.442	0.251	0.442	0.258	-0.792	0.144	0.814	0.152
180	-0.442	0.229	0.442	0.238				
225	-0.444	0.206	0.443	0.212	-0.813	0.077	0.820	0.085
270	-0.453	0.180			-0.812	0.061	0.824	0.071
315					-0.790	0.062	0.831	0.067

TABLE 19
Vortex core positions at section 2,
α = 22.45 deg, dα = 3.79 deg, f = 1.13 Hz

TABLE 50	x/c = 65.88 % b/2 = 225.00 mm	ALPHA = 22.45 deg DALPHA = 3.79 deg	FREQ = 1.13 Hz					
	STRAKE VORTEX				WING VORTEX			
	LEFT		RIGHT		LEFT		RIGHT	
PHI	2y/b	2z/b	2y/b	2z/b	2y/b	2z/b	2y/b	2z/b
0	-0.444	0.234	0.463	0.244	-0.789	0.132	0.814	0.145
45	-0.443	0.246	0.460	0.251	-0.789	0.148	0.798	0.168
90	-0.439	0.248	0.458	0.254	-0.787	0.157	0.790	0.167
135	0.439	0.237	0.456	0.242	-0.792	0.141	0.790	0.149
180	-0.441	0.229	0.462	0.239	-0.799	0.123	0.814	0.131
225	-0.446	0.222	0.464	0.230	-0.790	0.115	0.822	0.126
270	-0.444	0.216	0.467	0.222	-0.790	0.112	0.818	0.120
315	-0.444	0.223	0.471	0.229	-0.791	0.116	0.821	0.126

TABLE 20
Vortex core positions at section 2,
α = 22.41 deg, dα = 7.57 deg, f = 1.13 Hz

TABLE 51	x/c = 65.88 % b/2 = 225.00 mm	ALPHA = 22.41 deg DALPHA = 7.57 deg	FREQ = 1.13 Hz					
	STRAKE VORTEX				WING VORTEX			
	LEFT		RIGHT		LEFT		RIGHT	
PHI	2y/b	2z/b	2y/b	2z/b	2y/b	2z/b	2y/b	2z/b
0	-0.445	0.224	0.468	0.230	-0.792	0.117	0.822	0.129
45	-0.441	0.247	0.464	0.254	-0.766	0.172	0.788	0.175
90			0.443	0.271	-0.803	0.157		
135			0.452	0.259	-0.795	0.136	0.821	0.136
180	-0.438	0.225	0.463	0.232	-0.787	0.125	0.815	0.130
225	-0.446	0.203	0.467	0.210	-0.799	0.102	0.820	0.114
270	-0.446	0.191	0.468	0.194	-0.793	0.090	0.821	0.108
315	-0.452	0.198	0.470	0.204	-0.796	0.107	0.816	0.114

TABLE 21
Vortex core positions at section 2,
α = 22.42 deg, dα = 6.98 deg, f = 3 Hz

TABLE 57	x/c = 65.88 % ALPHA = 22.42 deg FREQ = 3.00 Hz b/2 = 225.00 mm DALPHA = 6.98 deg							
	STRAKE VORTEX				WING VORTEX			
	LEFT		RIGHT		LEFT		RIGHT	
PHI	2y/b	2z/b	2y/b	2z/b	2y/b	2z/b	2y/b	2z/b
0	-0.458	0.197	0.458	0.207	-0.800	0.105	0.804	0.115
45	-0.447	0.225	0.447	0.232	-0.794	0.142		
90	-0.446	0.247	0.446	0.252	-0.800	0.157		
135			0.449	0.244				
180	-0.442	0.219	0.442	0.226	-0.804	0.112		
225	-0.451	0.188	0.451	0.194	-0.808	0.086	0.816	0.093
270	-0.458	0.165	0.458	0.169	-0.810	0.070	0.809	0.079
315	-0.463	0.170	0.463	0.178	-0.806	0.088	0.804	0.094

TABLE 22
Vortex core positions at section 2 at 22.42 deg
α = 22.42 deg, dα = 6.88 deg, f = 6 Hz

TABLE 60	x/c = 65.88 % ALPHA = 22.42 deg FREQ = 6.00 Hz b/2 = 225.00 mm DALPHA = 6.88 deg							
	STRAKE VORTEX				WING VORTEX			
	LEFT		RIGHT		LEFT		RIGHT	
PHI	2y/b	2z/b	2y/b	2z/b	2y/b	2z/b	2y/b	2z/b
0	-0.469	0.195	0.469	0.205	-0.798	0.128	0.790	0.133
45	-0.457	0.227	0.457	0.235	-0.797	0.150		
90	-0.449	0.251	0.449	0.259				
135	-0.449	0.269	0.449	0.269				
180	-0.448	0.239	0.448	0.250				
225	-0.446	0.210	0.446	0.221				
270	-0.456	0.189	0.456	0.197	-0.824	0.085		
315	-0.466	0.179	0.466	0.188	-0.812	0.104	0.811	0.113

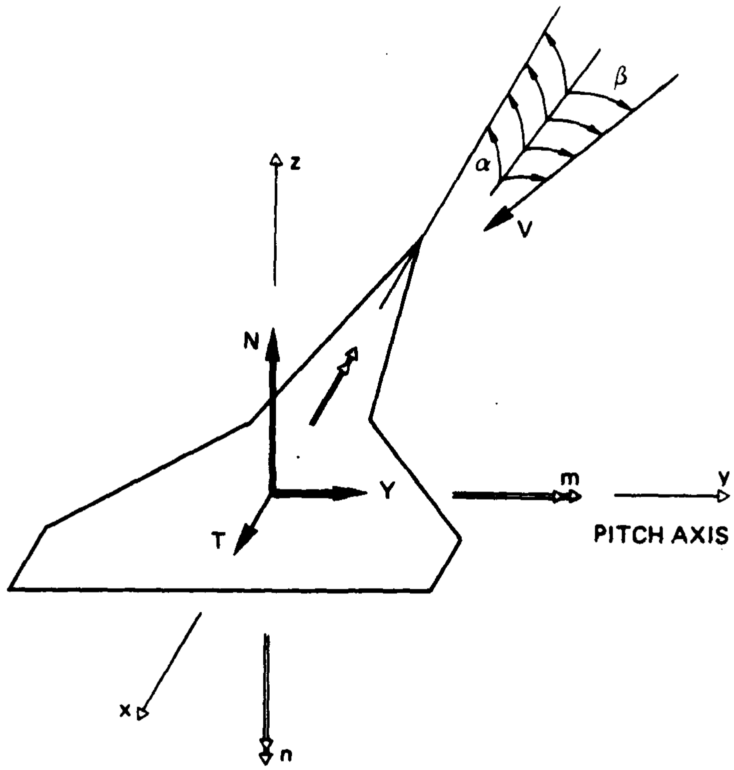

Fig. 1 Body fixed coordinate system

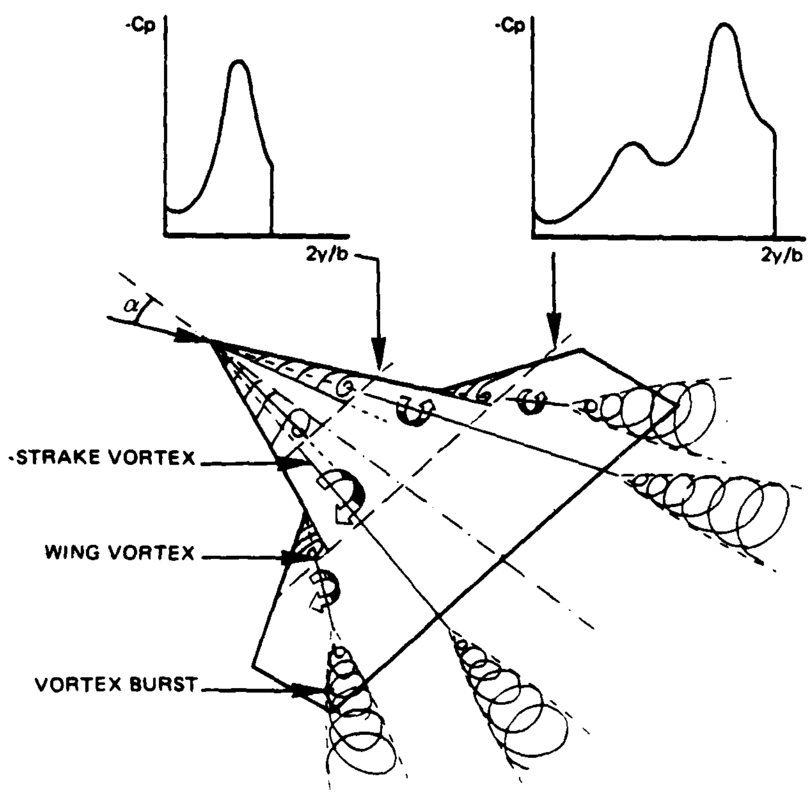

Fig. 2 The flow about a straked delta wing under incidence

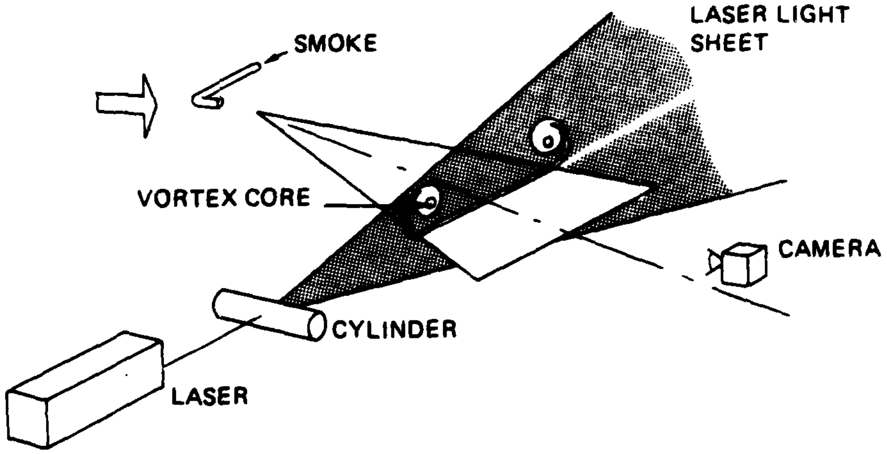

Fig. 3 Principle of laser light screen technique

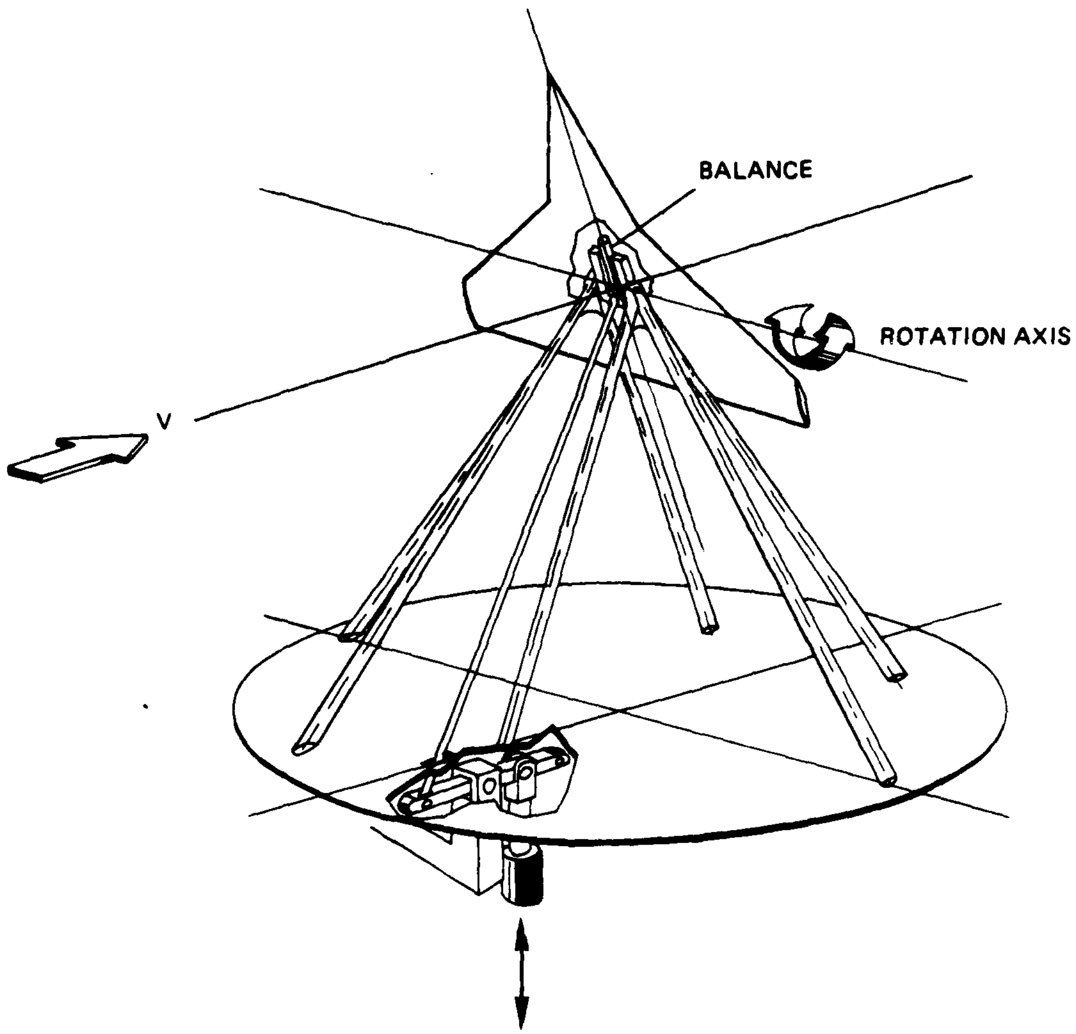

Fig. 4 Principle of the support mechanism

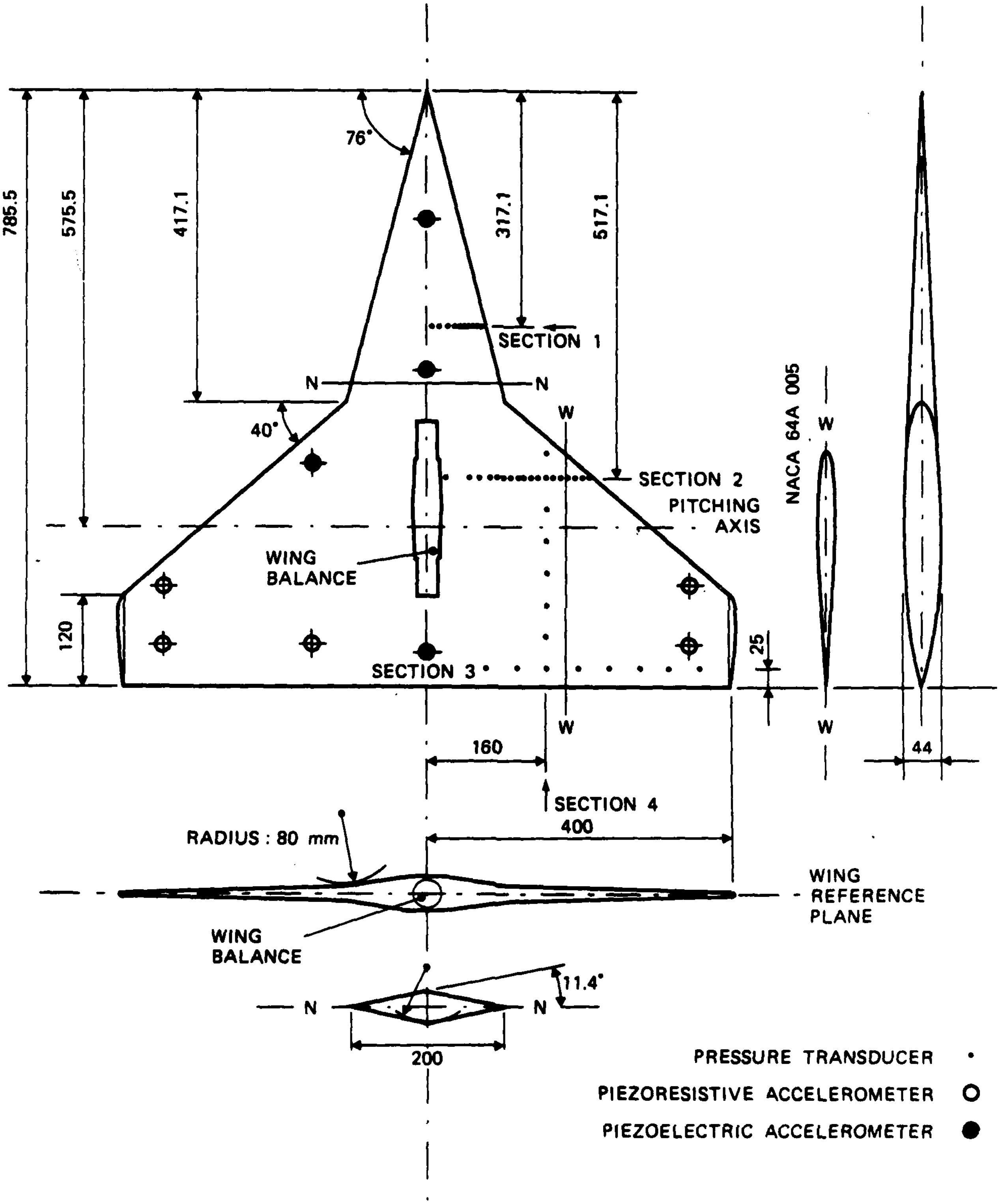

Fig. 5 Wing planform and model instrumentation
(dimensions in mm; pitching axis x/cr = 73.27 %)

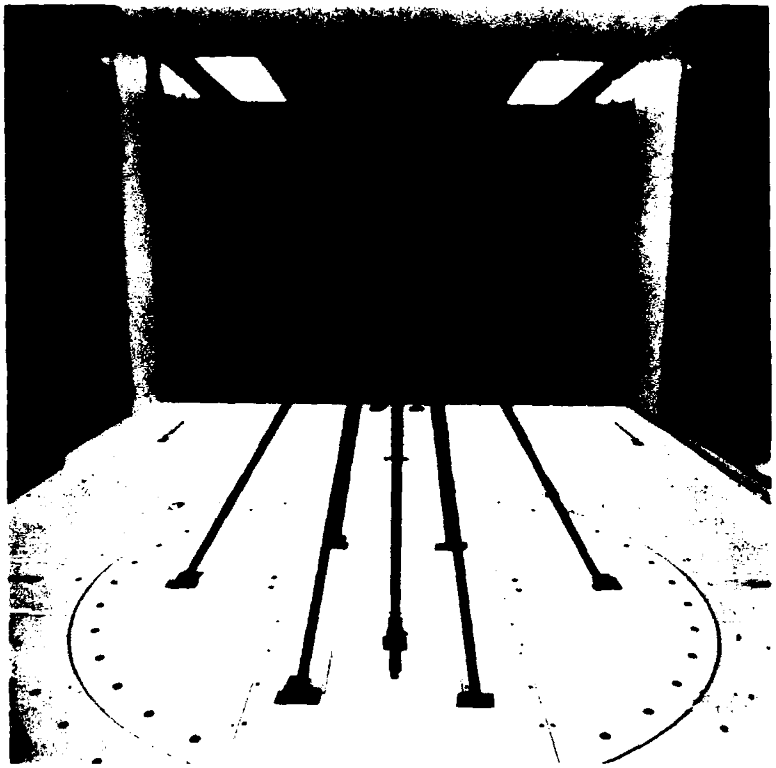

Fig. 6a Frontview of the model and the support mechanism
(pressure measurement configuration).

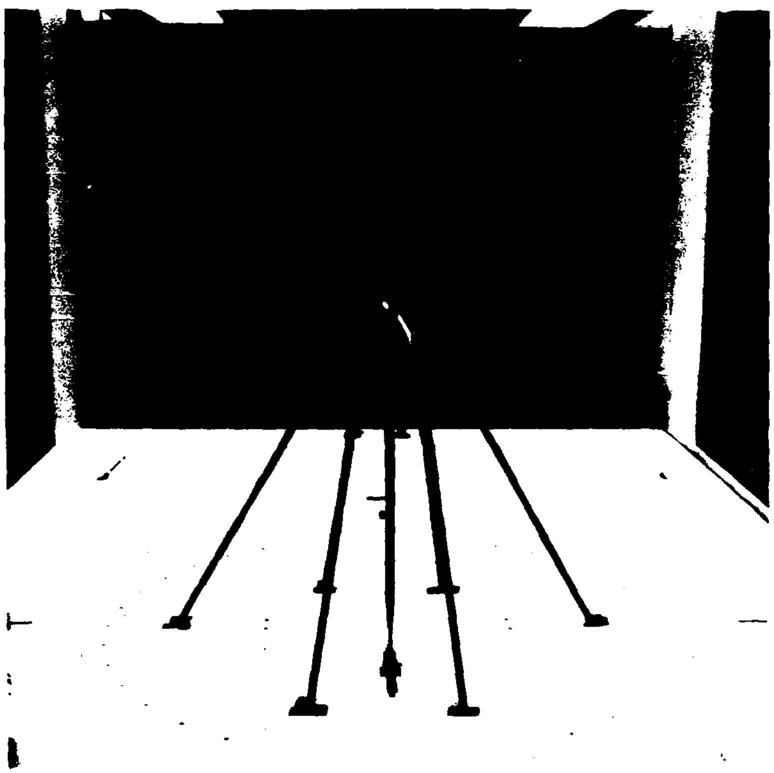

Fig. 6b Frontview of the model and the support mechanism
(visualization study configuration).

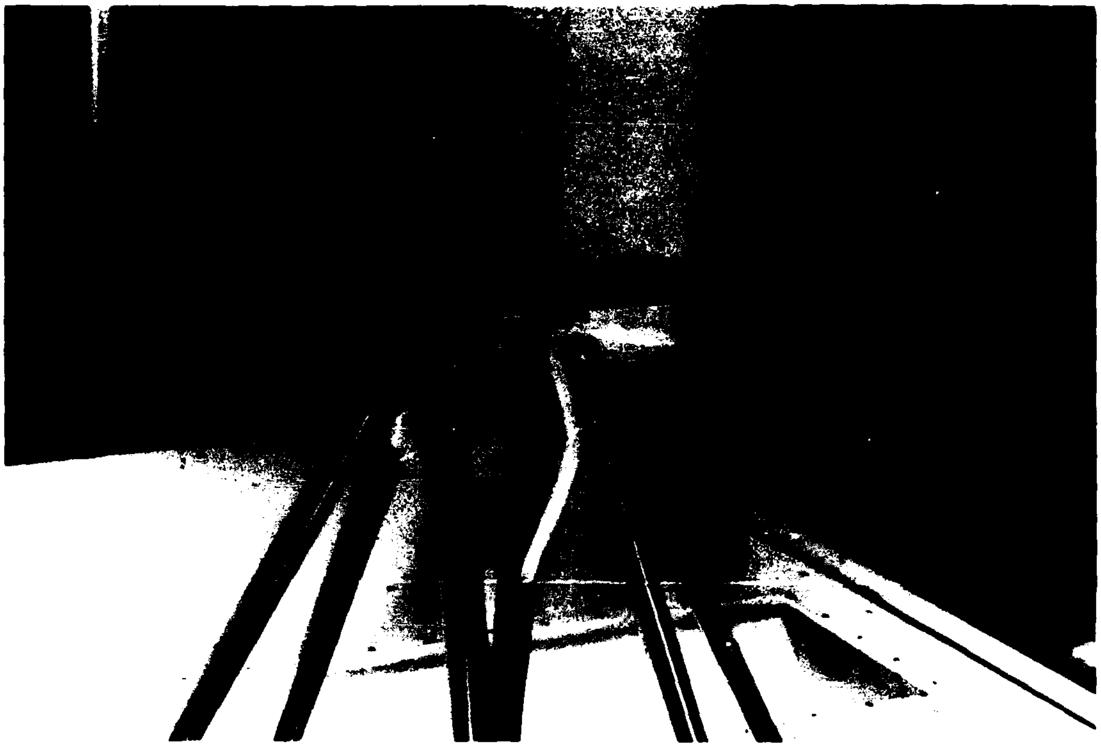

Fig. 6c Smoke tube attachment.

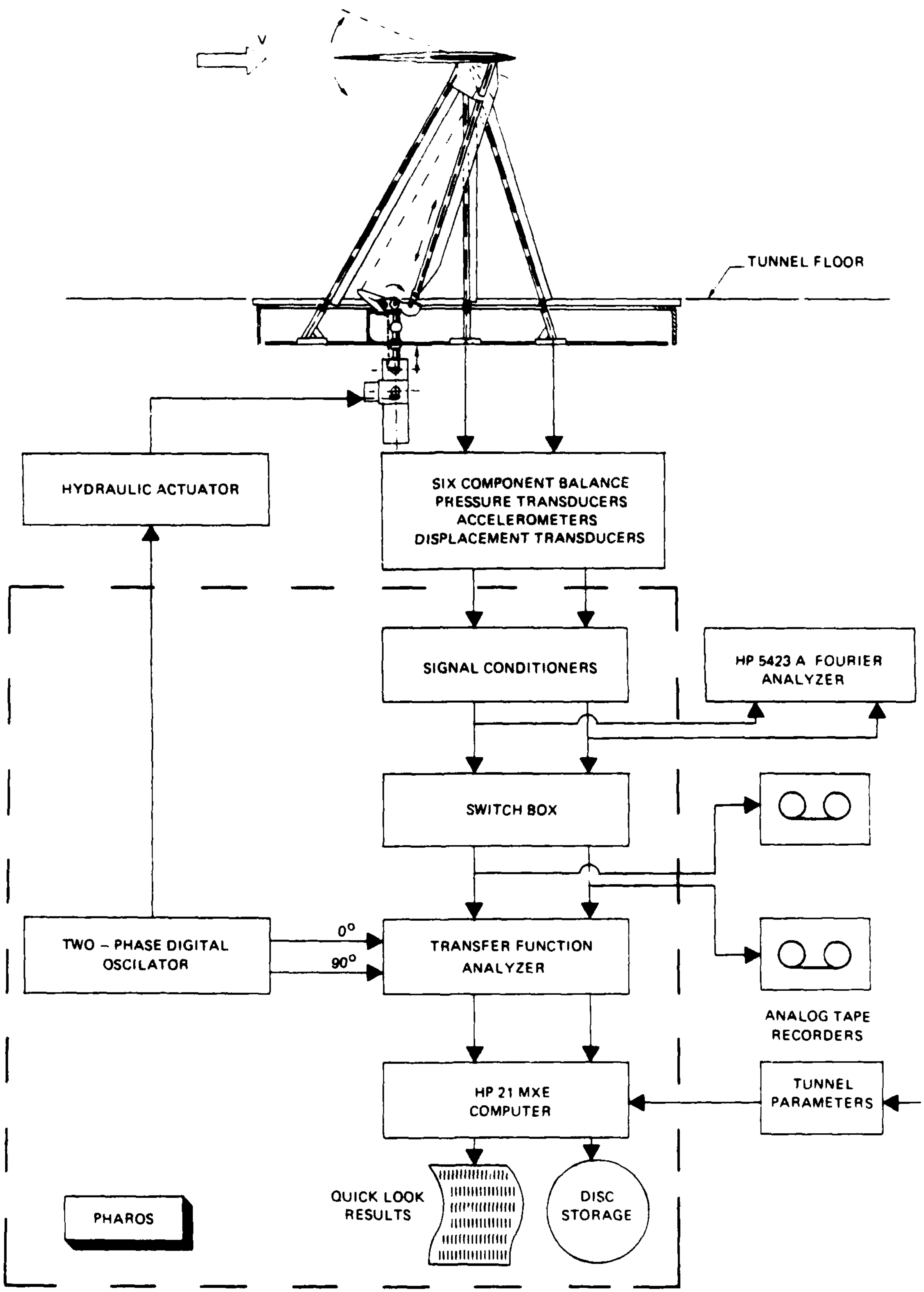

Fig. 7 Block-diagram of the test setup for measurements of forces, moments and pressures

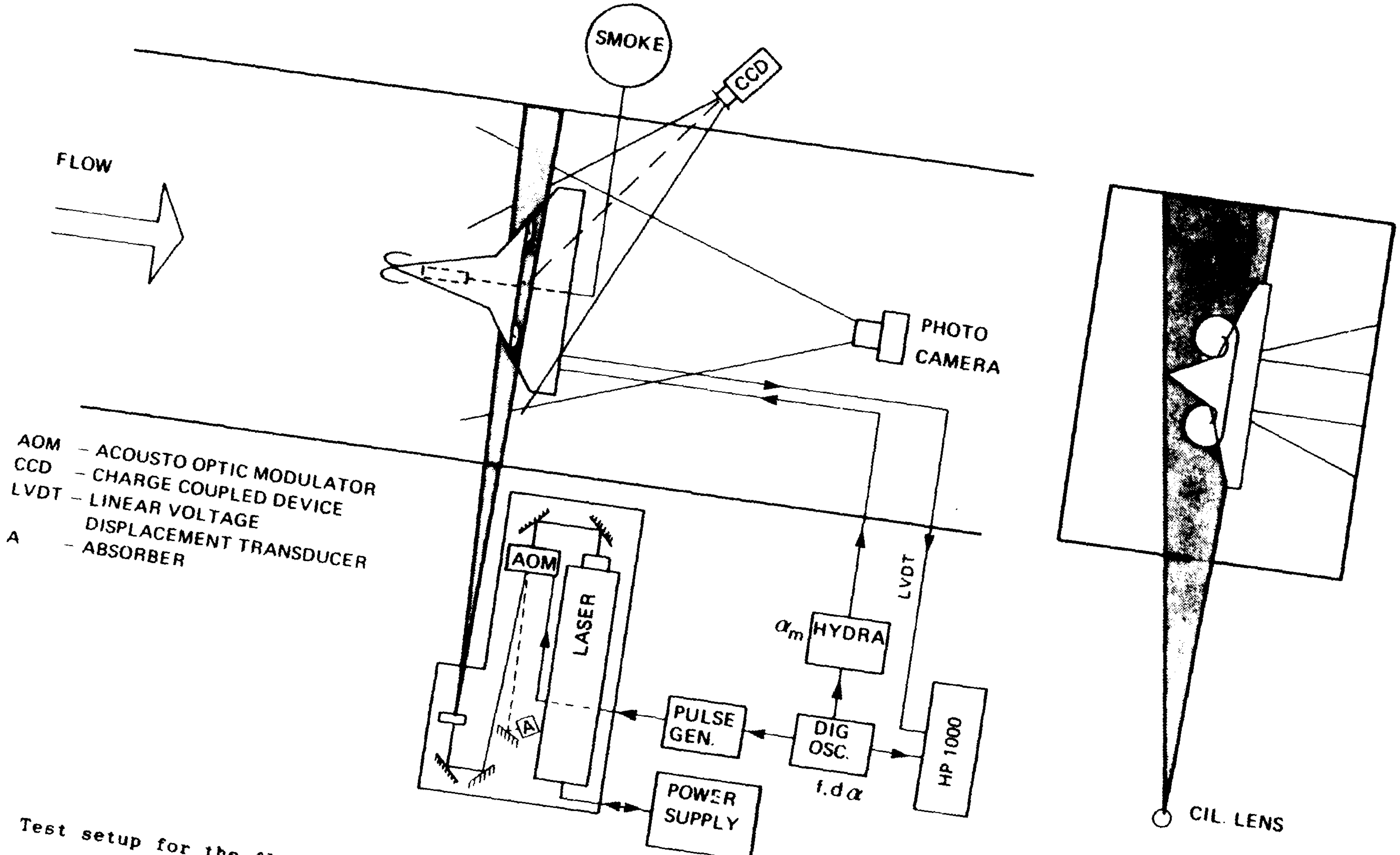

Fig. 8 Test setup for the flow visualization

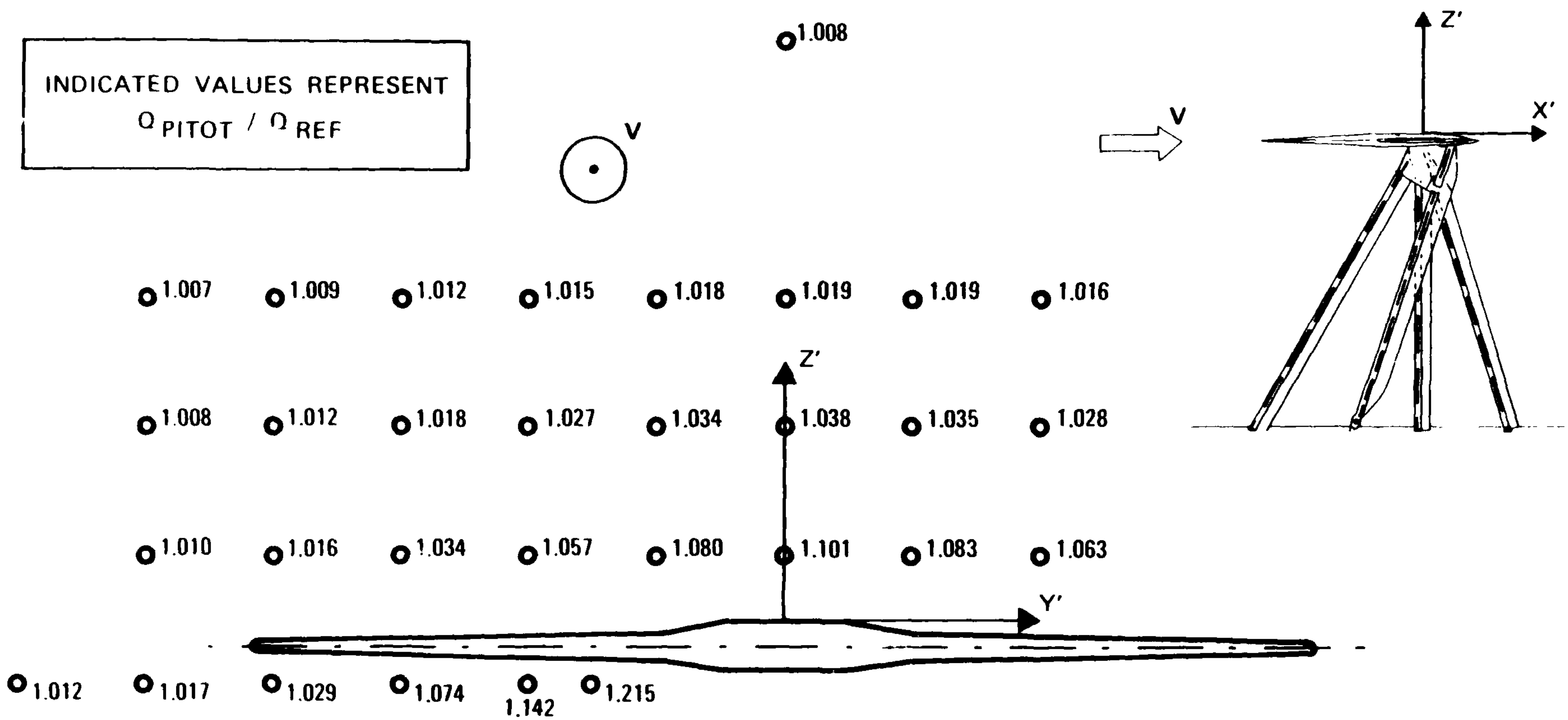

Fig. 9 Dynamic pressure distribution around model at zero lift

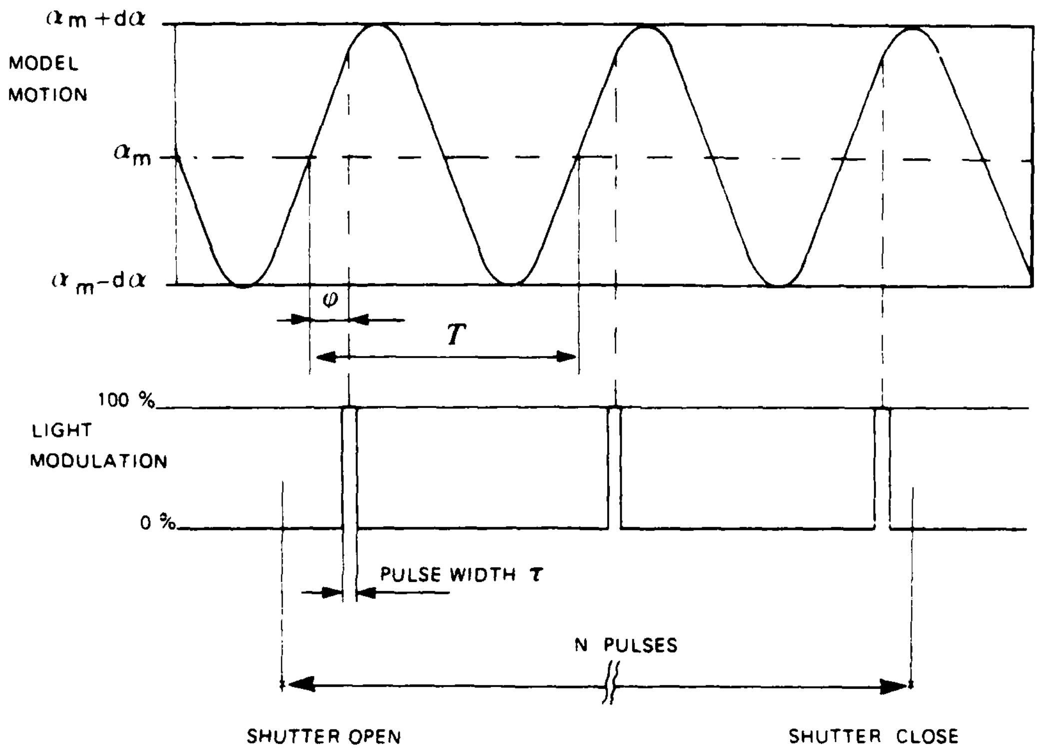

$$\text{EXPOSURE} = \sum_{i=1}^{N} \tau_i$$

<u>LIGHT SHEET</u> : PULSE DURATION τ INVERSELY PROPORTIONAL TO FREQUENCY
(1 – 8 DEG) ADJUSTABLE
PHASE φ WITH RESPECT TO MODEL MOTION
(0 – 360 DEG) ADJUSTABLE.

Fig. 10 Principle of unsteady flow visualization

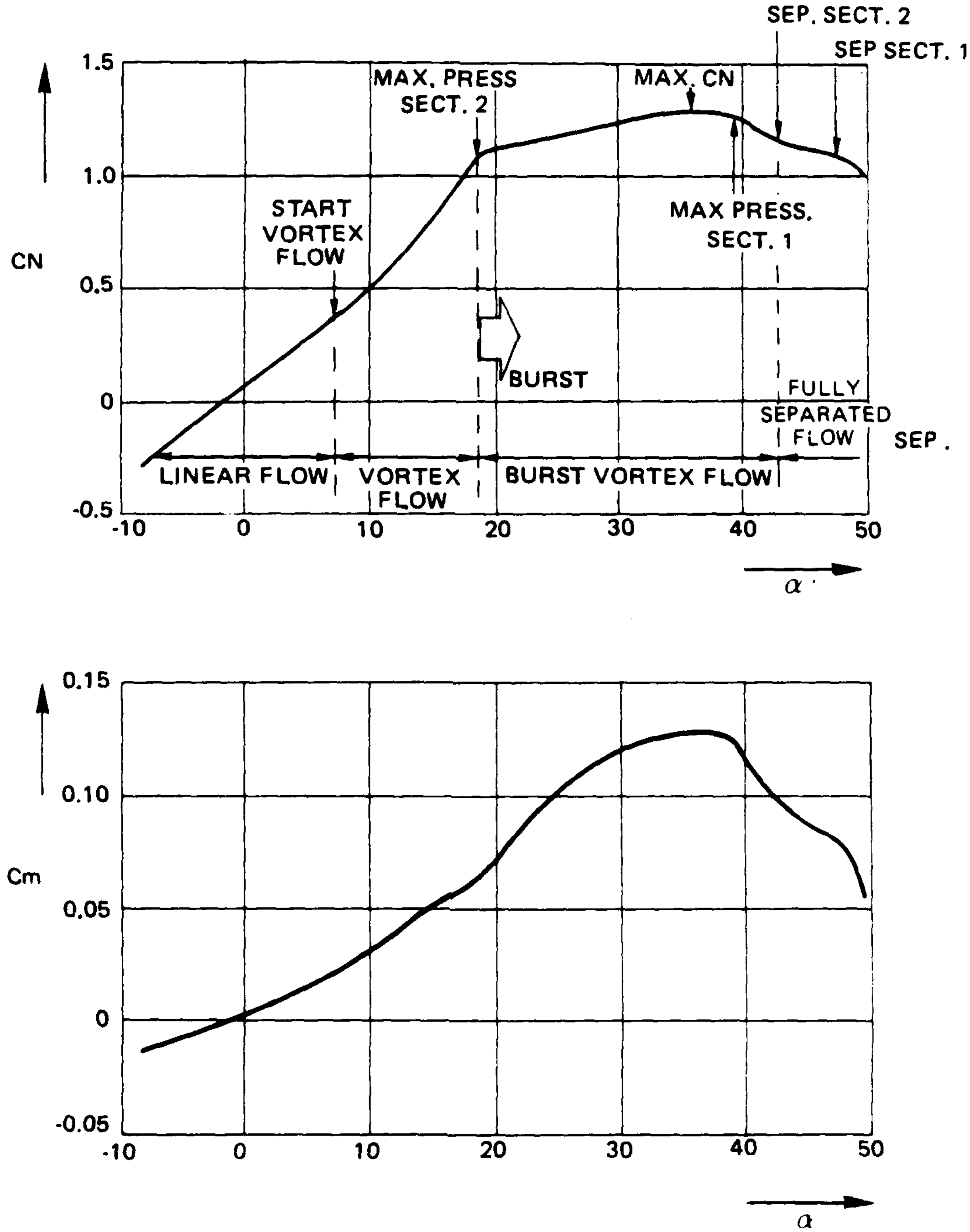

Fig. 11 Steady normal force and pitching moment coefficient vs. incidence

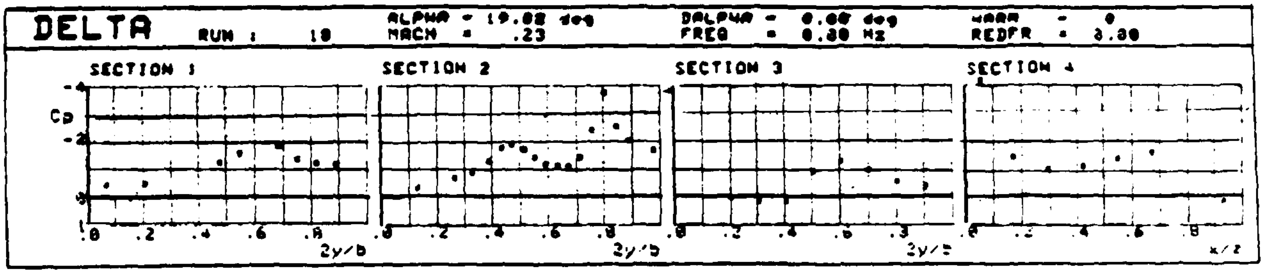

Fig. 12 Example of a plot of the pressure coefficients of a steady testrun (see also table 15)

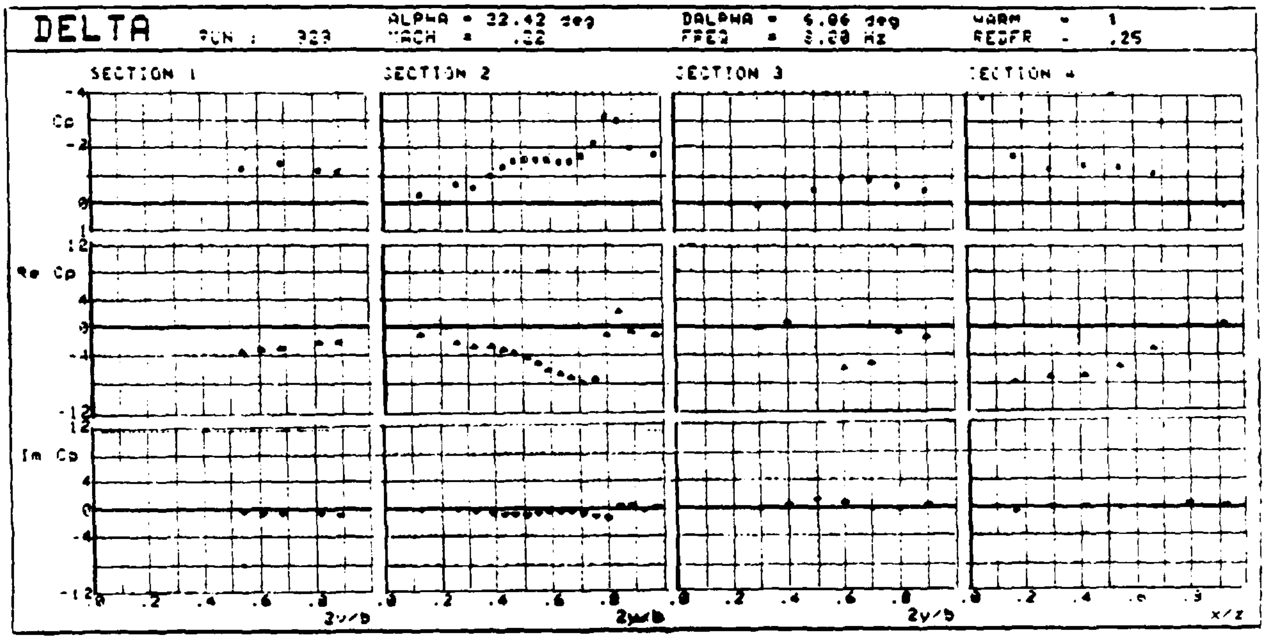

Fig. 13 Example of a plot of the pressure coefficients of an unsteady testrun (see also table 16)

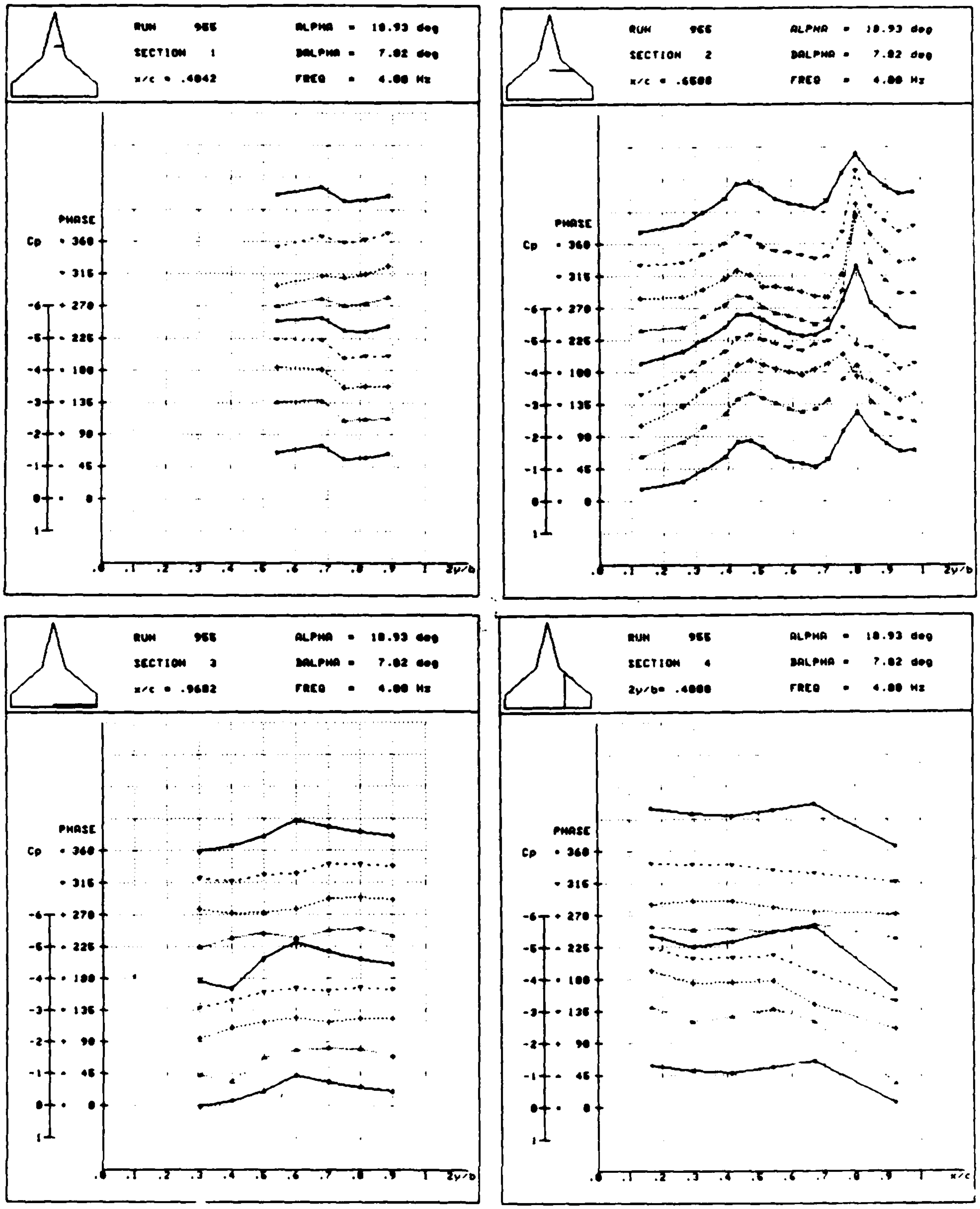

Fig. 14 Example of the time history of the pressure distributions

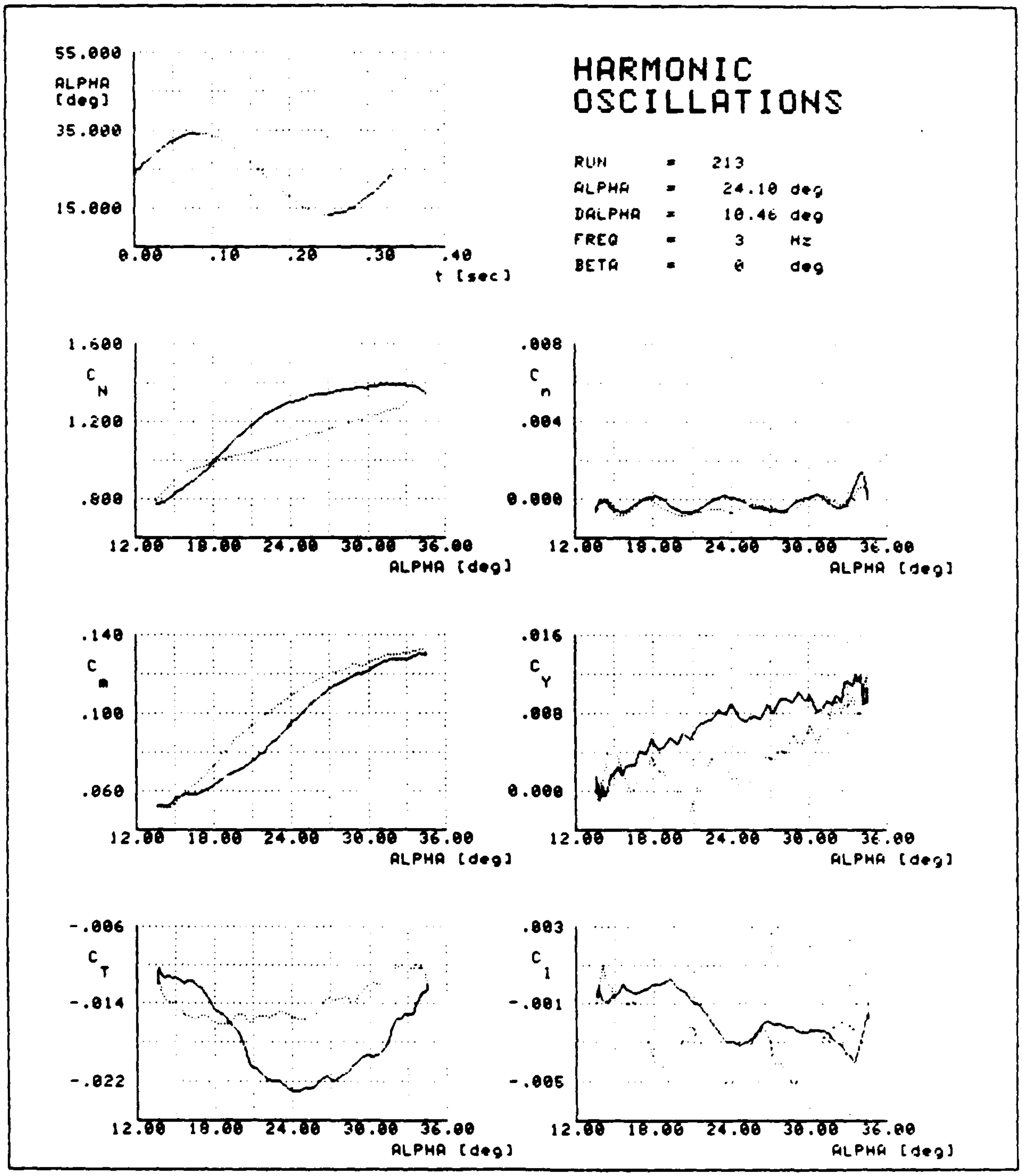

Fig. 15 Example of overall aerodynamic loads vs. incidence, derived from the recordings at harmonic oscillating model

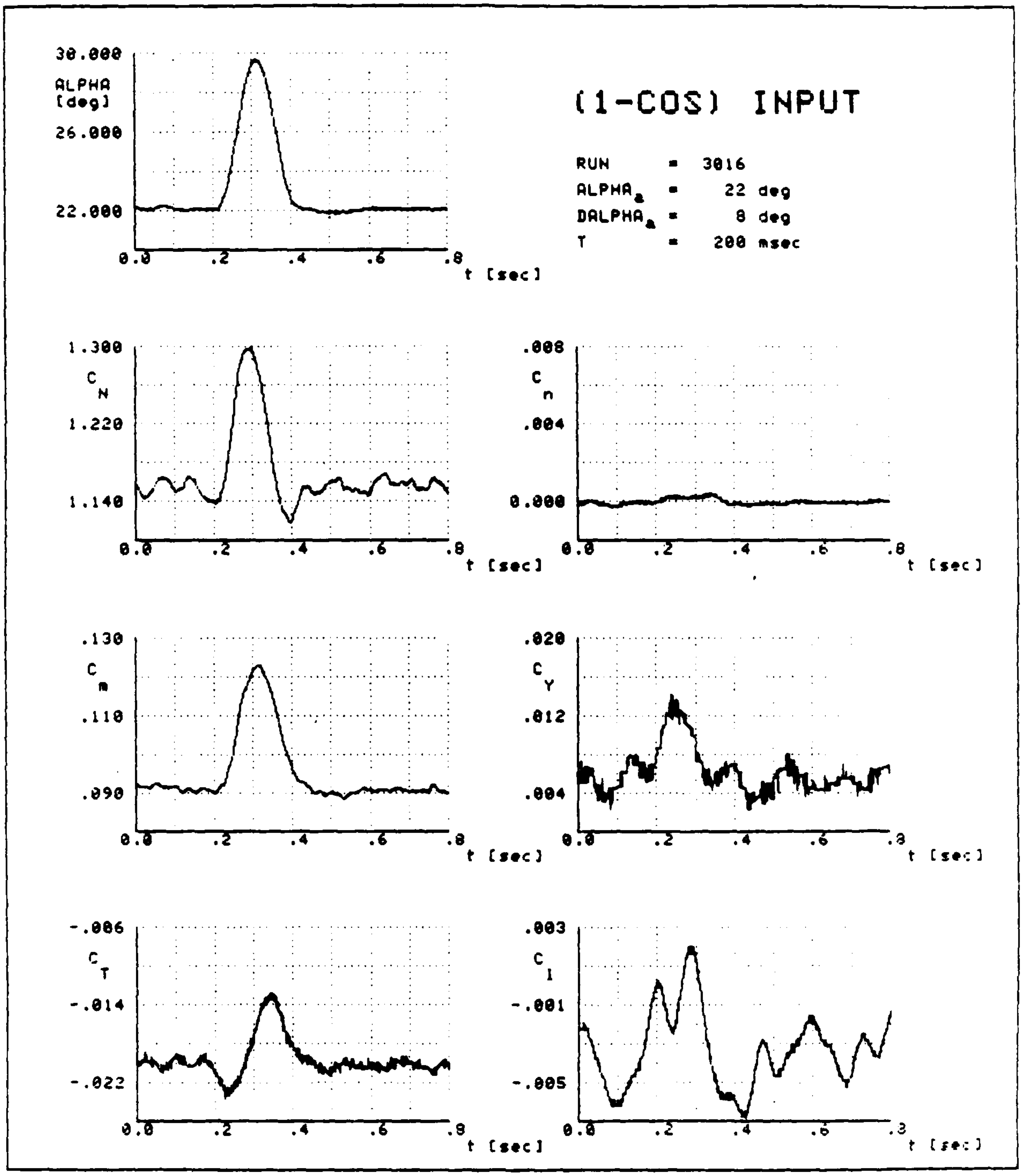

Fig. 16 **Example of the time history of the balance signals at the (1-cos) model motion**

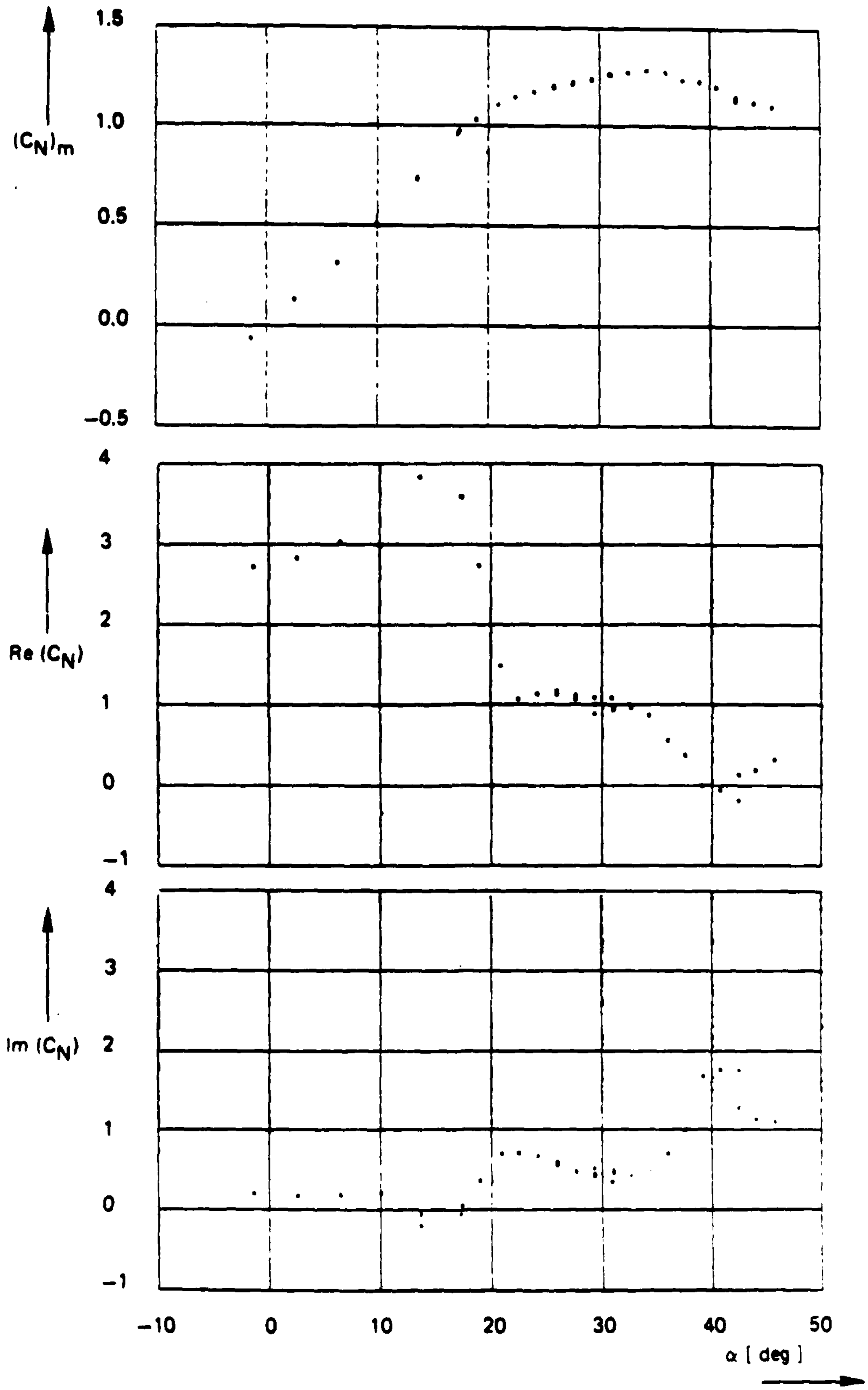

Fig. 17 Zeroth and first order harmonic components of unsteady normal force coefficient ($d\alpha \approx 3.5$ deg, $f = 3$ Hz, $\beta = 0$ deg, $V \approx 80$ m/s)

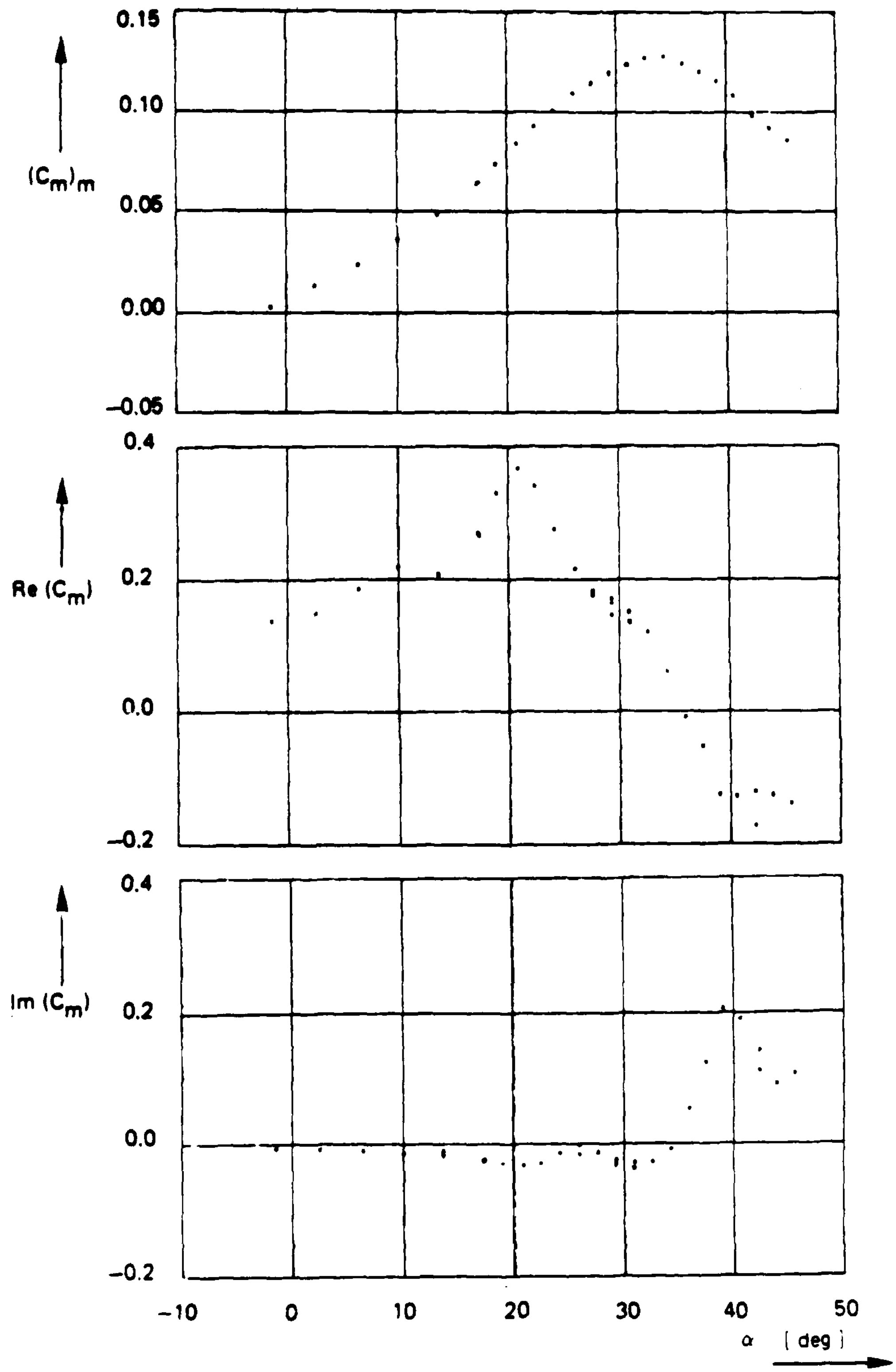

Fig. 18 Zeroth and first order harmonic components of unsteady pitching moment coefficient ($d\alpha \approx 3.5$ deg, $f = 3$ Hz, $\beta = 0$ deg, $V \approx 80$ m/s)

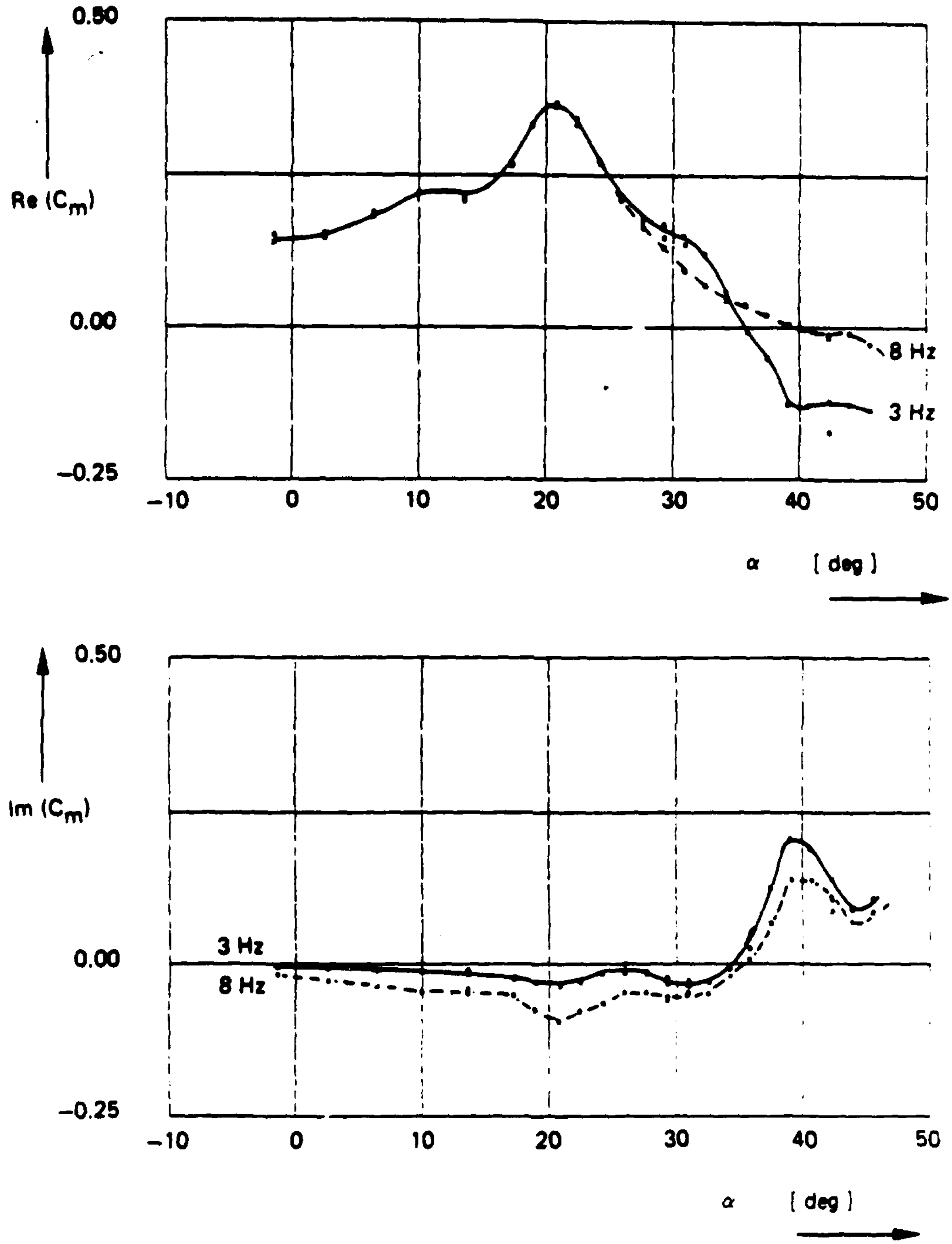

Fig. 19 First order harmonic components of unsteady pitching moment coefficients at 3 and 8 Hz ($d\alpha \approx 3.5$ deg, $\beta = 0$ deg, $V \approx 80$ m/s)

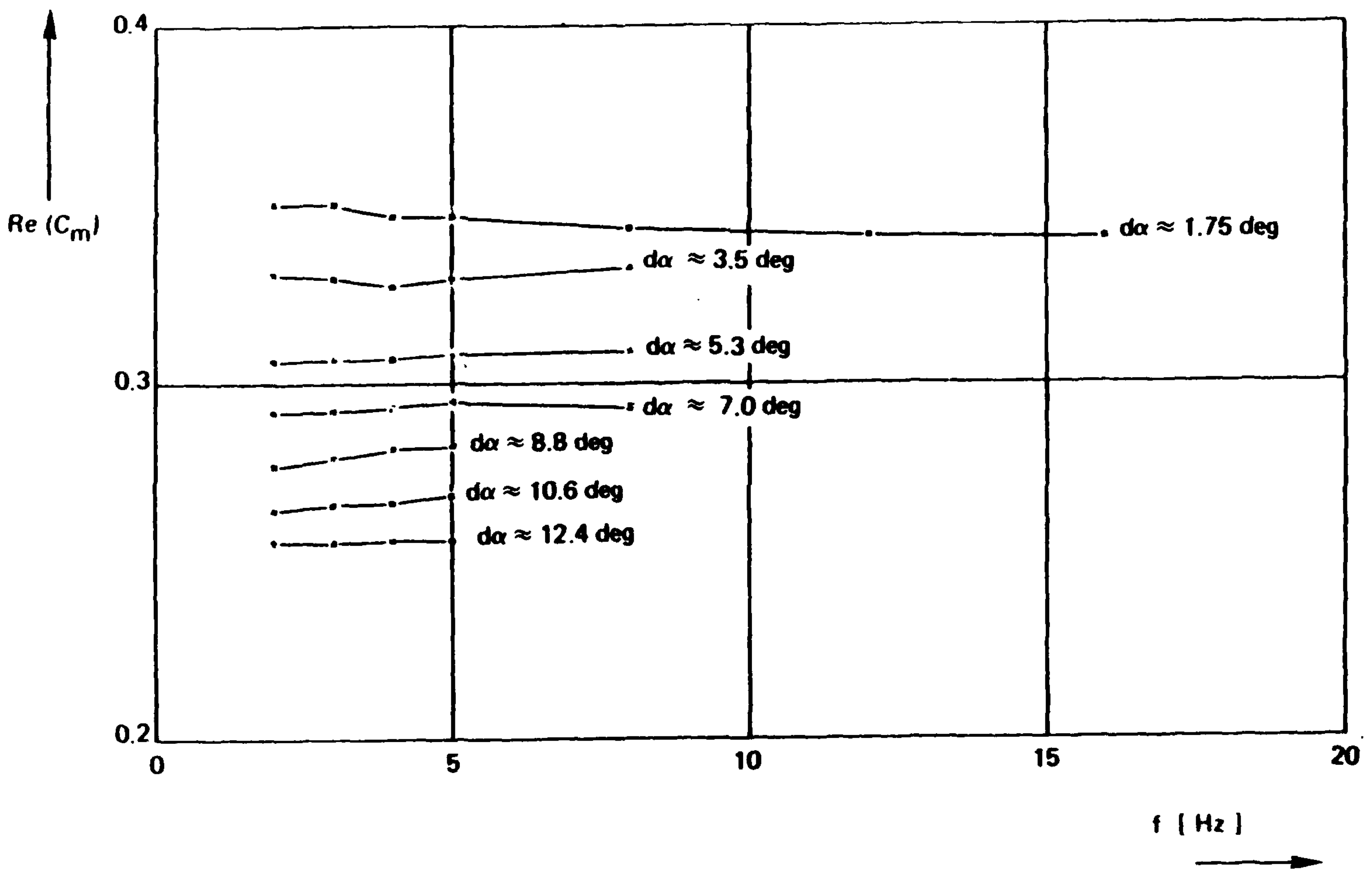

Fig. 20 Real part of first order harmonic component of unsteady pitching moment coefficient vs. frequency ($\alpha \approx 18.9$ deg, $\beta = 0$ deg, $V = 80$ m/s)

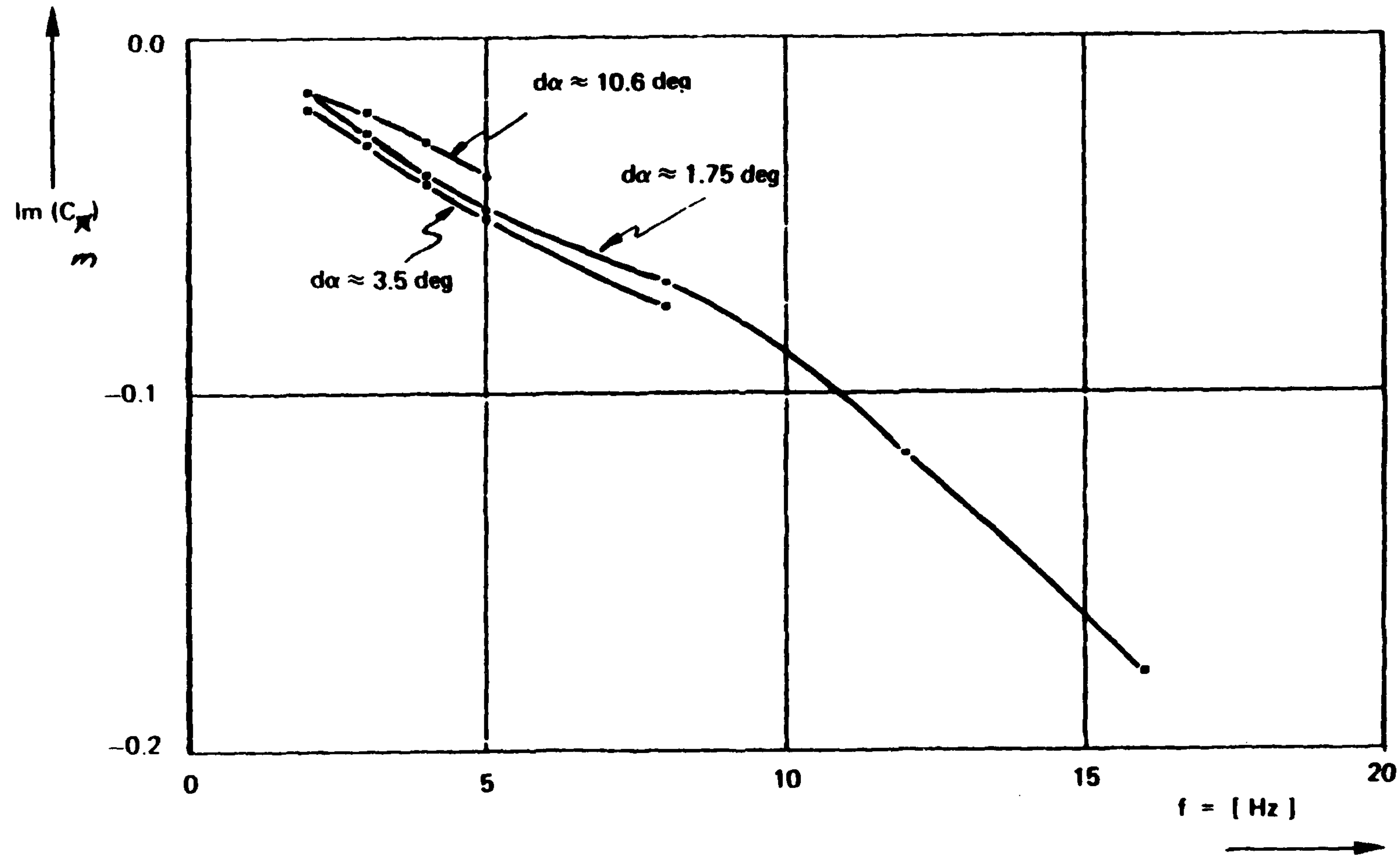

Fig. 21 Imaginary part of first order harmonic components of the unsteady pitching moment coefficient vs. frequency ($\alpha \approx 18.9$ deg, $\beta = 0$ deg, $V = 80$ m/s)

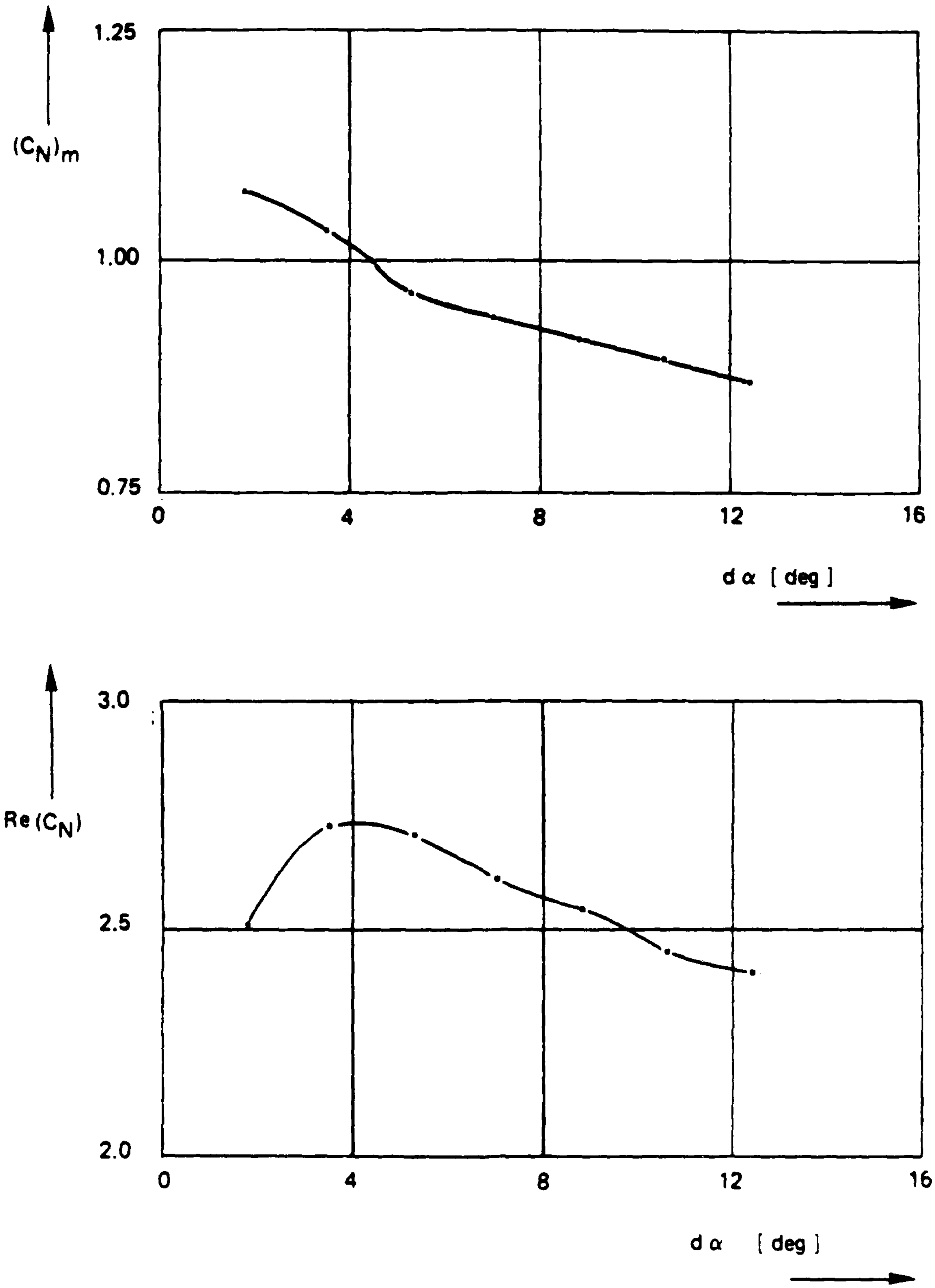

Fig. 22 Zeroth order harmonic component and real part of first order harmonic component of unsteady normal force coefficient vs. amplitude ($\alpha \sim 18.9$ deg, $f = 3$ Hz, $\beta = 0$ deg, $V \sim 80$ m/s)

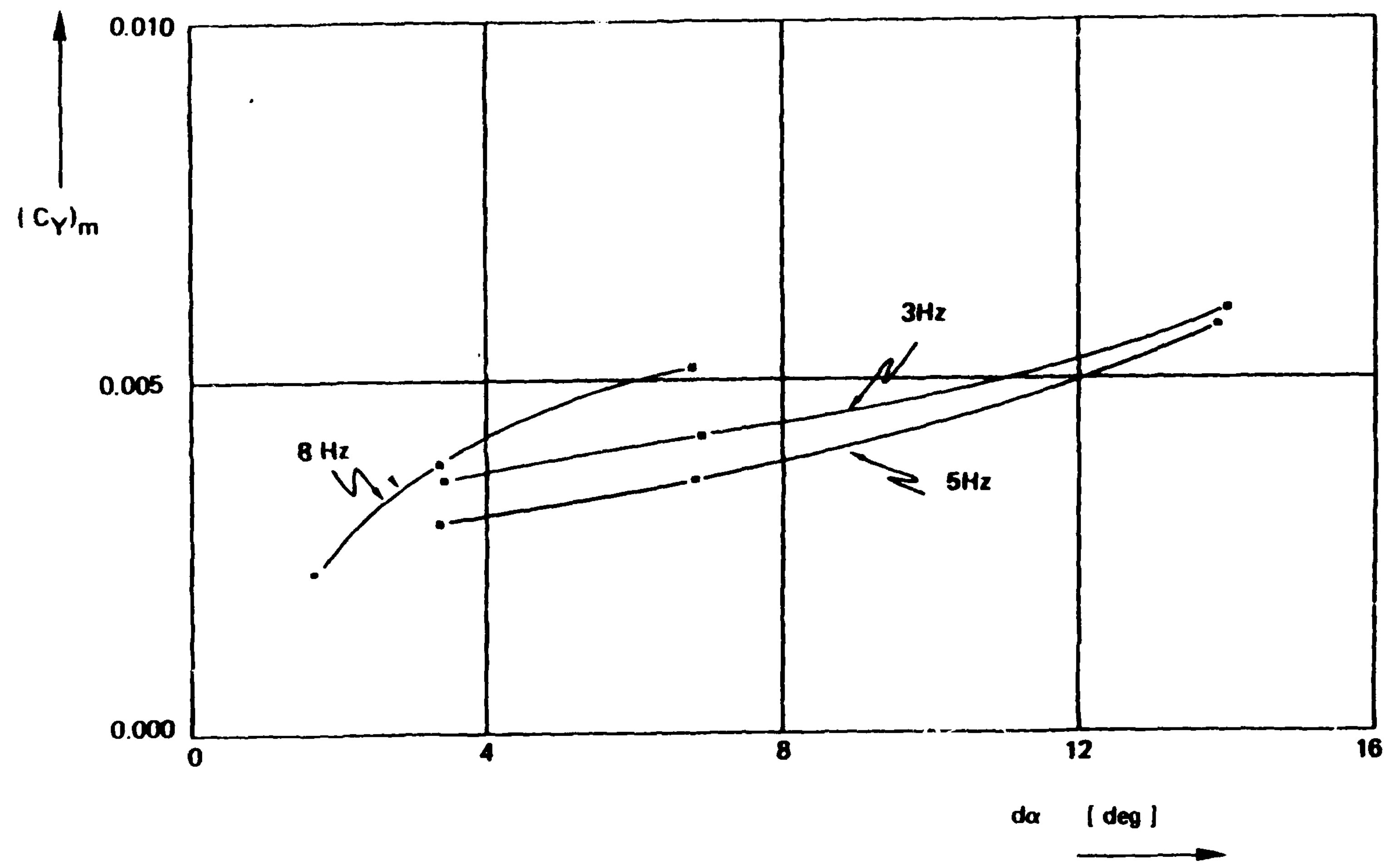

Fig. 23 Zeroth order harmonic component of unsteady side force coefficient vs. amplitude ($\alpha \approx 35.9$ deg, $\beta = 5$ deg, $V \approx 80$ m/s)

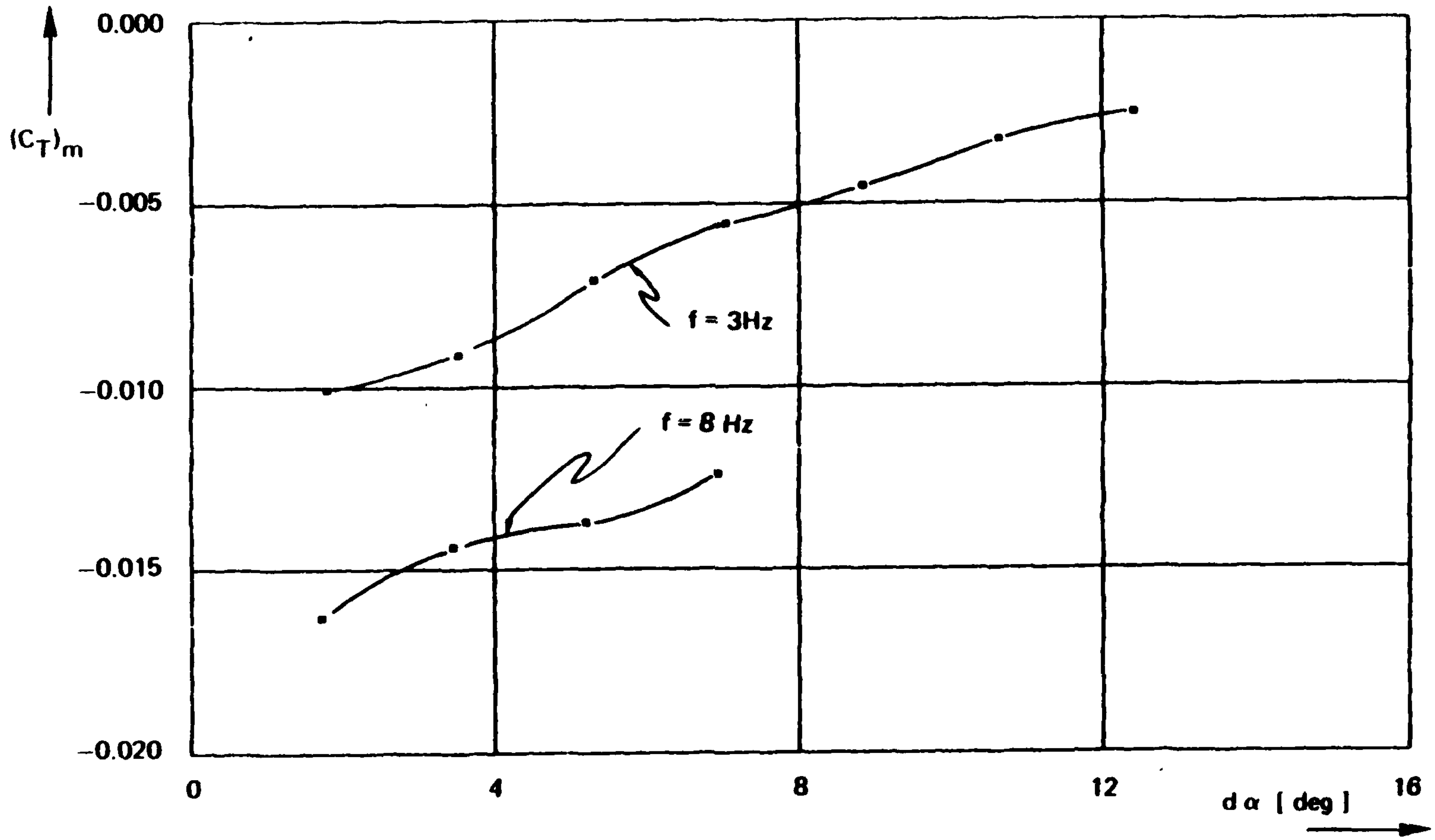

Fig. 24 Zeroth order harmonic component of unsteady tangential force coefficient vs. amplitude ($\alpha \approx 18.9$ deg, $\beta = 0$ deg, $V \approx 80$ m/s)

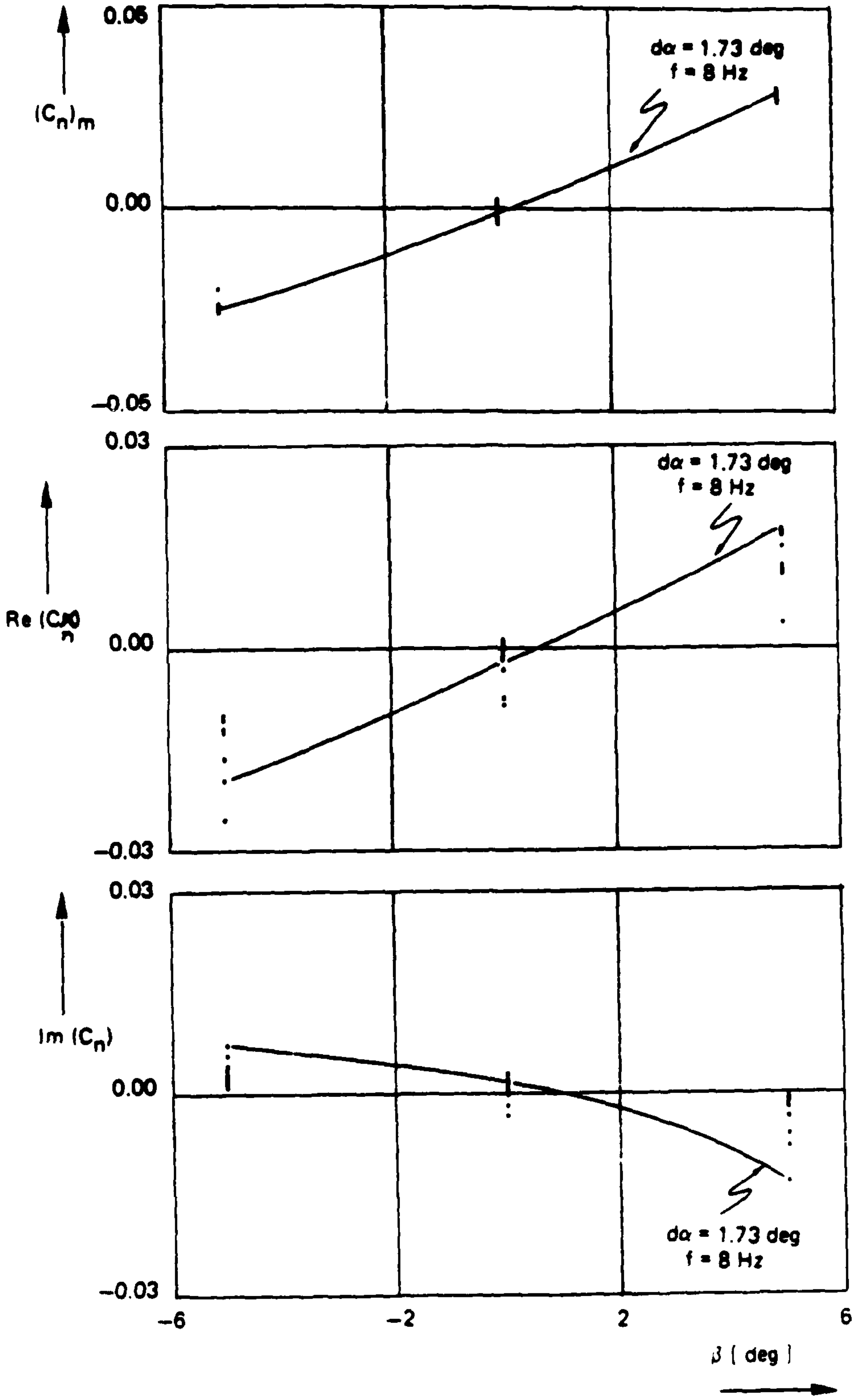

Fig. 25 The effect of sideslip on the zeroth and first order harmonic components of the unsteady yawing moment coefficient at various frequency amplitude combinations ($\alpha \sim 18.9$ deg, $V \sim 80$ m/s)

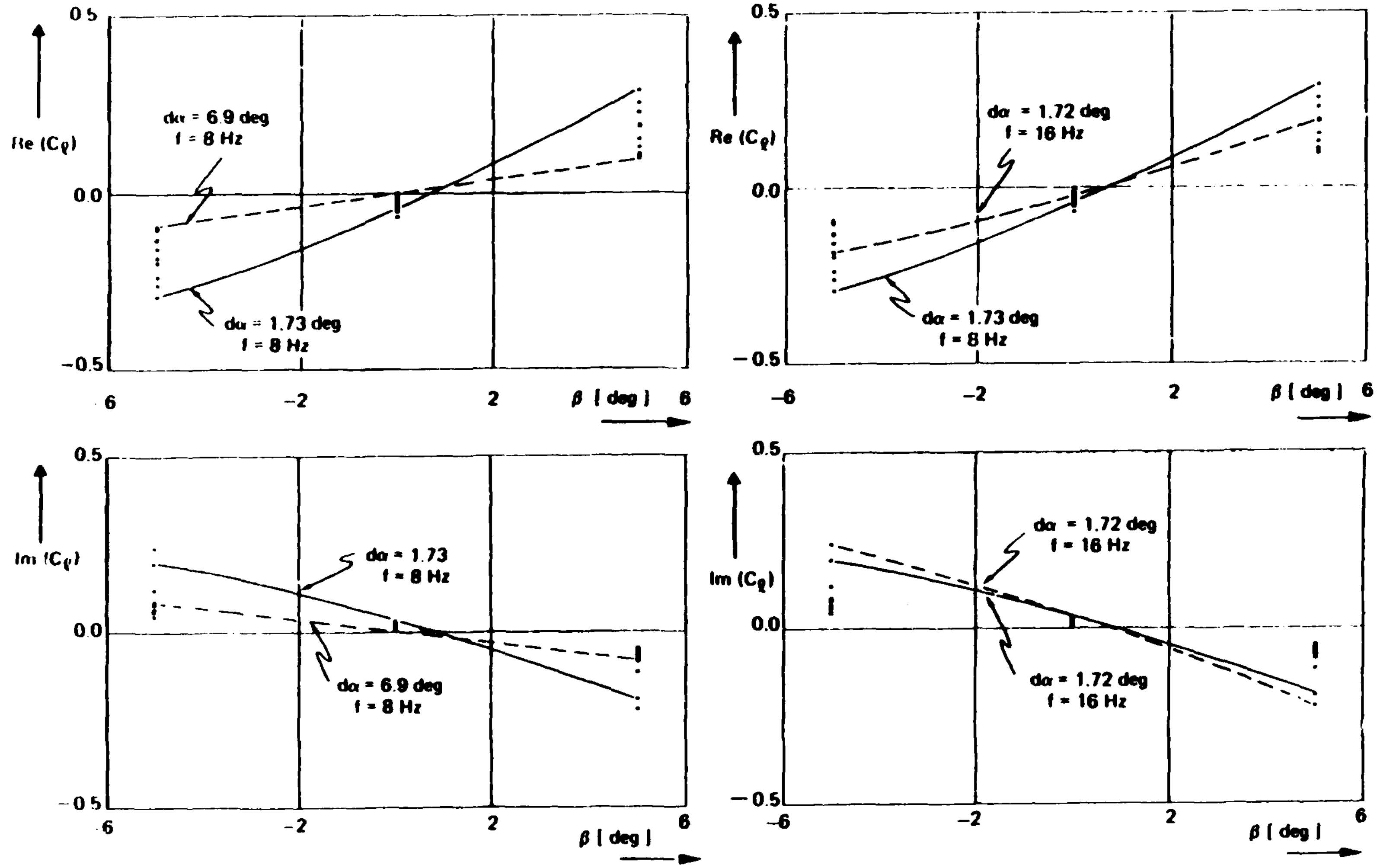

Fig. 26 The effect of sideslip on the first order harmonic component of the unsteady rolling moment coefficient ($\alpha \approx 18.9$ deg, $V \approx 80$ m/s)
Left side of figure : amplitude effect
Right side of figure: frequency effect

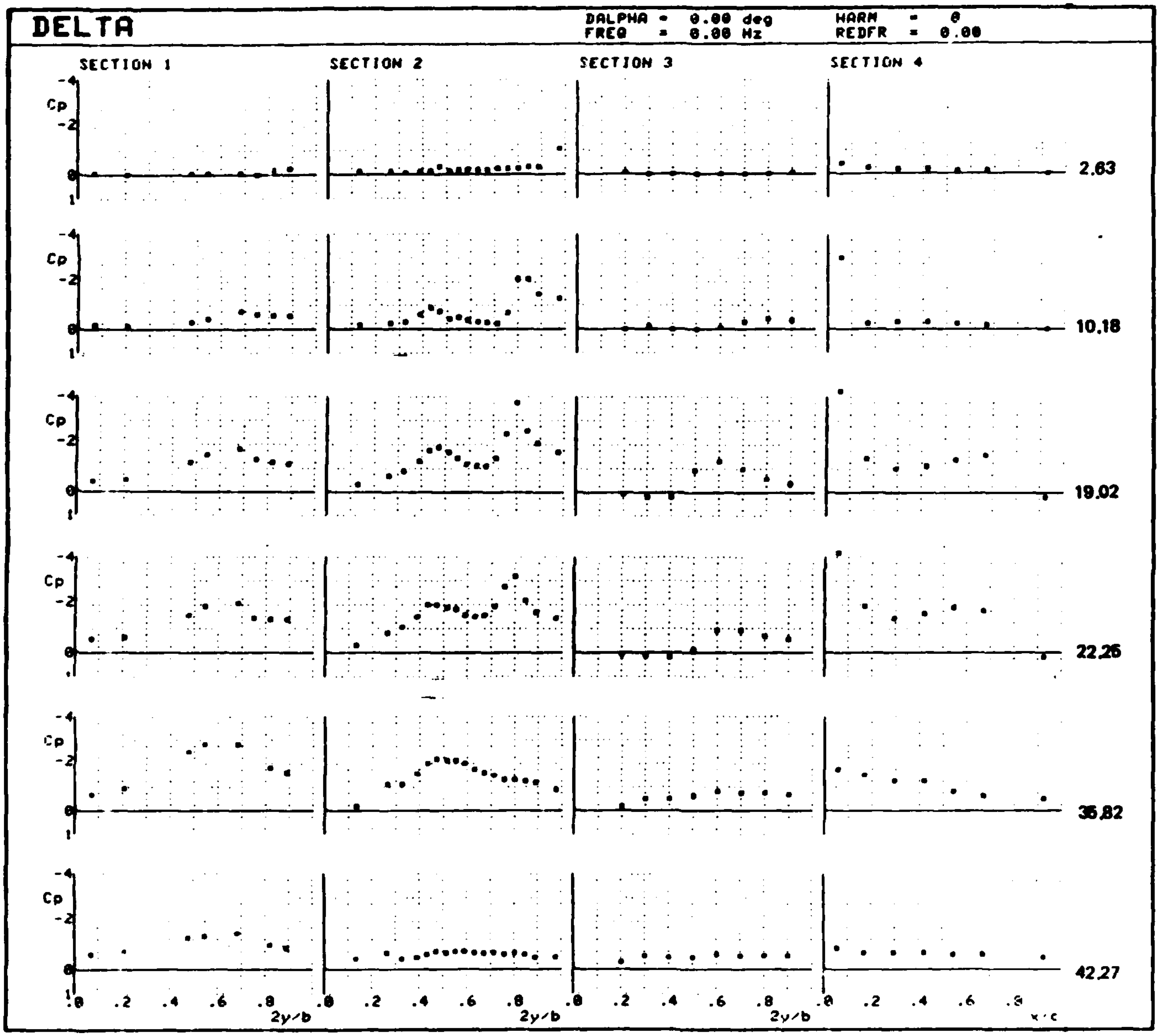

Fig. 27 Development of steady pressure distribution with incidence
(β = 0 deg, V ~ 80 m/s)

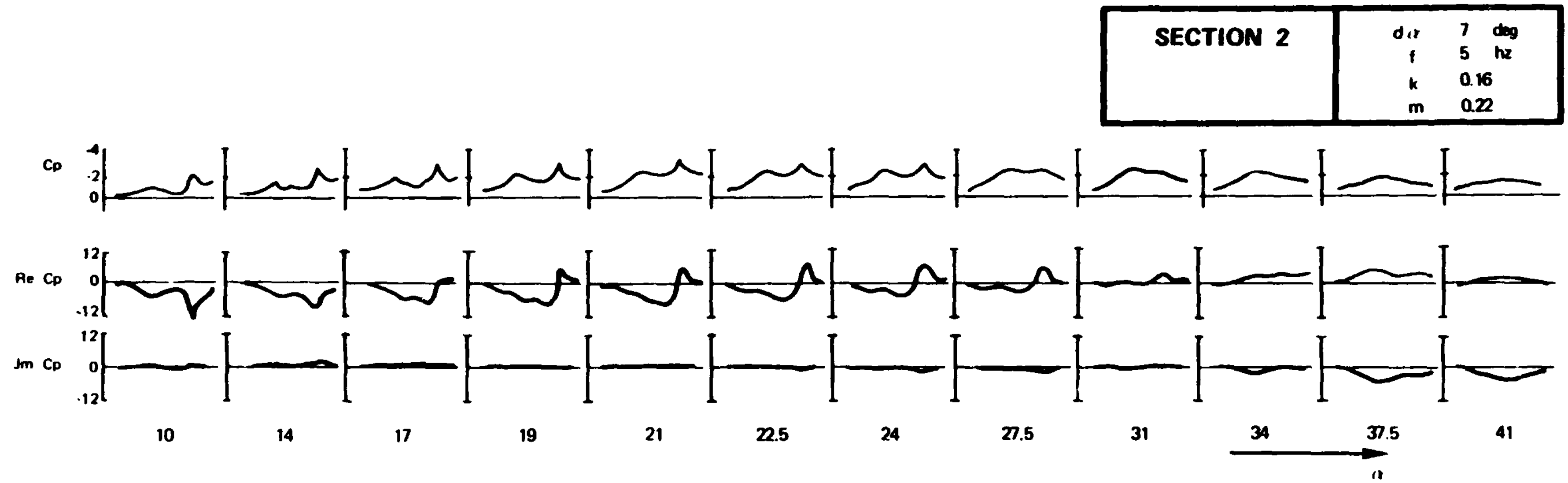

Fig. 28 Influence of angle of attack on the zeroth and first order harmonic components of the unsteady pressure distribution

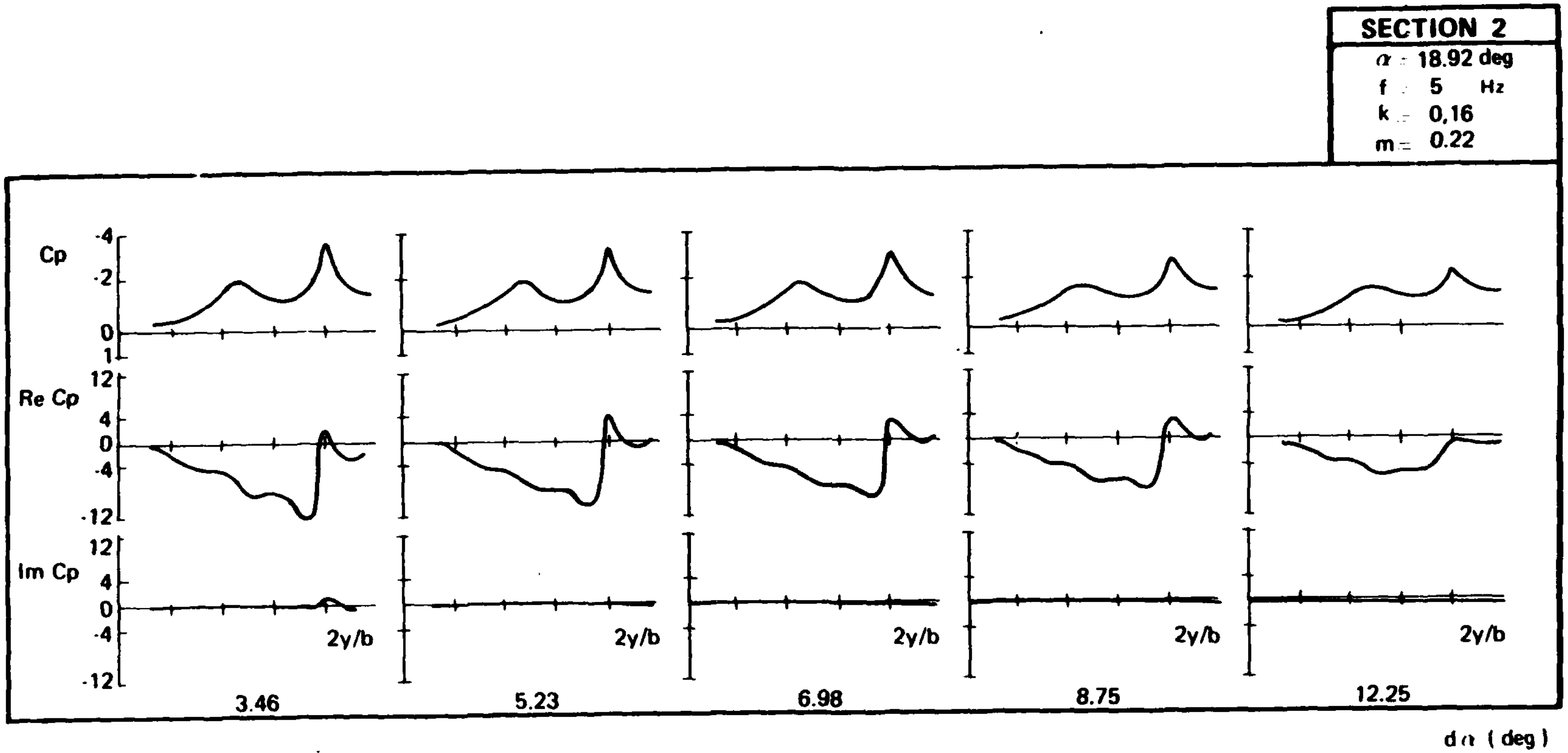

Fig. 29 Influence of amplitude on zeroth and first order dα (deg) harmonic components of the unsteady pressure distribution

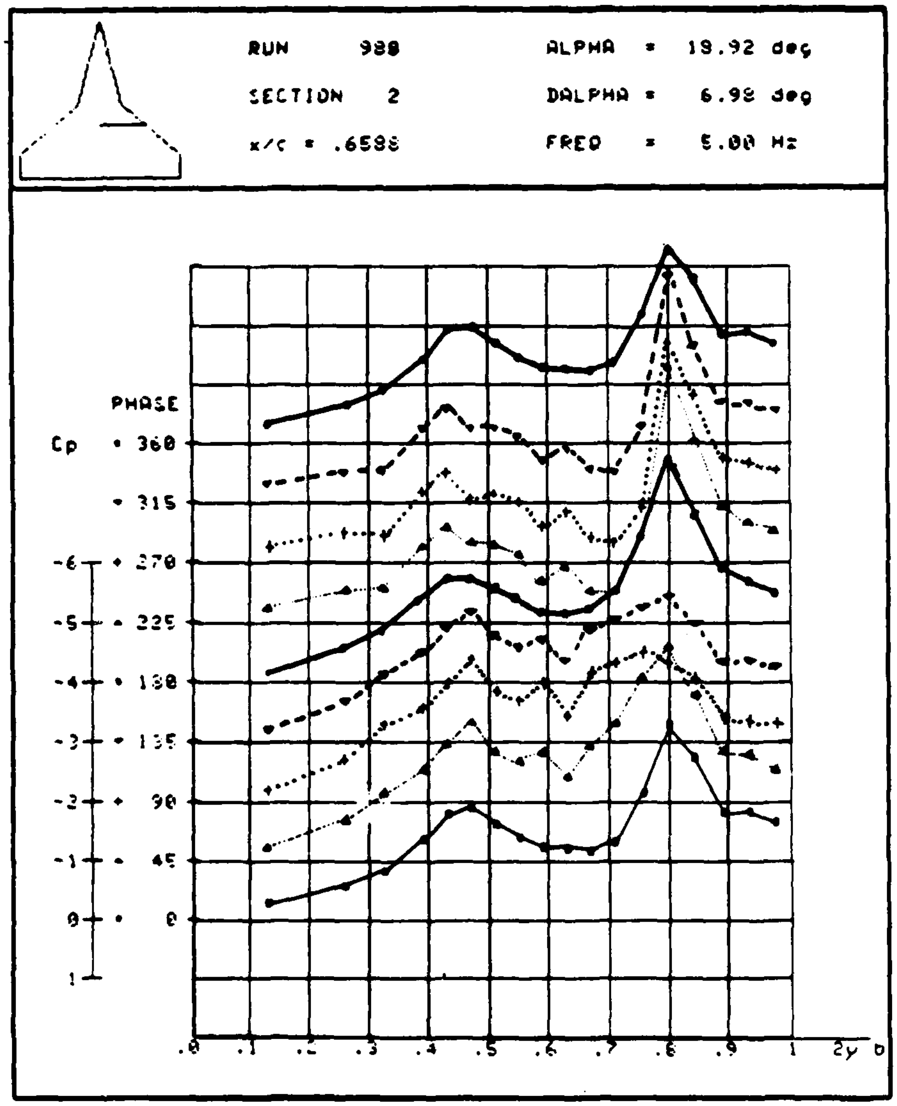

Fig. 30 Time history of the pressure distribution of section 2

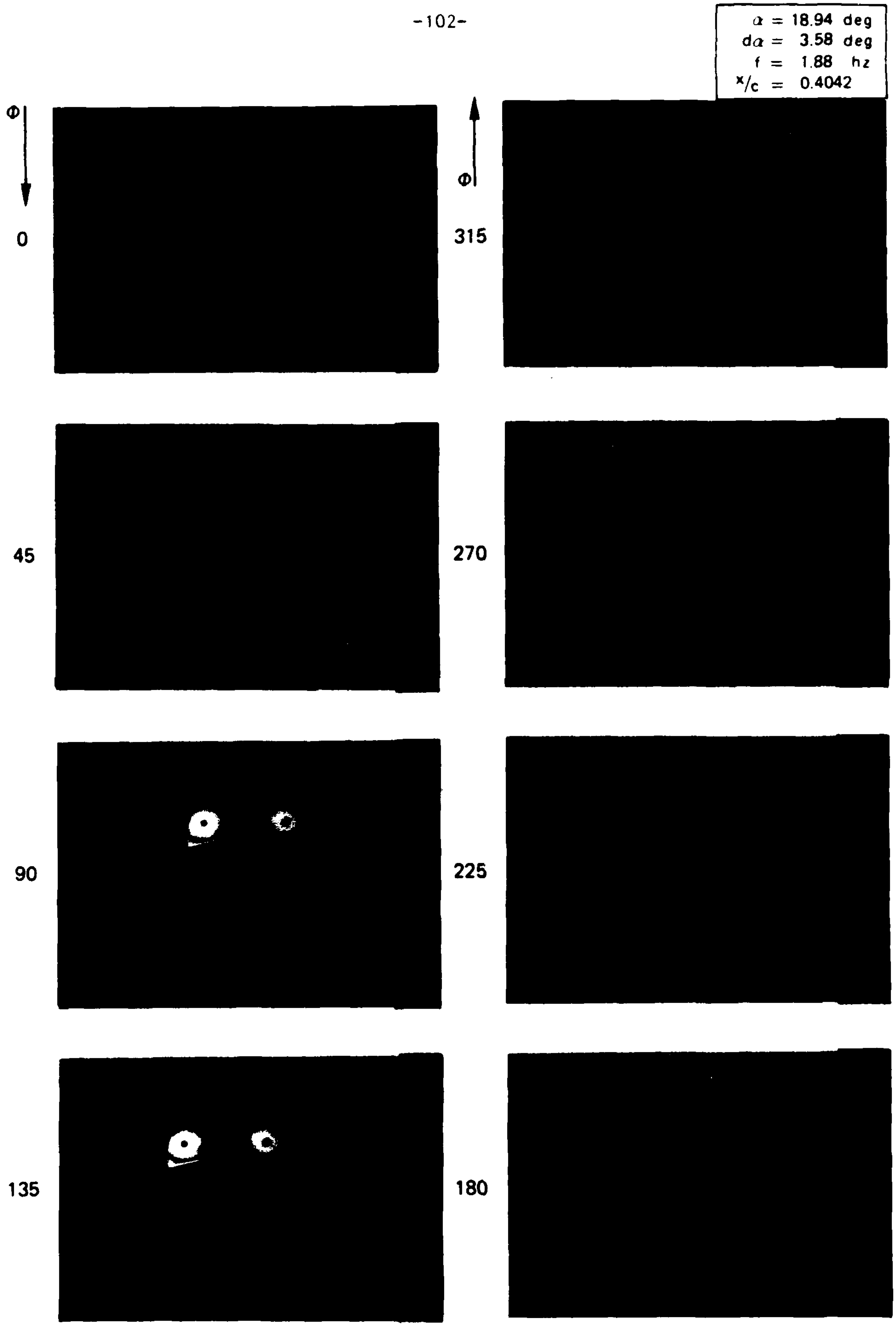

Fig. 31 Photographs showing the time history of the flow at section 1 (α = 18.94 deg, $d\alpha$ = 3.58 deg, f = 1.88 Hz)

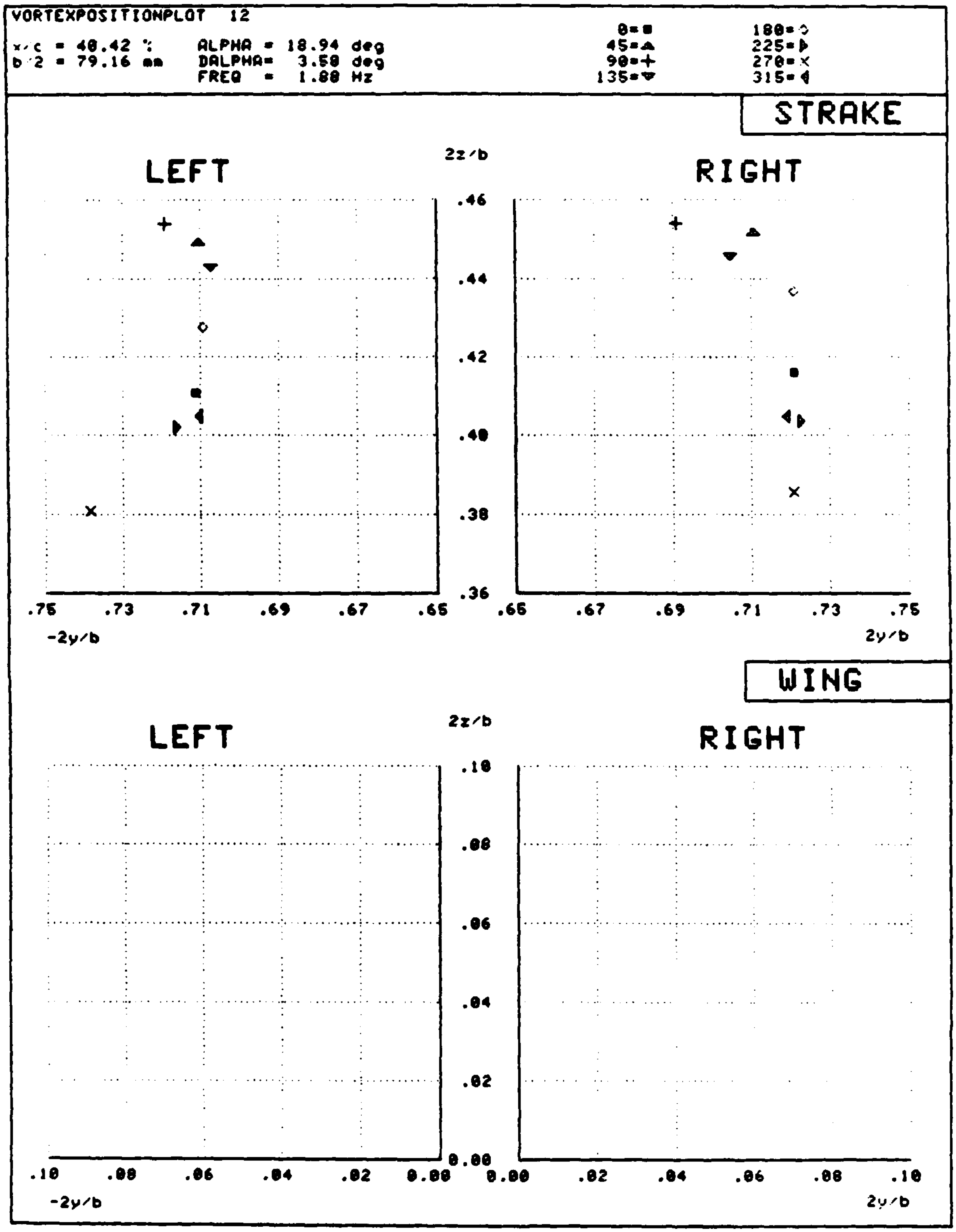

Fig. 32 Time history of the vortex core positions at section 1
(α = 18.94 deg, dα = 3.58 deg, f = 1.88 Hz)

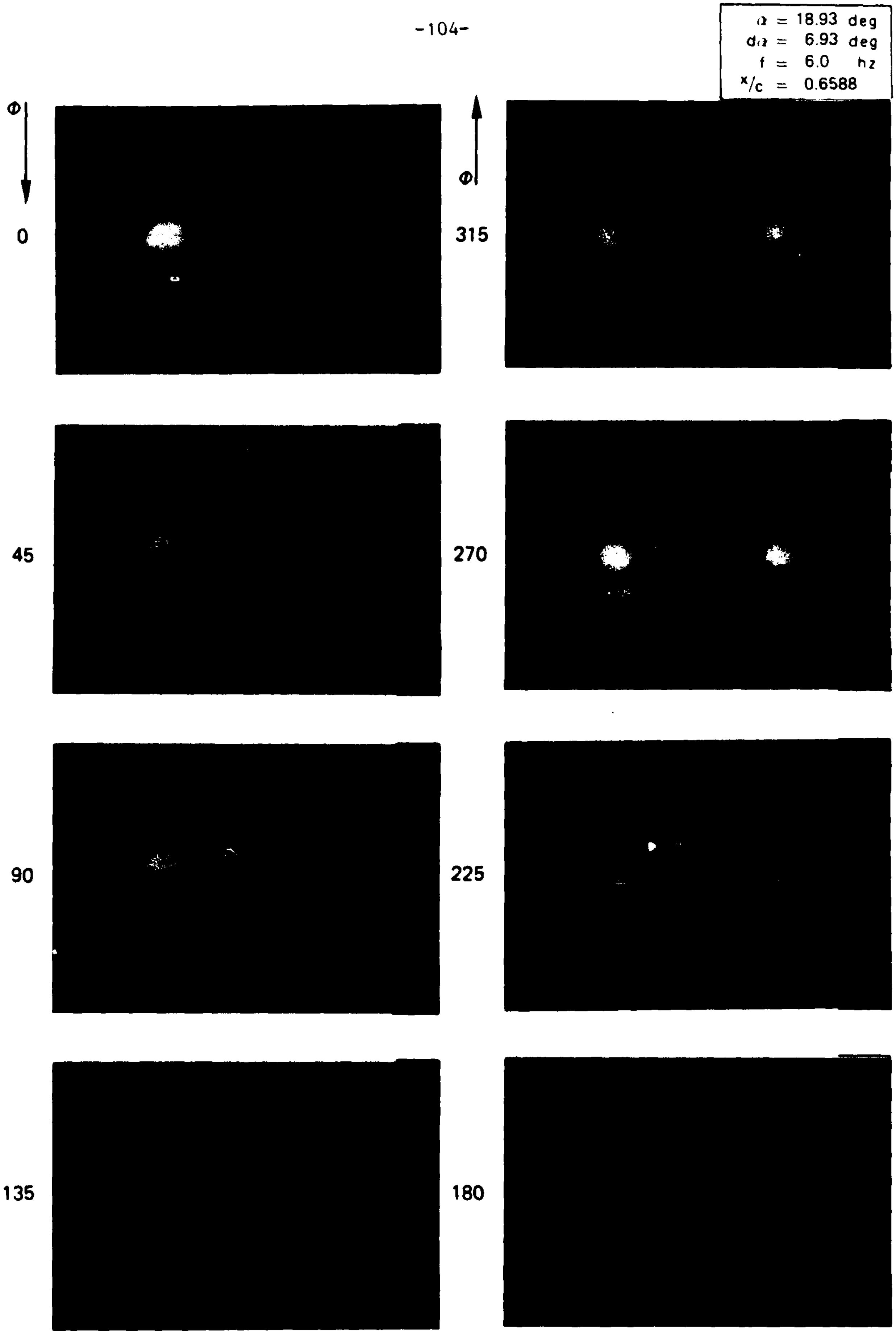

Fig. 33 Photographs showing the time history of the flow at section 2
(α = 18.93 deg, $d\alpha$ = 6.93 deg, f = 6 Hz)

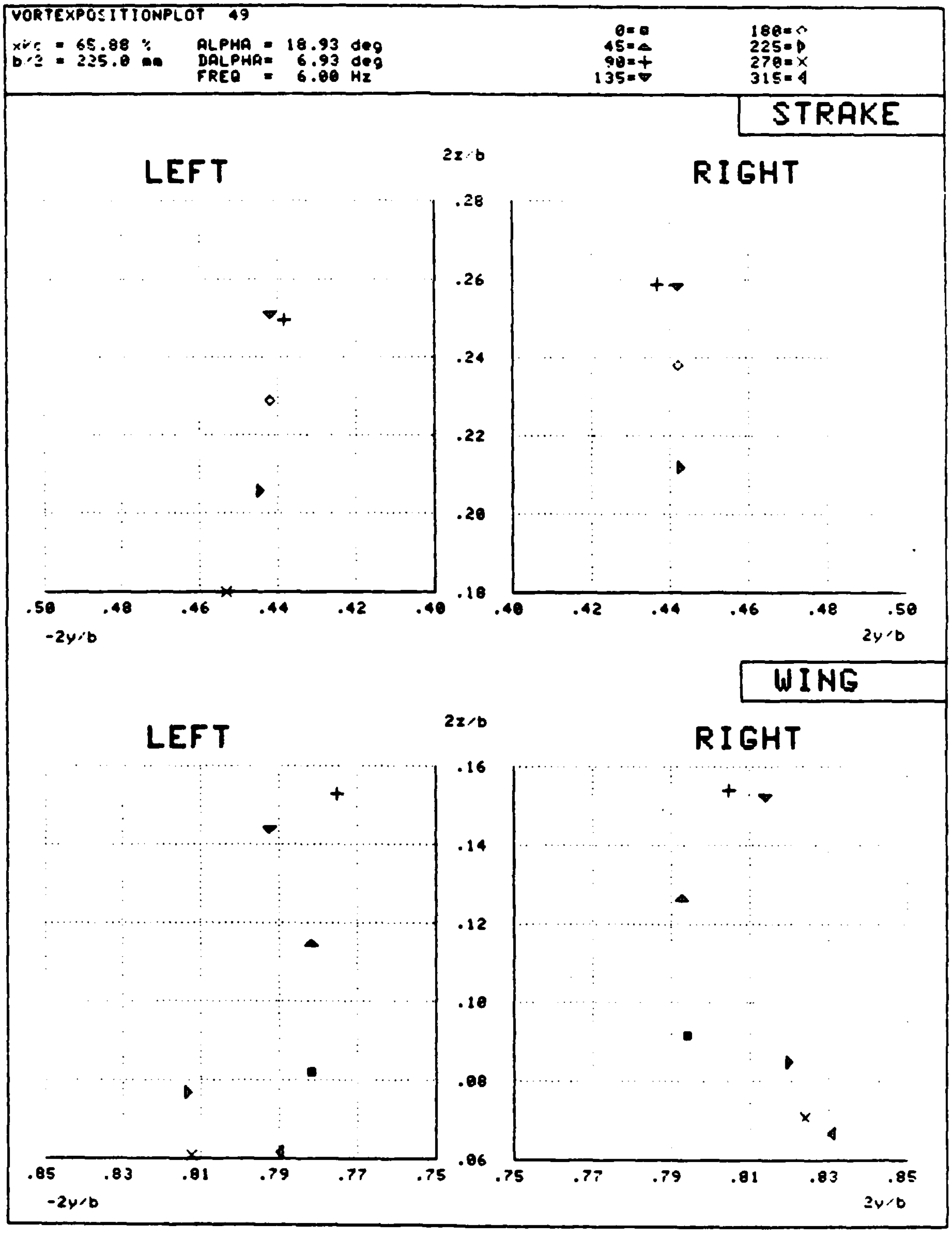

Fig. 34 Time history of the vortex core positions at section 2
(α = 18.93 deg, dα = 6.93 deg, f = 6 Hz)

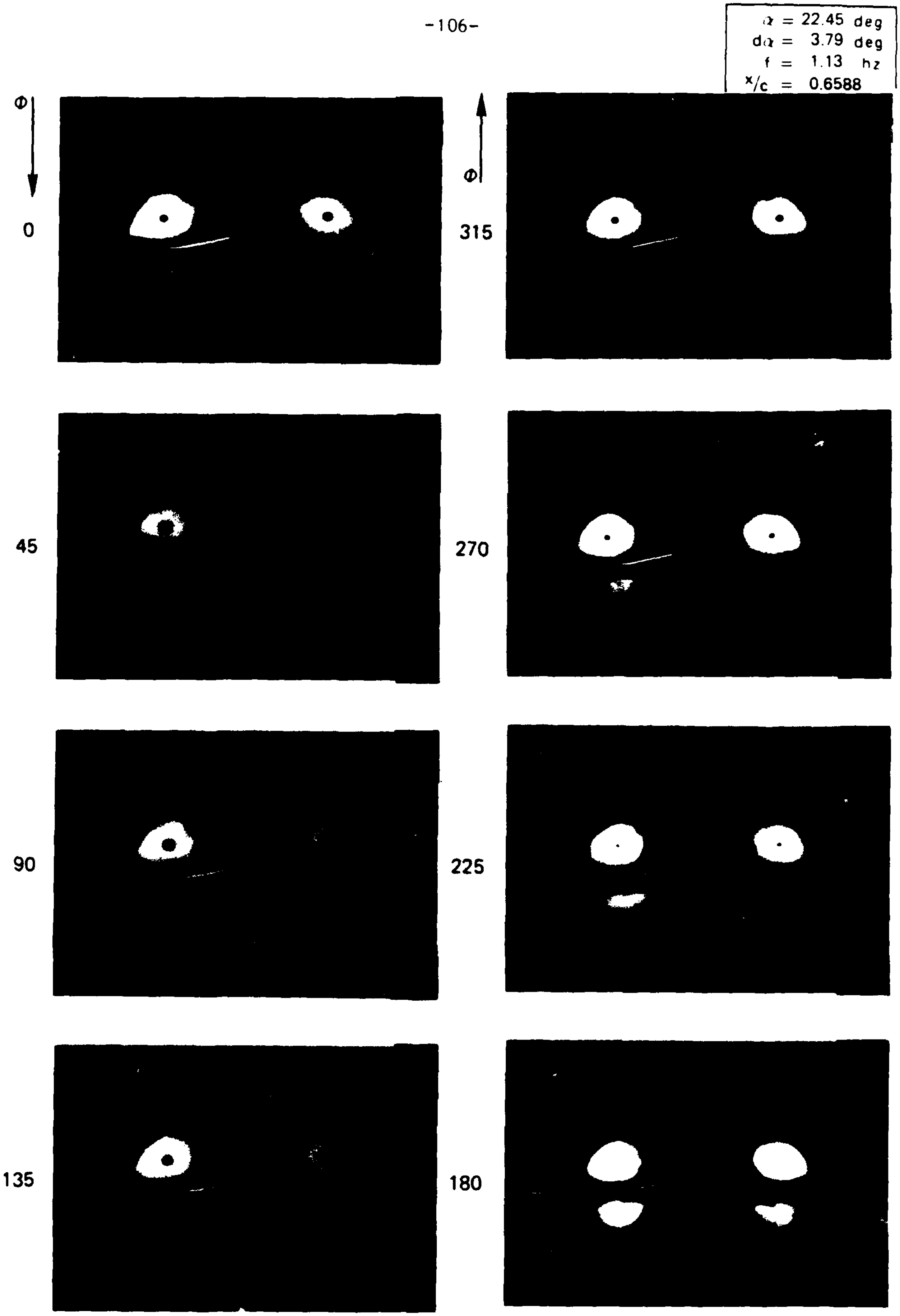

Fig. 35 Photographs showing the time history of the flow at section 2 (α = 22.45 deg, $d\alpha$ = 3.79 deg, f = 1.13 Hz)

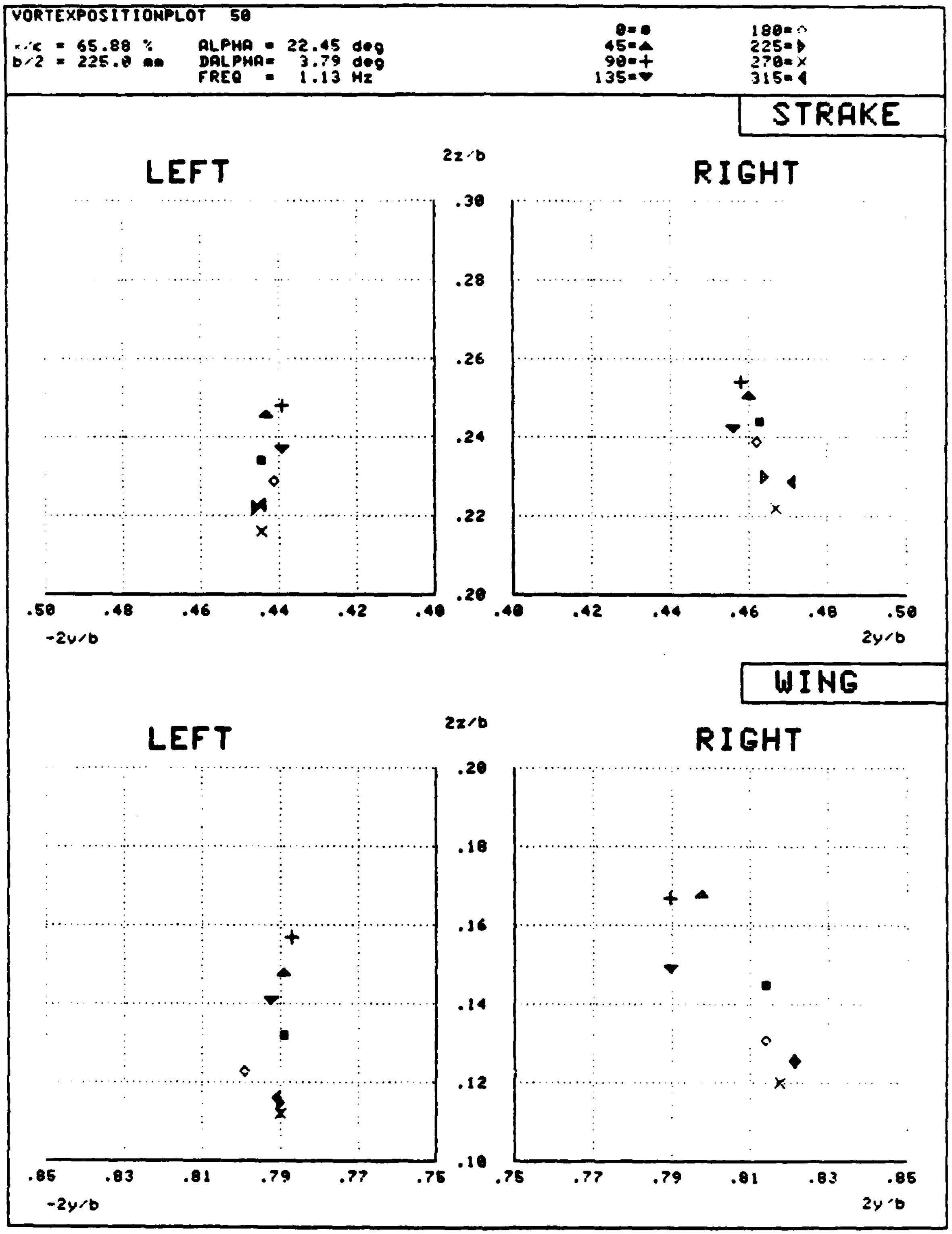

Fig. 36 Time history of the vortex core positions at section 2
(α = 22.45 deg, dα = 3.79 deg, f = 1.13 Hz)

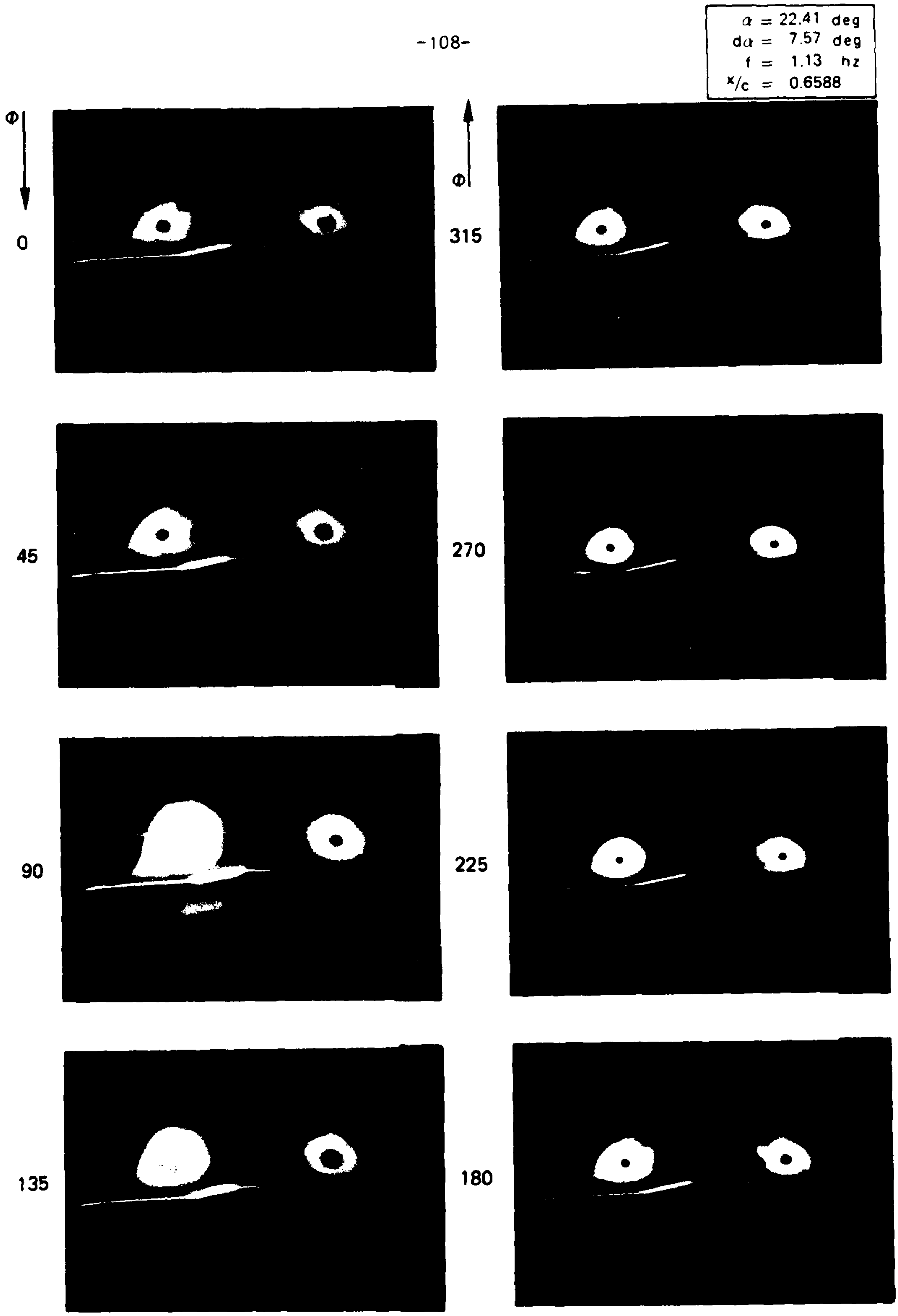

Fig. 37 Photographs showing the time history of the flow at section 2 (α = 22.41 deg, $d\alpha$ = 7.57 deg, f = 1.13 Hz)

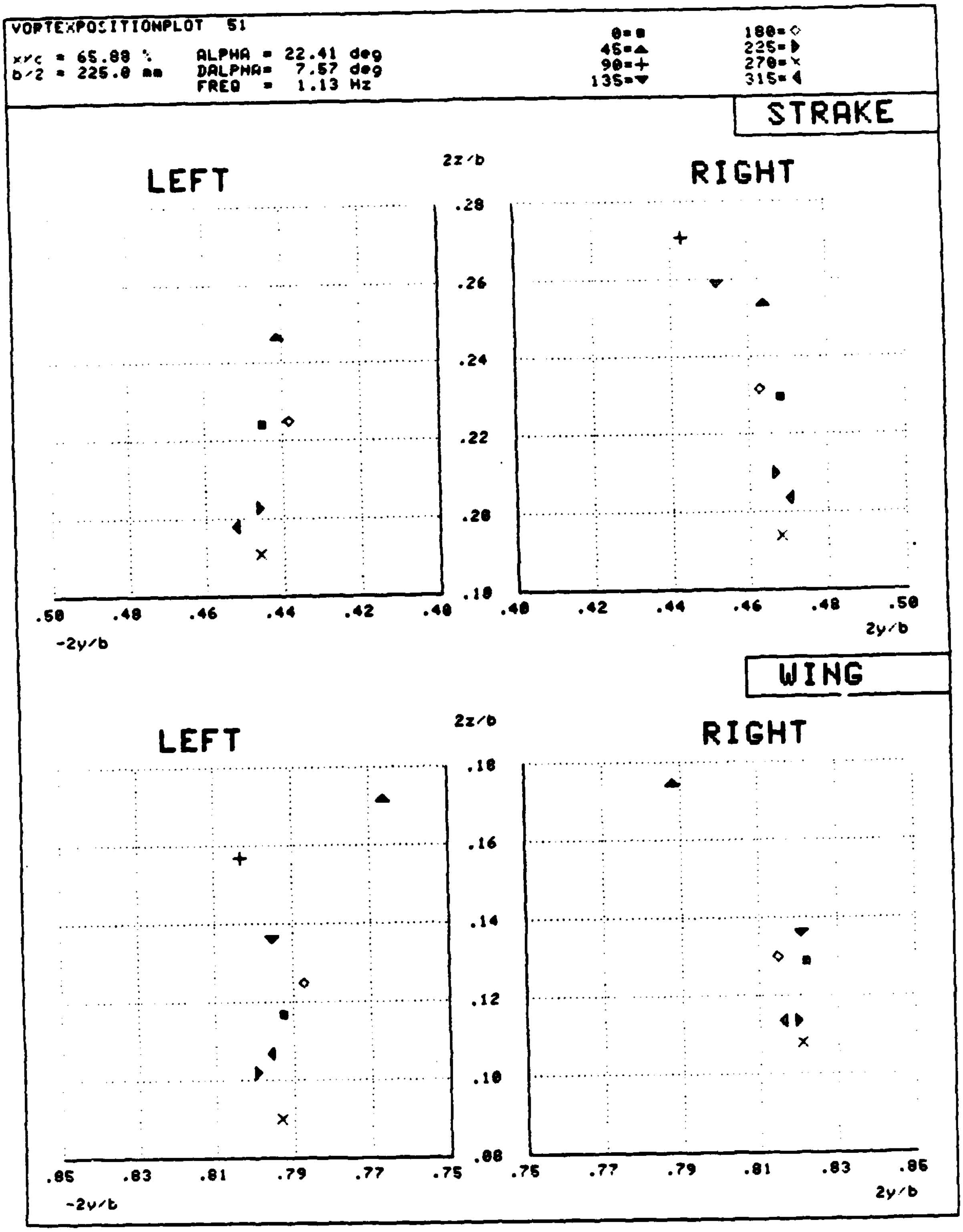

Fig. 38 Time history of the vortex core positions at section 2
(α = 22.41 deg, $d\alpha$ = 7.57 deg, f = 1.13 Hz)

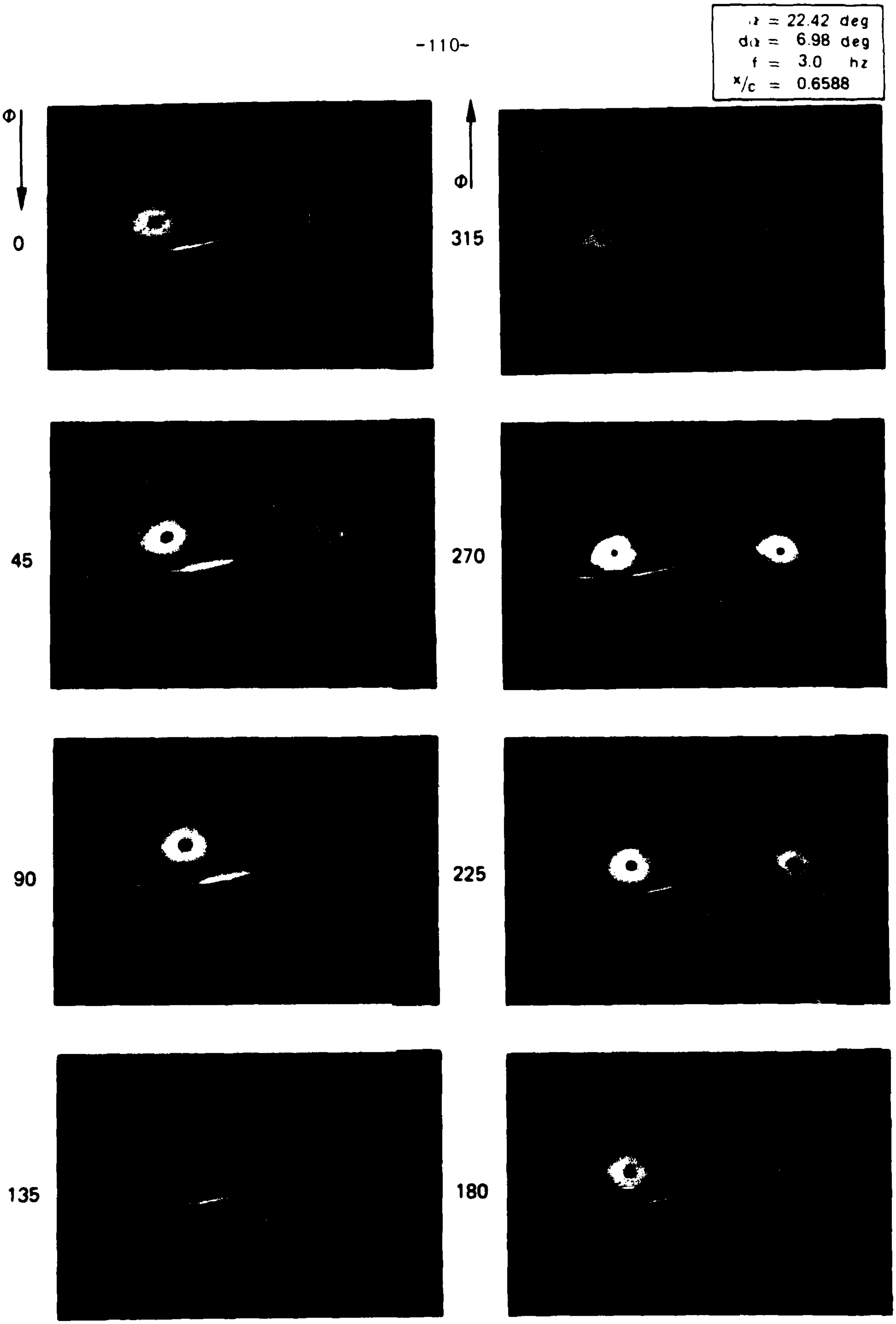

Fig. 39 Photographs showing the time history of the flow at section 2 (α = 22.42 deg, d_α = 6.98 deg, f = 3 Hz)

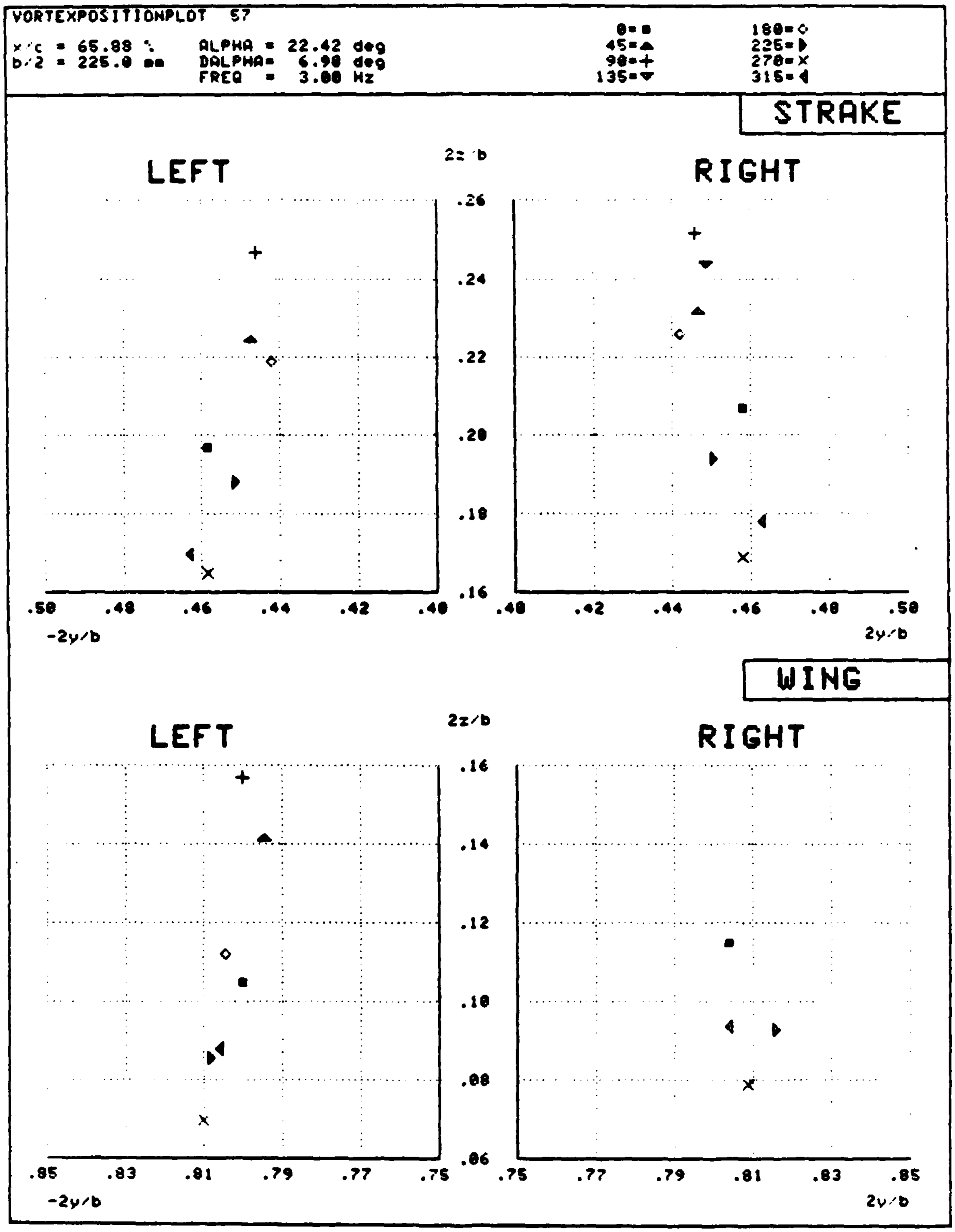

Fig. 40 Time history of the vortex core positions at section 2 (α = 22.42 deg, $d\alpha$ = 6.98 deg, f = 3 Hz)

α = 22.42 deg
$d\alpha$ = 6.88 deg
f = 6.0 hz
x/c = 0.6588

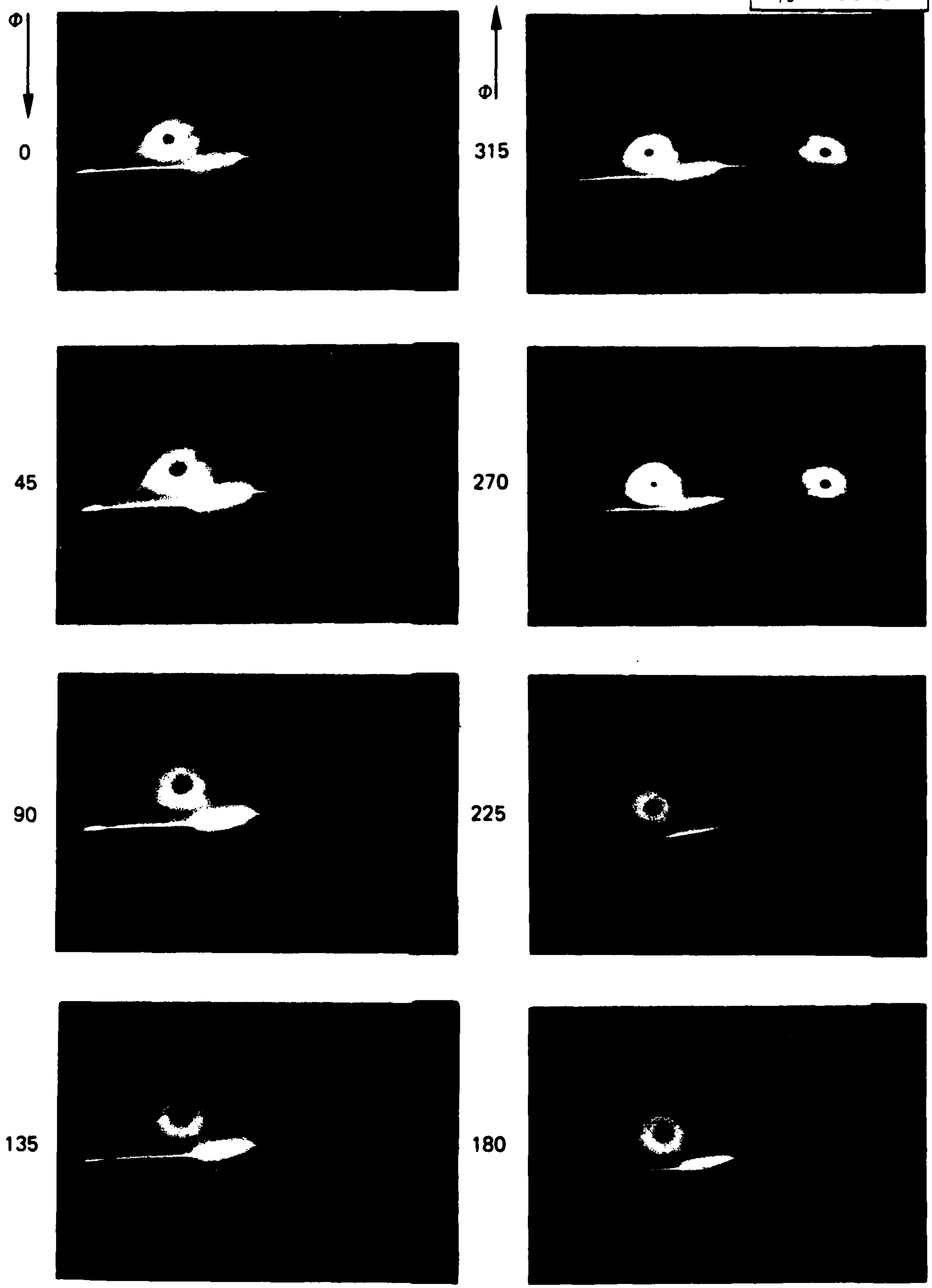

Fig. 41 Photographs showing the time history of the flow at section 2 (α = 22.42 deg, $d\alpha$ = 6.88 deg, f = 6 Hz)

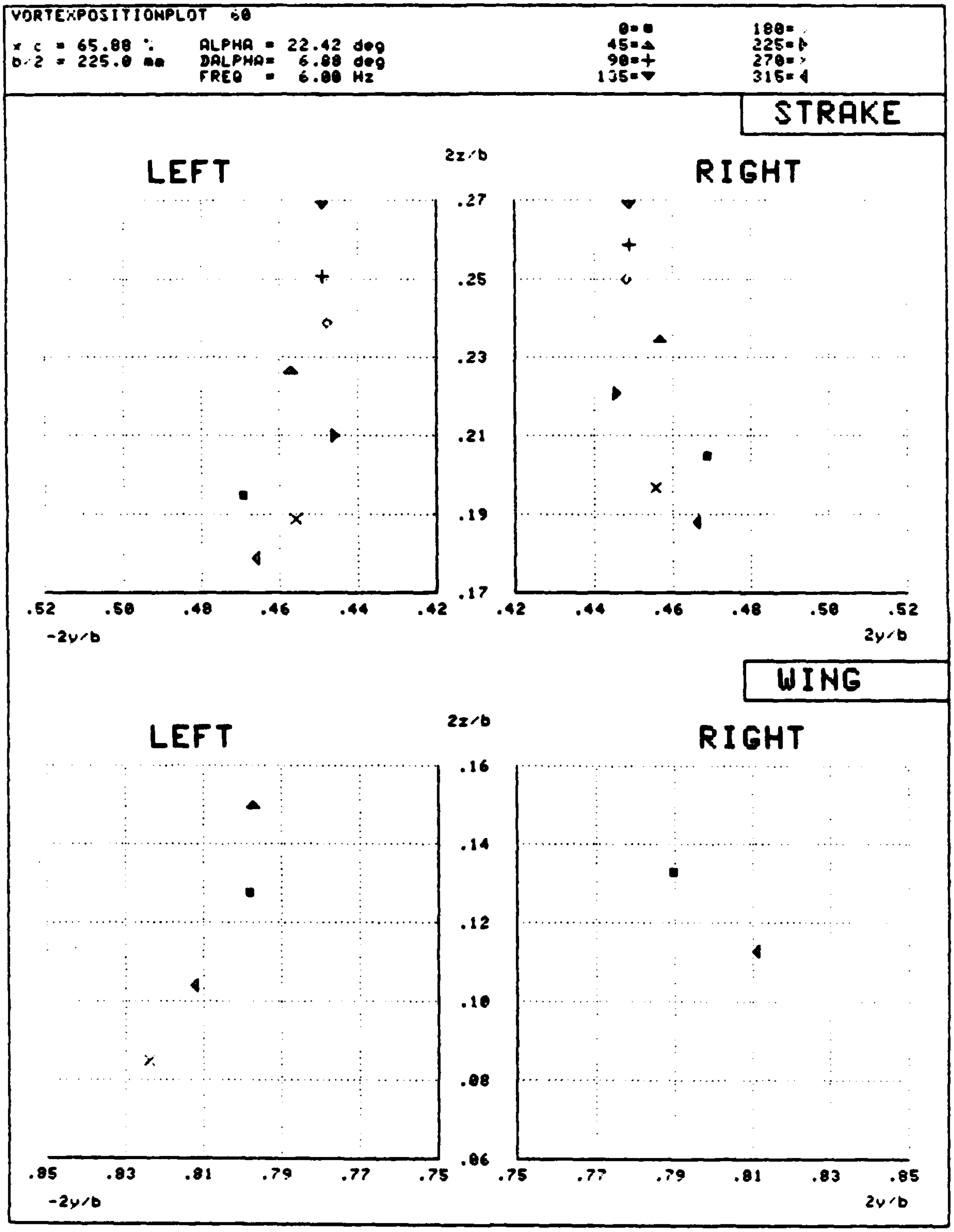

Fig. 42 Time history of the vortex core positions at section 2
(α = 22.42 deg, $d\alpha$ = 6.88 deg, f = 6 Hz)

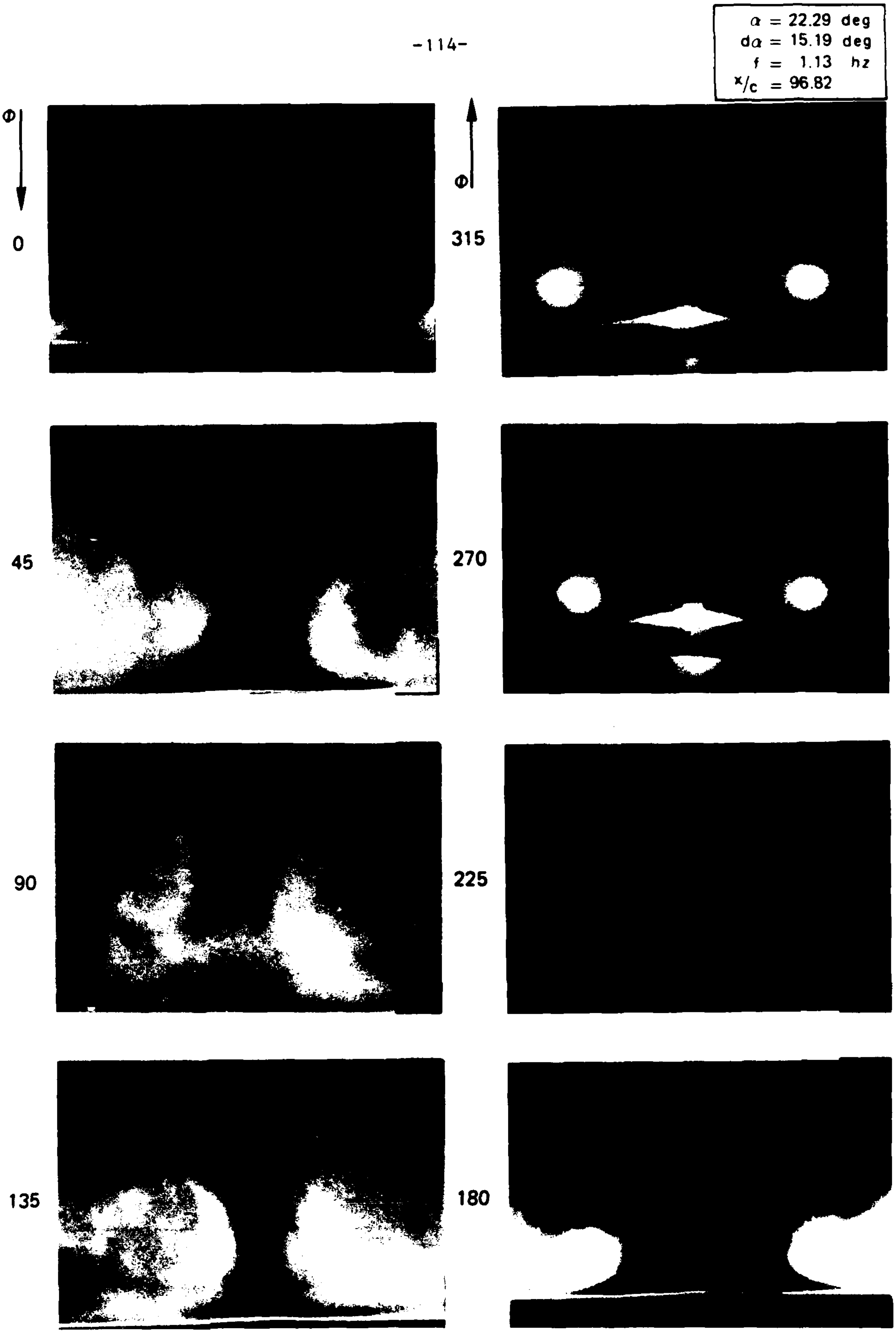

Fig. 43 Photographs showing the time history of the flow at section 3 (α = 22.29 deg, d_α = 15.19 deg, f = 1.13 Hz)

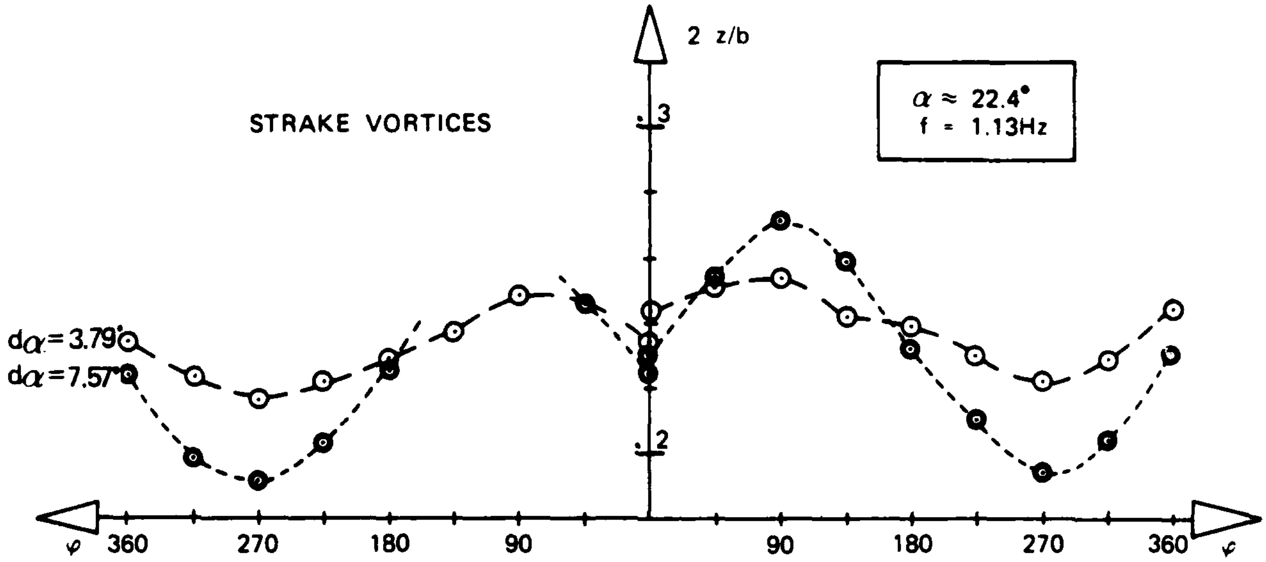

Fig. 44 Influence of amplitude on the time history of the vortex core positions

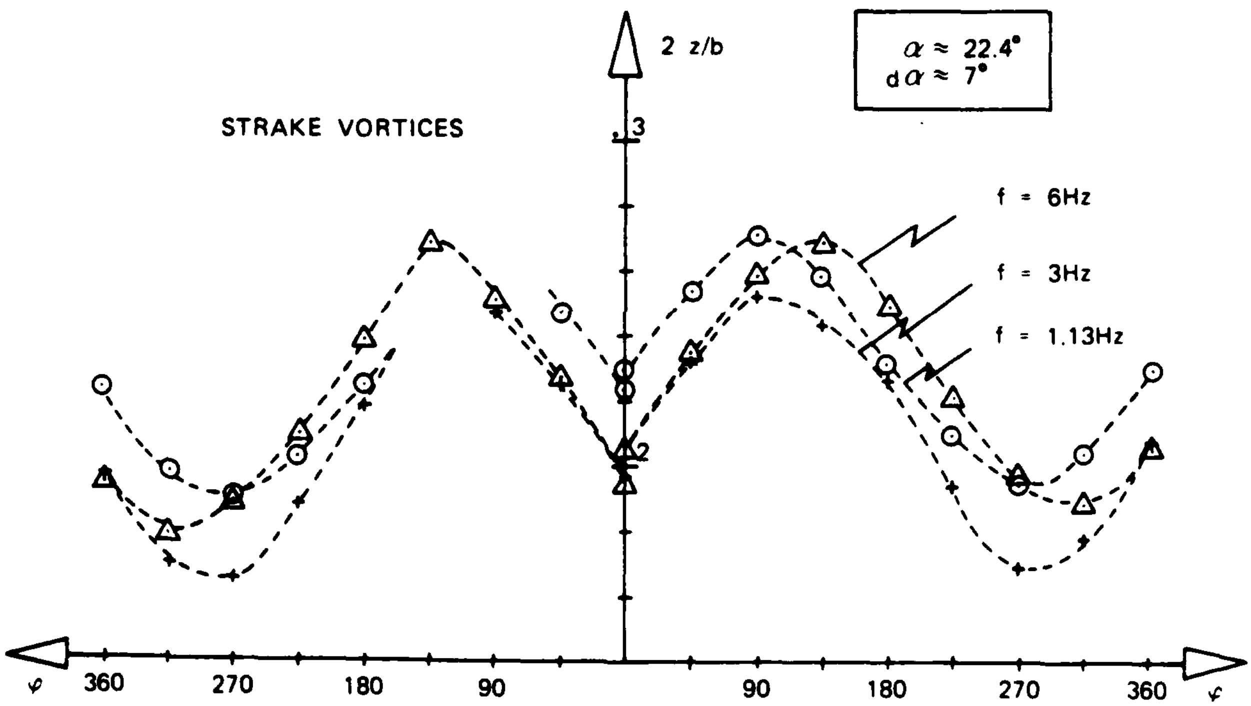

Fig. 45 Influence of frequency on the time history of the vortex core positions

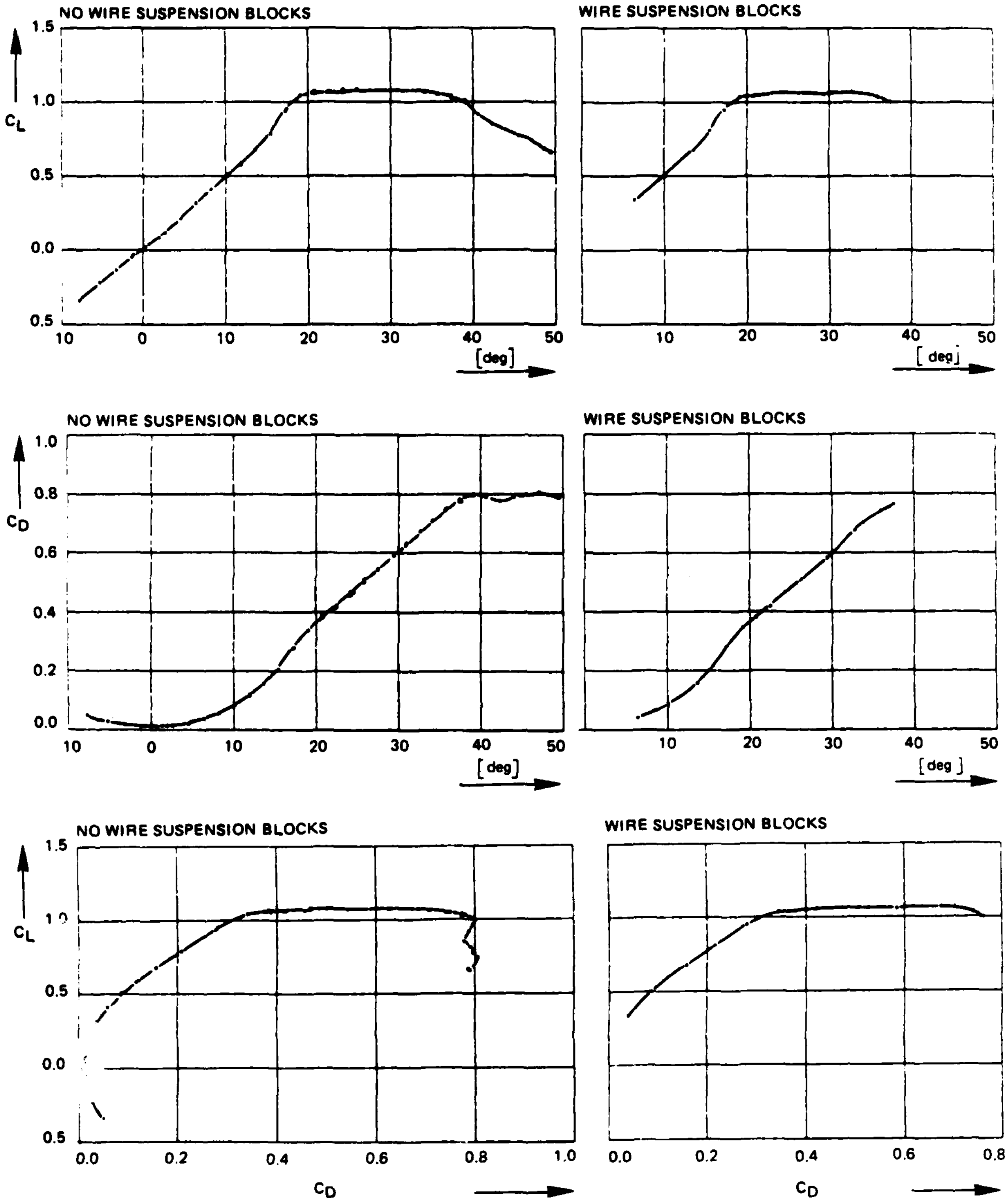

Fig. 46 The effect of the wire suspension blocks

APPENDIX A

MODEL GEOMETRY AND DIMENSIONS

span	800.0 mm
root chord	785.495 mm
tip chord	120.0 mm
sweep angle strake leading edge	76 deg
sweep angle wing leading edge	40 deg
area (wing + strake)	.264 m^2
airfoil of wing	NACA 64A005
aspect ratio	2.422 m
mean aerodynamic chord	.320 m
pitching axis	at 73.29 %cr

chordwise section no.	2y/b	c(mm)
1	+.30000	354.715
1	-.30000	354.755
2	+.63750	241.350
2	-.63750	241.410
3	+.97500	128.315
3	-.97500	128.340
4	.00000	785.495

spanwise section no.	2y/b	c(mm)
5	.12731	25.000
6	.31827	62.500
7	.50923	100.000
8	.87269	400.000
9	.93635	400.000

Note 1: All x-coordinates are measured relative to the leading edge of the local chord (see also figure A-1)

TABLE A1
Thickness distribution of section 1

SECTION 1		SECTION 1		SECTION 1		SECTION 1	
UPPER SIDE		LOWER SIDE		UPPER SIDE		LOWER SIDE	
2y/b = +.3000		2y/b = +.3000		2y/b = -.3000		2y/b = -.3000	
c = 354.715 mm		c = 354.715 mm		c = 354.755 mm		c = 354.755 mm	
x/c	z/c	x/c	z/c	x/c	z/c	x/c	z/c
0.00000	-.00024	.00003	-.00062	0.00000	-.00047	.00010	0.00000
.00004	0.00000	.00004	-.00092	.00001	0.00000	.00011	-.00075
.00017	.00037	.00017	-.00134	.00011	.00025	.00014	-.00092
.00025	.00062	.00027	-.00168	.00020	.00062	.00016	-.00062
.00041	.00092	.00070	-.00227	.00028	.00066	.00023	-.00135
.00072	.00124	.00078	-.00244	.00034	.00092	.00042	-.00168
.00100	.00168	.00151	-.00300	.00082	.00145	.00082	-.00213
.00152	.00197	.00316	-.00379	.00093	.00168	.00109	-.00244
.00190	.00244	.00488	-.00430	.00163	.00216	.00163	-.00279
.00316	.00307	.00740	-.00488	.00187	.00244	.00327	-.00355
.00489	.00375	.01240	-.00591	.00326	.00313	.00500	-.00407
.00740	.00450	.02491	-.00818	.00500	.00383	.00751	-.00474
.01240	.00574	.04993	-.01154	.00751	.00458	.01252	-.00588
.02491	.00808	.07495	-.01400	.01252	.00581	.02502	-.00827
.04993	.01136	.09995	-.01593	.02502	.00806	.02784	-.00874
.07493	.01380	.14999	-.01900	.05003	.01132	.05003	-.01166
.09995	.01573	.20002	-.02131	.07504	.01377	.07504	-.01409
.14999	.01879	.25006	-.02302	.10005	.01573	.10005	-.01604
.20002	.02109	.30009	-.02417	.15009	.01880	.15009	-.01710
.25006	.02279	.35013	-.02485	.20011	.02111	.20011	-.02142
.30009	.02391	.40015	-.02498	.25014	.02279	.25014	-.02311
.35013	.02458	.45019	-.02446	.30016	.02390	.30016	-.02421
.40015	.02471	.50022	-.02344	.35020	.02459	.35021	-.02488
.45019	.02420	.55026	-.02196	.40022	.02475	.40022	-.02505
.50022	.02315	.60028	-.02013	.45025	.02426	.45025	-.02450
.55026	.02167	.64236	-.01838	.50027	.02320	.50027	-.02344
.60028	.01983	.65616	-.01775	.55030	.02171	.55031	-.02194
.65031	.01773	.70035	-.01566	.60033	.01987	.60033	-.02014
.70035	.01538	.75038	-.01308	.65035	.01776	.65035	-.01804
.75038	.01286	.80042	-.01052	.70038	.01543	.70038	-.01567
.80042	.01030	.85044	-.00791	.75041	.01291	.75041	-.01316
.85044	.00772	.90048	-.00531	.80044	.01035	.80044	-.01060
.90048	.00513	.95051	-.00281	.85046	.00775	.80057	-.01058
.95051	.00262	.99999	-.00044	.90049	.00516	.85046	-.00798
1.00000	0.00000			.95052	.00269	.90049	-.00533
				1.00000	.00032	.95052	-.00276
						1.00000	-.00016

TABLE A2
Thickness distribution of section 2

SECTION 2		SECTION 2		SECTION 2		SECTION 2	
UPPER SIDE		LOWER SIDE		UPPER SIDE		LOWER SIDE	
2y/b = +.6375		2y/b = +.6375		2y/b = -.6375		2y/b = -.6375	
c = 241.350 mm		c = 241.350 mm		c = 241.410 mm		c = 241.410 mm	
x/c	z/c	x/c	z/c	x/c	z/c	x/c	z/c
0.00000	0.00000	0.00000	0.00000	0.00000	.00062	.00027	0.00000
.00012	.00062	.00004	-.00093	.00008	0.00000	.00037	-.00062
.00025	.00087	.00025	-.00128	.00031	.00168	.00054	-.00104
.00027	.00091	.00041	-.00168	.00054	.00184	.00058	-.00093
.00070	.00168	.00106	-.00230	.00124	.00244	.00097	-.00168
.00108	.00199	.00114	-.00244	.00137	.00244	.00137	-.00205
.00155	.00244	.00269	-.00327	.00298	.00325	.00180	-.00244
.00269	.00288	.00278	-.00340	.00313	.00340	.00298	-.00309
.00363	.00340	.00354	-.00379	.00474	.00389	.00348	-.00340
.00445	.00360	.00445	-.00398	.00721	.00468	.00474	-.00385
.00694	.00435	.00694	-.00476	.01224	.00590	.00723	-.00468
.01195	.00559	.01195	-.00605	.02475	.00822	.01222	-.00592
.02447	.00787	.02447	-.00833	.04979	.01137	.02475	-.00824
.04951	.01108	.04951	-.01162	.07481	.01379	.04979	-.01154
.07454	.01353	.07454	-.01403	.09983	.01574	.07481	-.01394
.09957	.01548	.10043	-.01601	.14989	.01883	.08744	-.01497
.14964	.01852	.14964	-.01898	.19995	.02106	.10308	-.01613
.19971	.02080	.19971	-.02132	.24999	.02274	.14989	-.01903
.24976	.02246	.24976	-.02300	.30005	.02388	.19995	-.02135
.29983	.02360	.29983	-.02418	.35011	.02450	.24999	-.02307
.34991	.02428	.34991	-.02480	.40017	.02456	.30005	-.02419
.39998	.02443	.39998	-.02490	.45021	.02405	.35011	-.02483
.45003	.02391	.45003	-.02438	.50027	.02307	.40017	-.02496
.50010	.02289	.50010	-.02337	.55033	.02162	.45021	-.02448
.55018	.02142	.55018	-.02188	.60037	.01976	.50027	-.02342
.60023	.01960	.60023	-.02003	.65043	.01769	.55033	-.02193
.65030	.01753	.65030	-.01782	.70049	.01541	.60037	-.02013
.70037	.01523	.70037	-.01560	.75053	.01292	.65043	-.01804
.75042	.01272	.75042	-.01305	.80059	.01034	.70049	-.01531
.80050	.01013	.80050	-.01044	.85065	.00777	.75053	-.01317
.85057	.00750	.85055	-.00783	.90069	.00524	.80059	-.01052
.90062	.00493	.90062	-.00526	.95075	.00282	.84124	-.00833
.95069	.00240	.95069	-.00276	1.00000	.00048	.85065	-.00783
1.00000	-.00017	.99985	-.00041			.86784	-.00690
						.89443	-.00547
						.90069	-.00514
						.92103	-.00406
						.94762	-.00265
						.95075	-.00249
						.97421	-.00130
						1.00000	.00004

TABLE A3
Thickness distribution of section 3

SECTION 3		SECTION 3		SECTION 3		SECTION 3	
UPPER SIDE		LOWER SIDE		UPPER SIDE		LOWER SIDE	
2y/b = +.9750		2y/b = +.9750		2y/b = -.9750		2y/b = -.9750	
c = 128.315 mm		c = 128.315 mm		c = 128.340 mm		c = 128.340 mm	
x/c	z/c	x/c	z/c	x/c	z/c	x/c	z/c
0.00000	0.00000	.00023	-.00062	0.00000	.00062	.00023	0.00000
.00012	0.00000	.00027	-.00094	.00008	.00168	.00051	-.00066
.00019	.00070	.00047	-.00168	.00016	0.00000	.00055	-.00094
.00023	.00062	.00097	-.00195	.00051	.00187	.00074	-.00168
.00027	.00094	.00109	-.00245	.00101	.00245	.00129	-.00230
.00066	.00168	.00210	-.00339	.00129	.00238	.00136	-.00245
.00097	.00183	.00261	-.00331	.00292	.00308	.00230	-.00339
.00132	.00245	.00323	-.00401	.00308	.00339	.00292	-.00327
.00261	.00296	.00436	-.00401	.00467	.00362	.00370	-.00401
.00284	.00339	.00686	-.00483	.00717	.00436	.00460	-.00409
.00436	.00347	.01188	-.00604	.01219	.00549	.00717	-.00503
.00686	.00417	.02439	-.00822	.02470	.00783	.01219	-.00623
.01188	.00526	.04941	-.01153	.04971	.01103	.02470	-.00842
.02439	.00764	.07443	-.01383	.07472	.01344	.04971	-.01165
.04941	.01091	.09940	-.01570	.09970	.01543	.07472	-.01406
.07443	.01329	.14944	-.01878	.14972	.01847	.09970	-.01609
.09940	.01531	.19947	-.02112	.19974	.02077	.14972	-.01917
.14944	.01839	.24950	-.02272	.24977	.02244	.19974	-.02151
.19947	.02073	.29954	-.02389	.29979	.02361	.24977	-.02326
.24950	.02241	.34957	-.02451	.34981	.02431	.29979	-.02443
.29954	.02369	.39960	-.02459	.39984	.02454	.34981	-.02505
.34957	.02439	.44964	-.02404	.39984	.02447	.39984	-.02517
.39960	.02455	.49967	-.02295	.44986	.02392	.44986	-.02470
.39960	.02459	.54970	-.02143	.49988	.02287	.49988	-.02361
.44956	.02412	.59973	-.01952	.54991	.02131	.54991	-.02221
.49967	.02307	.64973	-.01738	.59993	.01948	.59993	-.02041
.54970	.02159	.69820	-.01500	.64991	.01738	.64991	-.01851
.59973	.01980	.69976	-.01492	.69994	.01480	.69994	-.01570
.64973	.01777	.74976	-.01243	.74996	.01223	.74996	-.01321
.69976	.01531	.79983	-.00986	.79998	.00978	.79998	-.01044
.74980	.01270	.84986	- 00721	.85001	.00729	.85001	-.00775
.79983	.01009	.89989	-.00460	.90003	.00483	.89999	-.00514
.84986	.00740	.94993	-.00218	.95005	.00242	.95005	-.00284
.89989	.00483	.99852	-.00019	1.00000	.00312	.99856	-.00090
.94993	.00245						
.99844	.00051						
1.00000	.00312						

TABLE A4

Thickness distribution of section 4

SECTION 4			
upper side		lower side	
2y/b = 0.0		2y/b = 0.0	
cr = 785.495 mm		cr = 785.495 mm	
x/cr	z/cr	x/cr	z/cr
.57547	.02798	.57685	-.02806
.72125	.02915		
.73357	.02798		
.82962	.02799	.81258	-.02805

TABLE A5

Thickness distributions of sections 5 through 9

UPPER SIDE		LOWER SIDE		UPPER SIDE		LOWER SIDE	
SECTION 5 x/cr = .12731 b/2 = 25 mm							
2y/b	2z/b	2y/b	2z/b	2y/b	2z/b	2y/b	2z/b
.93420	.01140	.93420	-.00940	-.93420	.01100	-.93420	-.00980
.54220	.09060	.54220	-.08800	-.54220	.08980	-.54220	-.08840
.22840	.15360	.22840	-.15140	-.22840	.15280	-.22840	-.15140
SECTION 6 x/cr = .31827 b/2 = 62.5 mm							
2y/b	2z/b	2y/b	2z/b	2y/b	2z/b	2y/b	2z/b
.97752	.00320	.97760	-.00416	-.97752	.00360	-.97752	-.00416
.57048	.08504	.57048	-.08608	-.57048	.08552	-.57048	-.08608
.25032	.14944	.25032	-.15016	-.25032	.14992	-.25032	-.15016
SECTION 7 x/cr = .50923 b/2 = 100 mm							
2y/b	2z/b	2y/b	2z/b	2y/b	2z/b	2y/b	2z/b
.98155	.00610	.98155	-.00720	-.98155	.00605	-.98155	-.00690
.53045	.09340	.53045	-.09470	-.53045	.09360	-.53045	-.09435
.09770	.18055	.09770	-.18180	-.09770	.18115	-.09770	-.18135
SECTION 8 x/cr = .87269 b/2 = 400 mm							
2y/b	2z/b	2y/b	2z/b	2y/b	2z/b	2y/b	2z/b
.15000	.00241	.15000	-.00244	-.15000	.00241	-.15000	-.00242
.07500	.00340	.07500	-.00343	-.07500	.00340	-.07500	-.00342
SECTION 9 x/cr = .93635 b/2 = 400 mm							
2y/b	2z/b	2y/b	2z/b	2y/b	2z/b	2y/b	2z/b
.15000	.00120	.15000	-.00122	-.15000	-.00120	-.15000	-.00122
.07500	.00169	.07500	-.00172	-.07500	-.00170	-.07500	-.00171

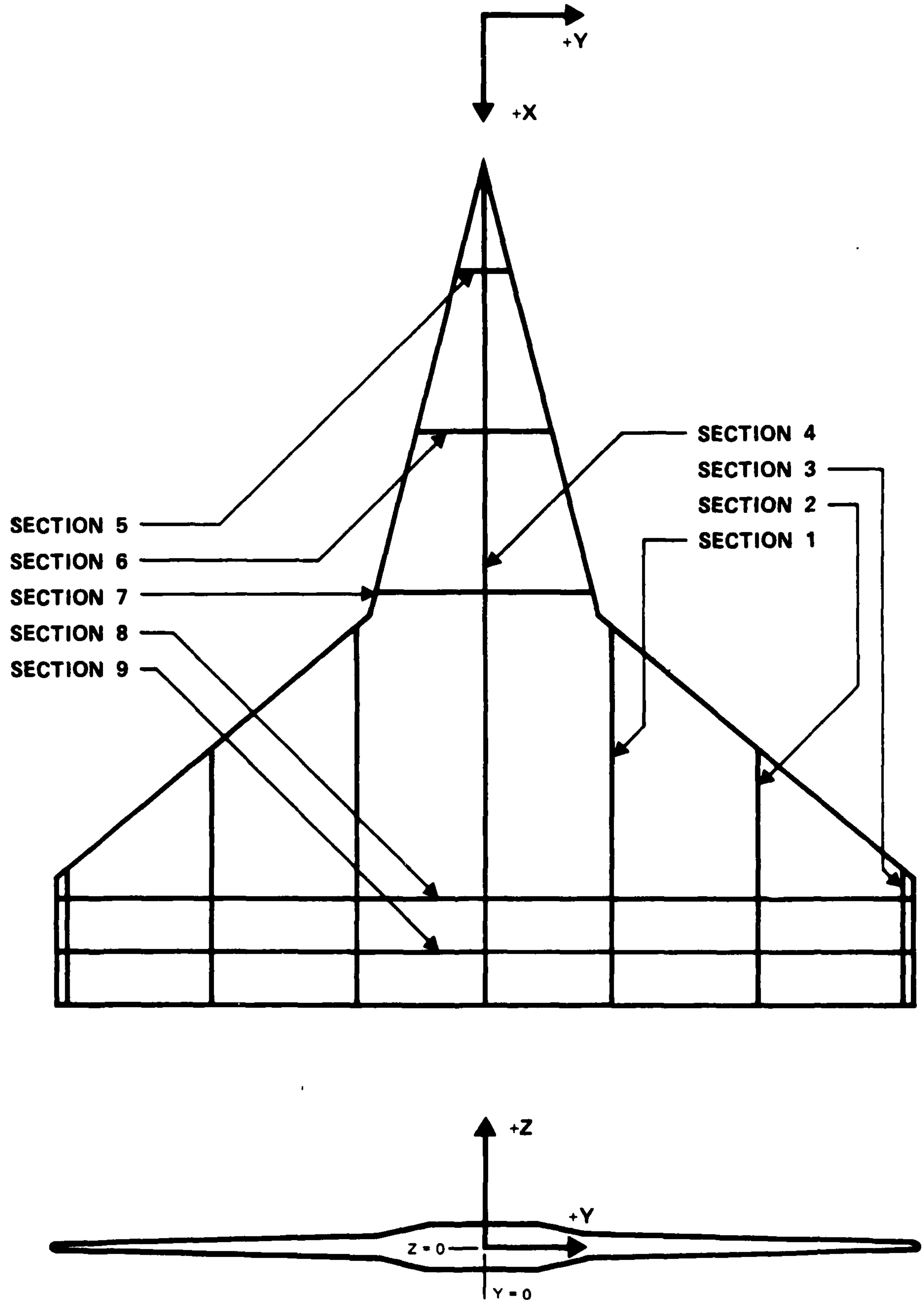

Fig. A1 Coordinate reference system and section positions

APPENDIX B

NON-AERODYNAMIC LOADS ON THE MODEL BALANCE

CONTENTS

LIST OF SYMBOLS

alf	wing incidence	(deg,rad)
$\dot{\text{alf}}$	wing angular velocity	(rad/s**2)
$\ddot{\text{alf}}$	wing angular acceleration	(kgm)
C_{mo_1}	model Constant ($M*dx_{c.g.}$) (see section 2)	(kgm)
C_{mo_2}	model Constant ($J_{y_{r.a.}} - M*dx_{c.g.}*dx_{b.c}$) (see section 2)	(kgm**^{2})
dx	distance in wing reference plane (see figure B.1)	(m)
f	frequency	(Hz)
g	gravitational acceleration	(m/s**2)
J_y	moment of inertia about axis parallel to y-axis	(kgm**2)
l	wing rolling moment (see figure B.1)	(Nm)
m	wind pitching moment (see figure B.1) ref. axis through balance center	(Nm)
M	mass (see section 2)	(kg)
N	wing normal force (see figure B.1)	(Nm)
n	wing yawing moment (see figure B.1)	(Nm)
T	wing tangential force (see figure B.1)	(N)
t	time	(s)
x	chordwise coordinate in wing reference plane; apex; x=0 (see figure B.1)	(m)
Y	wing force in y-direction (see figure B.1)	(N)
y	spanwise coordinate in wing reference plane (see figure B.1)	(m)
z	coordinate in plane of symmetry normal to wing	(m)

SUBSCRIPTS

0	zeroth order harmonic components
1	first order harmonic components
b	balance
b.c.	balance center
c.g.	center of gravity
g	gravity
i	inertia
mo	model
r.a.	rotation axis

1 LOADS ON THE MODEL BALANCE

The balance in the model measures:

- aerodynamic loads
- inertial loads
- gravitational loads
- wireloads caused by the electrical wires of the miniature pressure transducers and accelerometers leading from the model to the support system.

From wind-off tests it was concluded that the wireloads were extremely small. Therefore no correction for these loads was applied.

Gravitational loads on the balance are:

$$N_g = -M * g * \cos(alf) \quad (1)$$

$$T_g = +M * g * \sin(alf) \quad (2)$$

$$m_g = +M * g * (dx_{b.c.} - dx_{c.g.}) * \cos(alf) \quad (3)$$

Inertial loads on the balance are:

$$N_i = -M * dx_{c.g.} * \ddot{alf} \quad = -C_{mo_1} * \ddot{alf} \quad (4)$$

$$T_i = -M * dx_{c.g.} * (\dot{alf})^2 \quad = -C_{mo_1} * (\dot{alf})^2 \tag{5}$$

$$m_i = m_{i_{c.g.}} + N_i * (dx_{c.g.} - dx_{b.c.})$$

$$= -J_{y_{c.g.}} * \ddot{alf} - M * dx_{c.g.} * \ddot{alf} * (dx_{c.g.} - dx_{b.c.})$$

$$= \{-J_{y_{c.g.}} - M * dx^2_{c.g.}\} * \ddot{alf} + M * dx_{c.g.} * dx_{b.c.} * \ddot{alf}$$

$$= -J_{y_{r.a.}} * \ddot{alf} + M * dx_{c.g.} * dx_{b.c.} * \ddot{alf}$$

$$= -C_{mo_2} * \ddot{alf} \tag{6}$$

When the wing performs a harmonic pitching oscillation, described by $alf = alf_0 + alf_1 * \sin(2.pi.f.t)$,
the zeroth and first order harmonic components *of the inertial loads* become:

$$N_{i_1} = \quad C_{mo_1} * alf_1 * [(2.pi.f)**2] \tag{7}$$

$$T_{i_0} = -\tfrac{1}{2} * C_{mo_1} * [alf_1.2.pi.f]**2 \tag{8}$$

$$m_{i_1} = \quad C_{mo_2} * alf_1 * [(2.pi.f)**2] \tag{9}$$

2 MASS AND INERTIA PROPERTIES

This section describes how the constants M, C_{mo_1}, C_{mo_2}, $dx_{c.g.}$, $dx_{b.c}$, which show up in the formulae in section 1, are determined for this test setup.

Before the start of the windtunnel test, a very small mass was added to one of the wing tips, to position the center of gravity in the plane of symmetry of the model.
When the model is mounted on the balance, a part of the balance may be considered to move as an integral part of the model.

That part yields additional gravitational and inertial loads on the balance itself. Therefore, in the determination of the gravitational and inertial loads, the mass (M) and moment of inertia (C_{mo_2}) and the location of the center of gravity ($dx_{c.g.}$), of the wing and the part of the balance clamped to the model, must be used. These values are determined as follows:

- the mass is determined by positioning the model on the balance at different angles of attack and applying the formulae (1) and (2) ----> M

- by knowing the mass of the model only, also the mass of the part of the balance is known. Form the construction of that part its location of the c.g. can be determined. In combination with the c.g. and the mass of the wing only, the c.g. corresponding to the mass M, is determined ----> $dx_{c.g.}$

- $dx_{c.g.} * M =$ ----> C_{mo_1}

- by oscillating the model (at wind-off), the constant C_{mo_2} is determined ----> C_{mo_2}

- the location of the balance center is determined by the construction of the balance and the positioning of the balance with respect to the model ----> $dx_{b.c.}$

3 VARIOUS REMARKS

1. In the design of the model, it was decided to place the balance center a little forward of the rotation axis, providing a more smooth contouring of the thicker part of the model, containing the balance, on to the thin trailing edge. Consequently, also the center of gravity moved forward and so, both the b.c. and c.g. were not located in the rotation axis and the corrections (3), (4) and (5) (see section 1) became necessary.
2. The right way to determine the moment of inertia C_{mo_2} would have been vibrating the model in vacuum, measuring the output m_i of the balance

and $\ddot{\text{alf}}$ and application of formula (6). However, the measurement was done in the windtunnel at wind-off conditions. The effect of still air reactions was estimated to be small.

3. Because the b.c. was not located in the rotation axis, deformation of the balance would cause a change in the location of effective rotation axis. This effect was assumed to be small.
4. The maximum absolute value of the inertial and gravitational loads are:

$N_g = 70$ (alf = 0 deg)

$T_g = 50$ (alf = 50 deg)

$m_g = 0.35$ (alf = 0 deg)

$N_i = 75$ ($\ddot{\text{alf}} = 300$)

$N_{i_1} = 75$ ($\text{alf}_1 = 1.75$ deg, f = 16 Hz)

$T_i = 16$ ($\dot{\text{alf}} = 8$)

$T_{i_0} = 8$ ($\text{alf}_1 = 15$ deg, f = 5 Hz)

$m_i = 36$ ($\ddot{\text{alf}} = 300$)

$m_{i_i} = 36$ ($\text{alf}_1 = 1.75$ deg, f = 16 Hz)

5. The ratio between aerodynamic loads and non-aerodynamic loads depends on the incidence, angular velocity and angular acceleration. For the major part of the test runs, the non-aerodynamic loads are small (less than 10 %) as compared to the aerodynamic loads.
6. Only the symmetrical components are corrected for inertia effects.

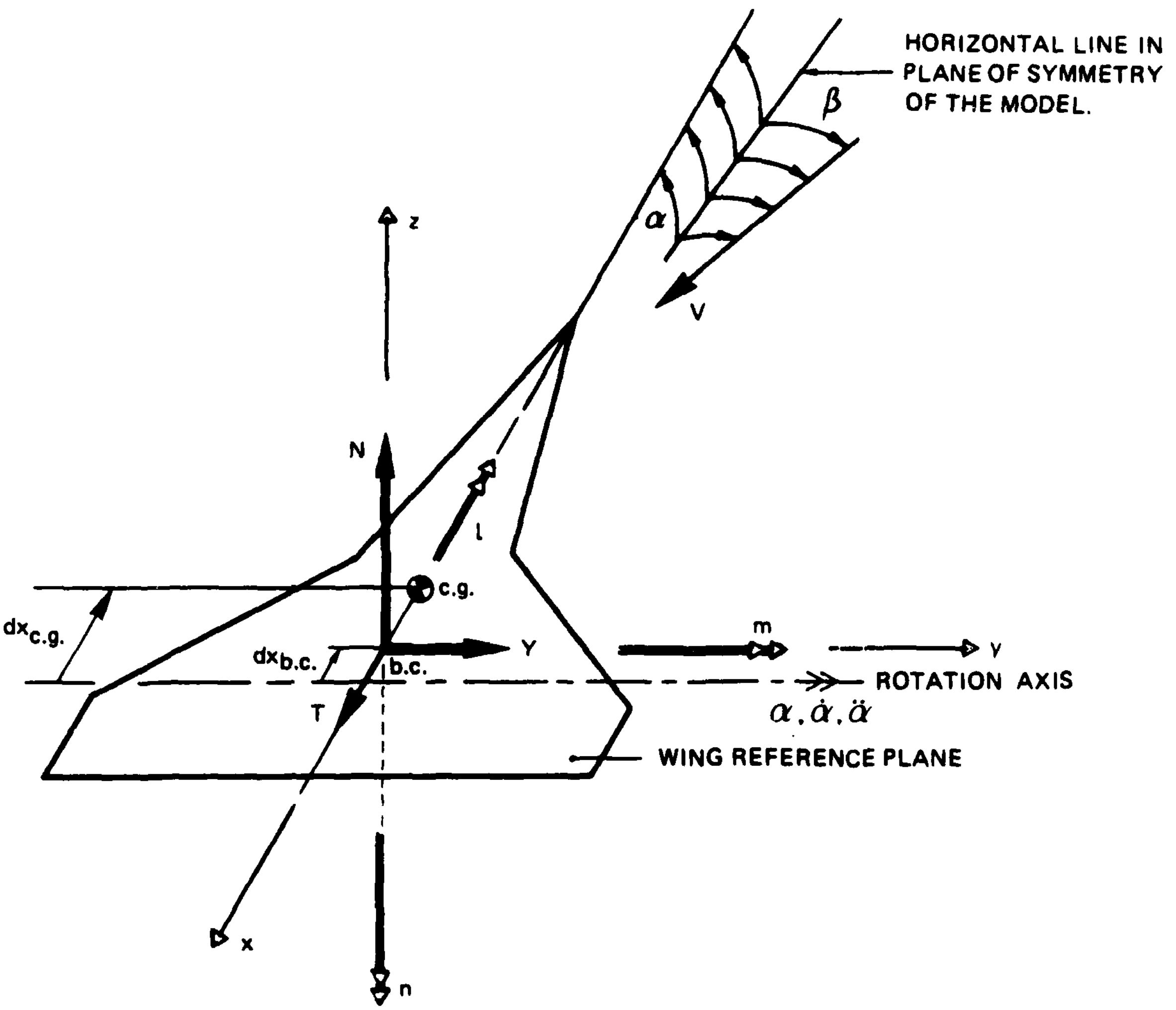

Fig. B1 Body-fixed coordinate system
Note: * y-axis through balance center
* wing reference plane is indicated in figure 5, Part I

APPENDIX C

UPDATED VALUES OF THE PITCHING MOMENT COEFFICIENT OF THE MODEL SUSPENDED IN WIRES

In report NLR TR 86047 C (reference 7) concerning "Force measurements in a low speed windtunnel on a model of the straked wing; suspended in wires", the values of the pitching moment coefficient were affected by the drag of the wires, which yield an additional pitching moment. Tables C1 through C7 and figure C1 present the correct pitching moment coefficients derived from only the force in the wire attached to the front part of the model.

NLR 1 ONLINE DATA-SYSTEM 1:48 PM THU., 22 OCT., 1987 PROC. 2 TEST 6602 SERIES 3 RUN 6 POL 1 PAGE 1

** CORR.ZERO DRIFT **

NATIONAL AEROSPACE LABORATORY (NLR) LST 3*2.25
DOUBLE DELTA FORCE MEASUREMENTS MEASURING DATE: 26- 2-1988

BETA = 0 degrees
At alpha > 20 degrees, a correction has been applied to Q

DPN	MACH	RE*E6	V	Q	ALFA	CL	CL^2	CD	CM	CC	CN	CR
64	.182	3.508	61.12	2392.5	-10.0	-.4803	.2307	.0945	-.0157	.0004	.0005	-.0005
65	.182	3.509	61.19	2397.0	-7.5	-.3666	.1344	.0587	-.0107	.0007	.0013	-.0014
66	.182	3.511	61.25	2400.8	-5.0	-.2339	.0547	.0331	-.0067	.0009	.0005	-.0006
67	.182	3.505	61.16	2393.5	-2.5	-.1067	.0114	.0210	-.0041	.0007	.0017	-.0018
68	.182	3.502	61.12	2390.6	.0	.0073	.0001	.0172	-.0013	.0002	-.0026	.0026
69	.182	3.499	61.12	2388.8	2.5	.1218	.0148	.0203	.0018	.0006	.0013	-.0014
70	.182	3.498	61.10	2387.2	5.0	.2542	.0646	.0330	.0048	.0003	.0018	-.0018
71	.182	3.495	61.09	2385.9	7.5	.3932	.1546	.0599	.0074	.0001	-.0010	.0009
72	.182	3.490	61.04	2380.8	10.0	.5051	.2551	.0950	.0148	-.0003	.0010	-.0010
73	.182	3.495	61.16	2389.9	12.5	.6238	.3889	.1401	.0220	.0003	.0022	-.0023
74	.182	3.494	61.17	2389.6	15.0	.7547	.5696	.2022	.0285	.0006	.0028	-.0029
76	.180	3.455	60.54	2339.8	17.5	.9669	.9349	.3000	.0314	-.0000	.0013	-.0013
77	.178	3.411	59.85	2285.2	20.0	1.0716	1.1483	.3802	.0431	-.0001	.0014	-.0014
78	.178	3.421	60.05	2299.8	22.5	1.0771	1.1602	.4360	.0801	-.0004	-.0018	.0018
79	.179	3.428	60.21	2310.9	25.0	1.1076	1.2268	.5028	.0699	-.0006	.0014	-.0013
80	.180	3.439	60.43	2327.8	27.5	1.0997	1.2093	.5837	.0784	.0002	.0005	-.0005
81	.175	3.355	59.04	2219.7	27.5	1.0940	1.1987	.5582	.0756	.0005	.0029	-.0030
82	.176	3.365	59.22	2232.9	30.0	1.1043	1.2194	.6264	.0841	-.0010	.0015	-.0014
83	.177	3.382	59.53	2256.2	32.6	1.1025	1.2155	.6996	.0903	.0029	-.0003	-.0002
84	.178	3.395	59.80	2275.7	35.1	1.0934	1.1955	.7594	.0934	.0028	.0027	-.0032
85	.178	3.404	59.98	2288.8	37.6	1.0545	1.1119	.8094	.1014	.0027	.0037	-.0043
86	.174	3.324	58.64	2186.5	37.5	1.0445	1.0910	.8000	.1037	.0023	.0044	-.0048
87	.175	3.333	58.81	2198.7	40.0	.9875	.9751	.8271	.0997	.0023	.0043	-.0047
88	.175	3.344	59.02	2214.1	42.5	.8755	.7665	.8041	.0704	.0008	.0008	-.0010

STOP

TABLE C1
Model with faired cavities at the wing lower side at M = 0.178

(NLR) OLIVE DATA-SYSTEM 1:48 PM THU., 22 OCT., 1987 PROC. 2 TEST 6602 SERIES 3 RUN 6 POL 5 PAGE 1

** CORR.ZERO DRIFT **

NATIONAL AEROSPACE LABORATORY (NLR) LST 3*2.25
DOUBLE DELTA FORCE MEASUREMENTS MEASURING DATE: 26- 2-1986

BETA = 0 degrees
At alpha > 20 degrees, a correction has been applied to Q

DPN	MACH	RE*E6	V	Q	ALFA	CL	CL^2	CD	CM	CC	CN	CR
89	.197	3.755	66.23	2789.7	-10.0	-.4783	.2288	.0953	-.0141	.0005	.0019	-.0019
90	.196	3.745	66.10	2777.9	-7.5	-.3636	.1322	.0607	-.0094	.0007	-.0001	-.0000
91	.196	3.746	66.17	2782.2	-5.0	-.2312	.0534	.0339	-.0062	.0003	.0016	-.0016
92	.196	3.746	66.16	2781.7	-2.5	-.1055	.0111	.0225	-.0031	.0011	.0008	-.0010
93	.196	3.746	66.20	2784.1	.0	.0090	.0001	.0180	-.0005	.0001	.0016	-.0016
94	.196	3.747	66.16	2780.2	2.5	.1238	.0153	.0208	.0024	.0004	.0012	-.0012
95	.196	3.744	66.24	2785.9	5.0	.2547	.0649	.0340	.0057	.0003	.0012	-.0012
96	.196	3.740	66.18	2780.6	7.5	.3899	.1520	.0602	.0088	.0003	.0017	-.0017
97	.196	3.739	66.23	2782.7	10.0	.5061	.2561	.0957	.0156	.0011	-.0002	-.0000
98	.197	3.741	66.31	2788.7	12.5	.6220	.3869	.1421	.0224	-.0001	.0013	-.0013
99	.196	3.736	66.24	2782.4	15.0	.7563	.5720	.2043	.0290	-.0002	.0020	-.0019
101	.196	3.735	66.30	2785.9	17.5	.9680	.9370	.3015	.0310	.0004	.0018	-.0019
102	.193	3.666	65.12	2686.7	17.5	.9691	.9391	.3017	.0311	-.0002	.0020	-.0019
103	.193	3.662	65.08	2682.7	20.0	1.0809	1.1684	.3849	.0418	-.0002	.0016	-.0015
104	.193	3.673	65.30	2699.5	22.5	1.0879	1.1834	.4401	.0585	-.0004	-.0007	.0007
105	.194	3.679	65.44	2710.8	25.0	1.1101	1.2324	.5058	.0698	-.0005	.0012	-.0011
106	.194	3.691	65.67	2729.1	27.5	1.1028	1.2161	.5664	.0756	.0012	.0018	-.0018
107	.191	3.620	64.46	2628.5	27.5	1.1029	1.2164	.5679	.0756	.0008	.0012	-.0014
108	.191	3.628	64.61	2640.5	30.0	1.1093	1.2306	.6285	.0856	-.0006	-.0001	.0002
109	.192	3.639	64.85	2658.6	32.5	1.1171	1.2478	.6963	.0928	.0008	.0009	-.0010
110	.193	3.655	65.15	2683.1	35.0	1.1050	1.2211	.7588	.1097	.0022	.0014	-.0018
113	.193	3.663	65.37	2699.5	37.5	1.0632	1.1304	.8207	.1021	.0038	.0048	-.0055
114	.190	3.596	64.23	2605.0	37.5	1.0600	1.1236	.8155	.1050	.0024	.0004	-.0009
115	.191	3.607	64.42	2619.9	40.0	.9961	.9921	.8396	.0961	.0053	.0020	-.0031
116	.191	3.621	64.69	2641.4	42.5	.8688	.7548	.8091	.0700	.0006	.0019	-.0020

STOP

TABLE C2
Model with faired cavities at the wing lower side at M = 0.193

(NLR) OLIVE DATA-SYSTEM 1:49 PM THU., 22 OCT., 1987 PROC. 2 TEST 6602 SERIES 3 RUN 6 POL 9 PAGE 1

** CORR.ZERO DRIFT **

NATIONAL AEROSPACE LABORATORY (NLR) LST 3*2.25
DOUBLE DELTA FORCE MEASUREMENTS MEASURING DATE: 26- 2-1986

BETA = 0 degrees
At alpha > 20 degrees, a correction has been applied to Q

TPN	MACH	RE*E6	V	Q	ALFA	CL	CL^2	CD	CM	CC	CN	CR
117	.074	1.409	25.14	399.4	-10.0	-.4734	.2241	.0925	-.0117	-.0004	-.0034	.0035
118	.074	1.411	25.15	400.0	-7.5	-.3572	.1276	.0549	-.0168	.0011	.0059	-.0061
119	.075	1.414	25.18	401.0	-5.0	-.2168	.0470	.0237	-.0119	.0051	.0106	-.0112
120	.075	1.415	25.19	401.6	-2.5	-.1016	.0103	.0171	-.0077	.0034	.0033	-.0037
121	.075	1.416	25.18	401.4	0.0	.0165	.0003	.0129	-.0057	.0024	-.0042	.0038
122	.075	1.417	25.19	401.8	2.5	.1360	.0185	.0061	.0004	.0050	.0055	-.0062
123	.075	1.417	25.18	401.6	5.0	.2669	.0713	.0184	.0048	.0019	.0016	-.0018
124	.075	1.417	25.17	401.3	7.5	.3948	.1559	.0451	.0095	.0045	.0011	-.0018
125	.074	1.416	25.15	400.7	10.0	.4906	.2407	.0810	.0198	.0024	-.0046	.0042
126	.074	1.415	25.12	399.7	12.5	.6035	.3642	.1262	.0304	.0025	-.0048	.0044
127	.074	1.413	25.06	398.2	15.0	.7292	.5318	.1850	.0409	.0040	.0013	-.0020
128	.074	1.409	24.99	395.8	17.5	.9268	.8589	.2776	.0477	.0027	-.0073	.0068
129	.074	1.410	24.99	396.1	20.0	1.0534	1.1097	.3604	.0580	-.0009	-.0070	.0072
130	.074	1.415	25.07	398.7	22.5	1.0373	1.0759	.4103	.0701	-.0001	-.0120	.0120
131	.075	1.420	25.13	401.0	25.0	1.0464	1.0949	.4649	.0792	-.0004	.0045	-.0045
132	.075	1.421	25.14	401.4	27.5	1.0634	1.1307	.5343	.0771	.0026	.0019	-.0024
133	.075	1.422	25.14	401.6	30.0	1.0857	1.1787	.6075	.0811	.0009	-.0065	.0063
134	.075	1.429	25.25	405.1	32.5	1.0715	1.1482	.6564	.1065	.0005	-.0018	.0017
135	.076	1.441	25.46	411.9	35.0	1.0334	1.0680	.7074	.1237	-.0008	.0030	-.0028
136	.076	1.446	25.53	414.2	37.5	.9898	.9798	.7481	.1279	.0013	.0027	-.0029
137	.076	1.456	25.69	419.5	40.0	.9461	.8951	.7854	.1201	.0023	-.0022	.0017
138	.077	1.461	25.78	422.7	42.5	.8585	.7371	.7834	.0964	.0013	.0005	-.0007

STOP
START

TABLE C3
Model with faired cavities at the wing lower side at M = 0.075

(NLR) OLIVE DATA-SYSTEM 1:44 PM THU., 22 OCT., 1987 PROC. 2 TEST 6602 SERIES 4 RUN 7 POL 1 PAGE 1

** CORR.ZERO DRIFT **

NATIONAL AEROSPACE LABORATORY (NLR) LST 3*2.25
DOUBLE DELTA FORCE MEASUREMENTS MEASURING DATE: 27- 2-1986

BETA = 0 degrees
At alpha > 20 degrees, a correction has been applied to Q

DPN	MACH	RE*E6	V	Q	ALFA	CL	CL^2	CD	CM	CC	CN	CR
141	.074	1.507	24.48	399.1	-10.0	-.4780	.2285	.0789	-.0040	.0002	.0060	-.0060
142	.074	1.507	24.51	399.5	-7.5	-.3676	.1351	.0472	-.0201	-.0040	-.0004	.0009
143	.074	1.506	24.52	399.9	-5.0	-.2365	.0559	.0275	-.0127	.0008	-.0000	-.0001
144	.074	1.506	24.53	400.0	-2.5	-.1139	.0130	.0115	-.0085	-.0013	.0002	-.0000
145	.074	1.505	24.53	399.9	0.0	.0167	.0003	-.0052	-.0060	.0002	.0032	-.0032
146	.074	1.504	24.53	399.5	2.5	.1246	.0155	.0103	-.0018	-.0011	-.0026	.0027
147	.074	1.502	24.52	399.2	5.0	.2538	.0644	.0211	.0063	-.0018	-.0015	.0017
148	.074	1.500	24.51	398.6	7.5	.3882	.1507	.0515	.0088	-.0024	-.0057	.0061
149	.074	1.498	24.48	397.7	10.0	.4955	.2456	.0807	.0214	-.0001	-.0007	.0008
150	.074	1.494	24.44	396.3	12.5	.6139	.3769	.1281	.0291	.0018	.0038	-.0041
151	.074	1.495	24.48	397.3	15.0	.7417	.5501	.1866	.0396	.0019	-.0001	-.0003
152	.074	1.494	24.48	397.1	17.5	.9469	.8967	.2773	.0480	.0016	.0042	-.0045
153	.074	1.489	24.42	394.9	20.0	1.0508	1.1043	.3614	.0589	-.0013	-.0004	.0006
154	.074	1.499	24.59	400.4	22.5	1.0586	1.1206	.4069	.0711	-.0004	.0032	-.0031
155	.075	1.499	24.60	400.7	25.0	1.0588	1.1210	.4670	.0784	.0011	.0008	-.0010
156	.074	1.498	24.60	400.4	27.5	1.0752	1.1561	.5374	.0790	-.0006	.0010	-.0009
157	.075	1.507	24.78	405.9	30.0	1.0969	1.2033	.6081	.0880	-.0005	-.0023	.0024
158	.076	1.520	25.00	413.1	32.5	1.0739	1.1532	.6626	.1122	-.0008	-.0012	.0014
159	.076	1.523	25.06	415.1	35.0	1.0347	1.0707	.7048	.1216	.0010	.0022	-.0024
160	.076	1.526	25.14	417.4	37.5	1.0109	1.0219	.7636	.1322	.0038	.0018	-.0025
161	.076	1.529	25.21	419.6	40.0	.9332	.8709	.7829	.1261	.0003	-.0014	.0013
162	.076	1.533	25.29	422.1	42.5	.8461	.7159	.7834	.0910	-.0014	.0013	-.0011

STOP

TABLE C4
Model with open cavities at the wing lower side at M = 0.075

(NLR) OLIVE DATA-SYSTEM   1:51 PM THU., 22 OCT., 1987   PROC.   2   TEST 6602 SERIES   4 RUN   7 POL   2 PAGE   1

** (CORR.ZERO DRIFT) **

NATIONAL AEROSPACE LABORATORY (NLR) LST 3*2.25
DOUBLE DELTA FORCE MEASUREMENTS   MEASURING DATE: 27- 2-1986

BETA = 0 degrees
At alpha > 20 degrees, a correction has been applied to Q

DPN	MACH	RE*E6	V	Q	ALFA	CL	CL^2	CD	CM	CC	CN	CR
163	.182	3.640	60.16	2386.2	-10.0	-.4752	.2258	.0964	-.0132	.0002	-.0015	.0015
164	.182	3.633	60.21	2386.2	-7.5	-.3645	.1329	.0602	-.0082	.0008	.0014	-.0015
165	.182	3.632	60.26	2389.0	-5.0	-.2325	.0541	.0351	-.0045	.0010	-.0018	.0017
166	.182	3.629	60.28	2388.8	-2.5	-.1048	.0110	.0227	-.0020	-.0003	.0017	-.0016
167	.182	3.625	60.29	2388.1	0.0	.0117	.0001	.0190	.0002	.0001	.0002	-.0002
168	.182	3.620	60.28	2385.5	2.5	.1248	.0156	.0227	.0037	.0003	-.0026	.0026
169	.182	3.616	60.33	2386.8	5.0	.2558	.0654	.0348	.0067	-.0001	-.0002	.0003
170	.182	3.607	60.29	2381.1	7.5	.3944	.1555	.0618	.0097	.0003	.0004	-.0004
171	.182	3.605	60.34	2383.5	10.0	.5072	.2572	.0983	.0168	.0003	-.0007	.0007
172	.182	3.601	60.33	2381.6	12.5	.6244	.3899	.1453	.0240	.0000	-.0027	.0027
173	.182	3.605	60.48	2391.4	15.0	.7609	.5789	.2073	.0307	.0002	-.0002	.0002
174	.182	3.598	60.44	2386.5	17.5	.9716	.9440	.3039	.0334	-.0001	.0011	-.0010
175	.178	3.519	59.24	2290.1	17.5	.9723	.9453	.3043	.0336	.0005	-.0003	.0002
176	.178	3.512	59.22	2286.3	20.0	1.0747	1.1551	.3849	.0451	.0003	-.0010	.0009
177	.178	3.508	59.21	2284.0	22.5	1.0843	1.1758	.4409	.0607	-.0007	-.0001	.0003
178	.179	3.523	59.55	2308.4	25.0	1.1101	1.2324	.5058	.0736	.0003	.0014	-.0014
179	.180	3.533	59.77	2324.7	27.5	1.1029	1.2164	.5667	.0790	.0001	.0026	-.0026
180	.176	3.450	58.48	2222.6	27.5	1.1010	1.2121	.5646	.0802	.0001	.0018	-.0018
181	.176	3.458	58.66	2235.6	30.0	1.1006	1.2113	.6329	.0882	.0021	.0001	-.0005
182	.177	3.468	58.90	2252.5	32.5	1.1050	1.2210	.6993	.0988	.0013	.0011	-.0013
183	.177	3.479	59.17	2271.3	35.0	1.0898	1.1876	.7590	.0970	.0021	.0023	-.0027
184	.178	3.486	59.35	2283.8	37.5	1.0597	1.1229	.8133	.1076	.0046	.0033	-.0042
185	.174	3.402	58.02	2180.5	37.5	1.0556	1.1144	.8107	.1046	.0038	.0047	-.0055
186	.174	3.411	58.22	2194.3	40.0	.9924	.9849	.8305	.1075	.0064	.0018	-.0030
187	.175	3.422	58.47	2211.4	42.5	.8664	.7506	.8102	.0673	.0007	.0042	-.0043

STOP

TABLE C5
Model with open cavities at the wing lower side at M = 0.178

(NLR) OLIVE DATA-SYSTEM 1:52 PM THU., 22 OCT., 1987 PROC. 2 TEST 6602 SERIES 4 RUN 7 POL 6 PAGE 1

** CORR.ZERO DRIFT **

NATIONAL AEROSPACE LABORATORY (NLR) LST 3*2.25
DOUBLE DELTA FORCE MEASUREMENTS MEASURING DATE: 27- 2-1986

BETA = 0 degrees
At alpha > 20 degrees, a correction has been applied to Q

DPN	MACH	RE*E6	V	Q	ALFA	CL	CL^2	CD	CM	CC	CN	CR
188	.196	3.833	65.64	2784.7	-10.0	-.4794	.2299	.0565	-.0117	.0014	.0009	-.0010
189	.196	3.827	65.62	2780.6	-7.5	-.3657	.1338	.0612	-.0079	.0009	.0013	-.0014
190	.196	3.826	65.66	2782.7	-5.0	-.2326	.0541	.0360	-.0040	.0008	-.0012	.0011
191	.196	3.823	65.68	2782.7	-2.5	-.1071	.0115	.0237	-.0011	.0006	.0003	-.0004
192	.196	3.820	65.70	2783.1	0.0	.0094	.0001	.0192	.0009	.0005	.0015	-.0015
193	.197	3.820	65.81	2789.4	2.5	.1241	.0154	.0224	.0037	.0009	.0004	-.0005
194	.196	3.814	65.73	2782.4	5.0	.2563	.0657	.0341	.0070	.0010	.0025	-.0027
195	.197	3.812	65.81	2786.3	7.5	.3916	.1533	.0623	.0099	.0006	.0006	-.0007
196	.197	3.809	65.83	2786.3	10.0	.5095	.2596	.0981	.0165	.0004	.0014	-.0015
197	.196	3.803	65.82	2783.0	12.5	.6250	.3907	.1454	.0235	.0001	-.0005	.0005
198	.197	3.802	65.88	2786.1	15.0	.7593	.5766	.2086	.0300	.0002	-.0006	.0006
199	.196	3.793	65.82	2779.5	17.5	.9714	.9437	.3056	.0328	-.0000	-.0004	.0004
200	.193	3.772	64.67	2681.5	17.5	.9708	.9421	.3050	.0329	.0001	.0006	-.0006
201	.193	3.725	64.84	2692.5	20.0	1.0812	1.1689	.3884	.0434	.0003	.0002	-.0002
202	.193	3.724	64.91	2696.3	22.5	1.0905	1.1892	.4442	.0589	.0002	.0035	-.0035
203	.194	3.730	65.08	2708.6	25.0	1.1074	1.2264	.5092	.0694	-.0003	.0009	-.0008
204	.195	3.742	65.36	2730.2	27.5	1.1048	1.2207	.5714	.0764	-.0005	.0007	-.0007
205	.191	3.669	64.18	2630.7	27.5	1.1077	1.2269	.5727	.0759	.0006	.0016	-.0017
206	.192	3.678	64.38	2644.9	30.0	1.1024	1.2153	.6325	.0792	-.0000	.0005	-.0004
207	.192	3.686	64.62	2663.0	32.5	1.1034	1.2176	.7084	.0895	.0007	.0027	-.0029
208	.193	3.696	64.87	2681.5	35.0	1.0977	1.2049	.7697	.1005	.0034	.0008	-.0014
209	.194	3.706	65.19	2704.6	37.5	1.0654	1.1350	.8187	.0995	.0043	.0027	-.0036
210	.190	3.628	63.88	2596.3	37.5	1.0735	1.1525	.8285	.1079	.0039	.0036	-.0043
211	.191	3.644	64.23	2622.7	40.0	.9992	.9985	.8505	.0982	.0068	.0013	-.0026
212	.191	3.649	64.36	2631.9	42.5	.8599	.7394	.8076	.0687	-.0001	.0017	-.0017

STOP
START

TABLE C6
Model with open cavities at the wing lower side at M = 0.193

```
( NLR )  OLIVE DATA-SYSTEM   1:53 PM  THU., 22  OCT., 1987    PROC.    2    TEST 6602  SERIES    5  RUN   8  POL    1  PAGE    1

 ** CORR.ZERO DRIFT **

NATIONAL AEROSPACE LABORATORY (NLR)  LST 3*2.25
DOUBLE DELTA FORCE MEASUREMENTS             MEASURING DATE: 27- 2-1986

BETA = 0 degrees
At alpha > 20 degrees, a correction has been applied to Q
```

DPN	MACH	RE*E6	V	Q	ALFA	CL	CL^2	CD	CM	CC	CN	CR
215	.175	3.347	58.96	2210.7	42.5	.8656	.7493	.8013	.0664	.0007	.0022	-.0024
216	.175	3.334	58.84	2199.5	40.0	.9950	.9901	.8463	.0996	.0048	.0045	-.0054
217	.174	3.319	58.64	2183.0	37.5	1.0585	1.1204	.8106	.1044	.0030	.0015	-.0021
218	.178	3.393	60.11	2290.9	37.5	1.0588	1.1211	.8093	.1039	.0032	.0041	-.0047
219	.178	3.378	59.89	2273.0	35.0	1.0942	1.1974	.7628	.1054	.0025	.0012	-.0016
220	.177	3.360	59.61	2251.0	32.5	1.1039	1.2185	.7011	.0964	.0011	-.0002	-.0000
221	.176	3.350	59.45	2238.7	30.0	1.1010	1.2121	.6302	.0935	-.0016	-.0021	.0024
222	.176	3.335	59.25	2222.3	27.5	1.1003	1.2107	.5639	.0871	-.0007	.0025	-.0023
223	.179	3.407	60.55	2320.4	27.5	1.0974	1.2044	.5659	.0879	.0001	.0010	-.0010
224	.179	3.397	60.42	2309.8	25.0	1.1073	1.2262	.5050	.0784	-.0011	.0016	-.0014
225	.178	3.386	60.25	2295.9	22.5	1.0840	1.1750	.4388	.0628	-.0010	.0025	-.0023
226	.178	3.378	60.15	2287.7	20.0	1.0765	1.1588	.3831	.0452	-.0002	.0022	-.0021
227	.178	3.377	60.16	2287.8	17.5	.9742	.9491	.3023	.0328	-.0005	-.0005	.0005
228	.182	3.448	61.45	2386.2	17.5	.9756	.9518	.3030	.0324	-.0008	.0025	-.0024
229	.182	3.442	61.38	2379.8	15.0	.7616	.5801	.2054	.0305	-.0006	.0001	.0000
230	.182	3.443	61.43	2383.6	12.5	.6275	.3938	.1426	.0238	.0001	.0022	-.0023
231	.182	3.446	61.53	2390.1	10.0	.5119	.2620	.0959	.0165	.0004	.0020	-.0021
232	.182	3.444	61.51	2387.8	7.5	.3936	.1549	.0604	.0105	-.0006	.0015	-.0014
233	.182	3.444	61.52	2388.5	5.0	.2598	.0675	.0339	.0071	-.0003	-.0011	.0012
234	.182	3.439	61.45	2382.9	2.5	.1274	.0162	.0218	.0043	-.0001	.0006	-.0005
235	.182	3.436	61.45	2382.4	0.0	.0131	.0002	.0166	.0015	.0004	.0005	-.0005
236	.182	3.438	61.46	2383.0	-2.5	-.1037	.0108	.0207	-.0005	.0003	-.0007	.0006
237	.182	3.441	61.55	2388.9	-5.0	-.2287	.0523	.0316	-.0024	.0002	.0021	-.0021
238	.182	3.435	61.48	2382.5	-7.5	-.3626	.1315	.0593	-.0052	-.0007	-.0007	.0007
239	.182	3.437	61.52	2385.9	-10.0	-.4782	.2287	.0941	-.0102	-.0010	-.0012	.0013

STOP

TABLE C7

Model with open cavities at the wing lower side at $M = 0.178$, measured in a reversed order (from positive α to negative α)

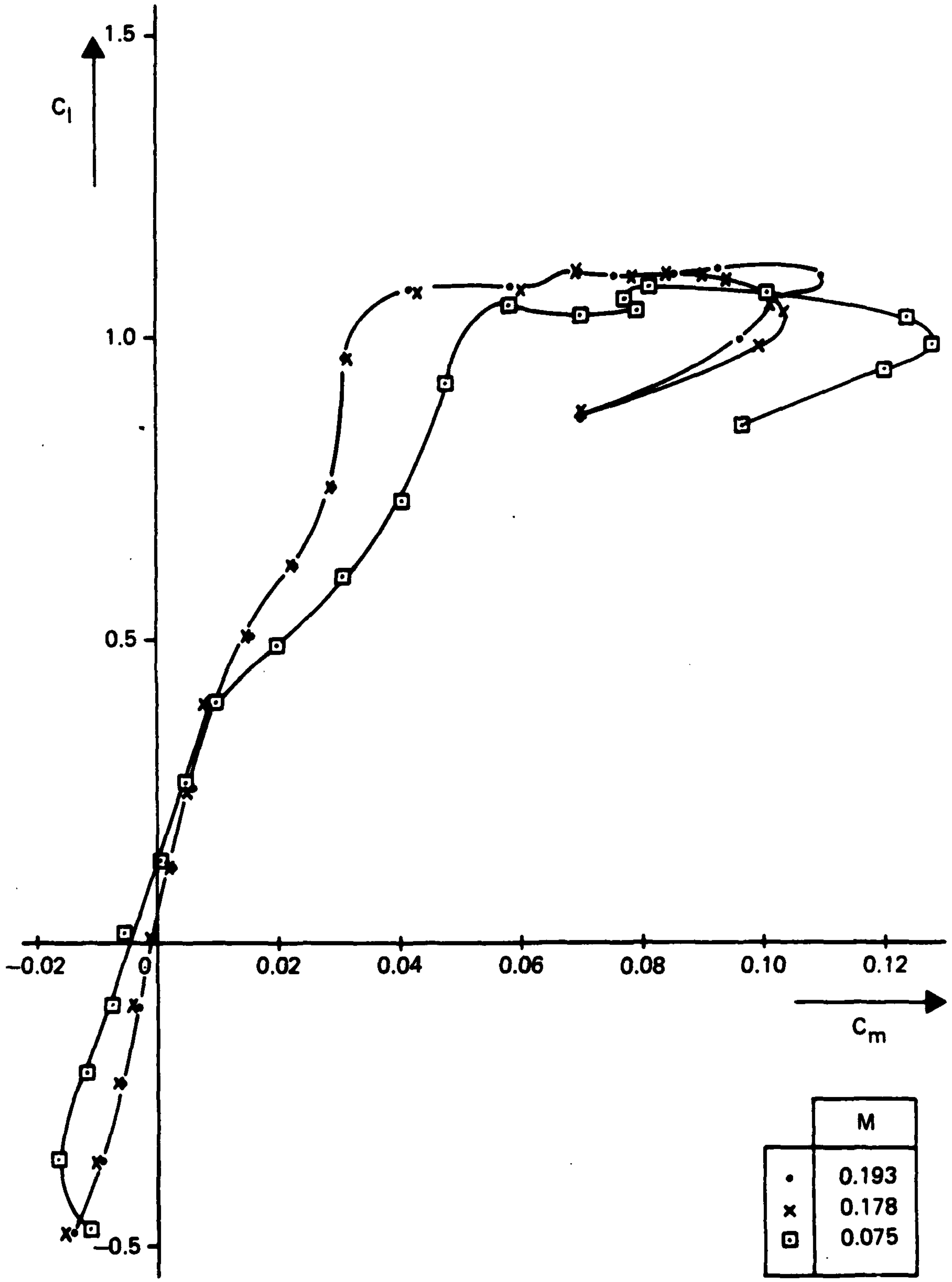

Fig. C1 Model with faired cavities in the lower wing surface. Influence of the tunnel speed on C_L versus C_m